ELECTRON PARAMAGNETIC RESONANCE AND STRUCTURAL PHASE TRANSITION STUDIES OF Mn^{2+} DOPED SINGLE CRYSTALS OF SOME METAL PERCHLORATE HEXAHYDRATES

By

RAGHUBAR DAYAL

DEPARTMENT OF PHYSICS

INDIAN INSTITUTE OF TECHNOLOGY KANPUR

JANUARY, 1977

ELECTRON PARAMAGNETIC RESONANCE AND STRUCTURAL PHASE TRANSITION STUDIES OF Mn^{2+} DOPED SINGLE CRYSTALS OF SOME METAL PERCHLORATE HEXAHYDRATES

A Thesis Submitted
In Partial Fulfilment of the Requirements
for the Degree of

DOCTOR OF PHILOSOPHY

By

RAGHUBAR DAYAL

to the

DEPARTMENT OF PHYSICS

INDIAN INSTITUTE OF TECHNOLOGY KANPUR

JANUARY, 1977

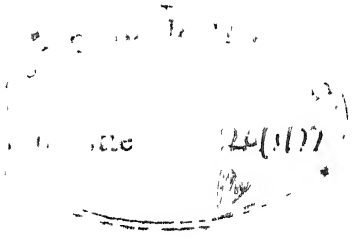

Certificate

This is to certify that the work presented in the thesis entitled "Electron Paramagnetic Resonance and Structural Phase Transition Studies of Mn^{2+} doped Single Crystals of Some Metal Perchlorate Hexahydrates" is the original work of Mr. Raghubar Dayal carried out under our joint supervision, and it has not been submitted elsewhere for a degree.

D. Ramachandra Rao
Professor Physics
I.I.T., Kanpur

Putcha Venkateswarlu
Professor of Physics
I.I.T., Kanpur

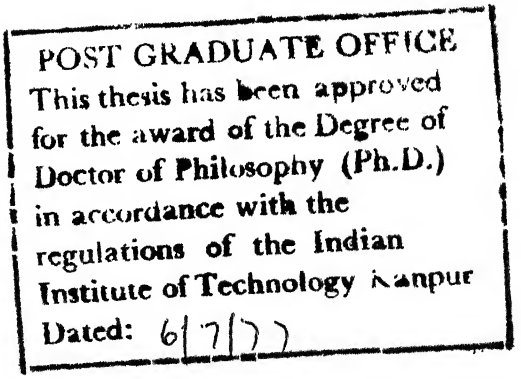

ACKNOWLEDGEMENTS

I express my deep sense of indebtedness to Prof. P. Venkateswarlu and Prof. D. Ramachandra Rao for their guidance and encouragement. Their interest in the progress of this work is gratefully acknowledged.

I am very much thankful to the authorities of Aligarh Muslim University (specially to the Vice-Chancellor, Dr. A.M. Khusro and the Head of the Physics Department, Prof. M.Z.R. Khan) for kindly sanctioning the study leave for completing my Ph.D. programme .

I thank Dr. M.V. Ramaniah, the Head of the Radio Chemistry Division, BARC, Bombay for extending me the facilities to work on the EPR apparatus, and Dr. M.D. Sastri for his kind co-operation and valuable suggestions.

I have benefitted highly from the discussions I had with Dr. S.D. Pandey of P.P.N. College, Kanpur, and Drs. T.V. Ramakrishnan, N.C. Vizia and U.V. Kumar of our department. I thank Dr. R.P. Singh and Dr. J.G. Mohanty of Chemistry department for the help in preparing the compounds

It is a pleasure to thank my colleagues and friends M/s. A.V. Jain, R.S. Saraswat, V.K. Jain, A.A. Ansari, V.M. Malhotra and M.S. Ansari, for the co-operation they

have extended to me. Mr. A.V. Jain has been a source of help and assistance althrough. I am very much thankful to h I thank all my friends who have helped me in the preparation of this thesis.

My thanks are due to the staff of Glass-blowing Shop for the necessary jobs done for my work and Mr. D.S. Rawat for supplying the nitrogen gas whenever needed. I thank Mr. B.B. Srivastava for the tracings, Mr. C.M. Abraham for neat and patient typing of the manuscript, and Mr. H.K. Panda for the cyclostyling work.

The financial assistance from the National Bureau of Standards, Washington, U.S.A., is gratefully acknowledged.

RAGHUBAR DAYAL

CONTENTS

LIST OF FIGURES

LIST OF TABLES

SYNOPSIS

Electron paramagnetic resonance has been employed to investigate several solid state problems associated with irradiation effects, radiation damage, point defects, conduction band and trapped electrons in metals etc. It has proved to be a powerful tool to measure the g values and their anisotropy and thus to extract direct information about the magnetic field dependent ground state energy levels of the transition metal and rare earth ions doped in crystalline solids. It also helps to determine the structural phase transitions. The S-state ions with $S > \frac{1}{2}$ such as Fe^{3+}, Mn^{2+}, Eu^{2+}, Gd^{3+} etc. have been found very much suitable for the study of the phase transitions because they possess orbitally non-degenerate ground states which remain unaffected by Jahn-Teller effect and thus they do not disturb the local symmetry. Further the fine structure splittings of the states with $S > \frac{1}{2}$ could be used in symmetry determination.

In the work described in the thesis, divalent manganese (Mn^{2+}) which has $S = 5/2$, is chosen for the EPR study of the structural phase transitions occurring in a series of isomorphic compounds involving both diamagnetic and paramagnetic systems $M(ClO_4)_2.6H_2O$ (where M = Mg, Zn, Cd and Fe, CO, Ni).

A general introduction to the phenomenon of EPR is given in the first chapter. Various paramagnetic systems that can be studied by EPR and the information which can be obtained, are also included. The general theory of EPR and structural phase transitions, zero-field splitting mechanisms for Mn^{2+} and the role of EPR in determining the transition temperatures, order parameters etc. are described in Chapter II.

Chapter III deals with the experimental details along with the EPR study of Mn^{2+} doped $Mg(ClO_4)_2.6H_2O$ at different temperatures. Changes in the line shape and splittings due to angular and temperature variation are easily seen in this system. $Mg(ClO_4)_2.6H_2O$ has a pseudohexagonal structure with a binolecular orthorhombic unit cell (C^7_{2v}). Mn^{2+} substitutes for Mg^{2+} at the sites of trigonal symmetry and exhibits the characteristic 30-line hyperfine spectrum for the static magnetic field parallel to the c-axis (trigonal symmetry axis). When the magnetic field does not coincide with c-axis, each hyperfine line splits into three components indicating that there are three inequivalent sites for(Mn^{2+}) and hyperfine forbidden ($\Delta M = \pm 1$, $\Delta m = \pm 1$) transitions are also observed. Linewidth has been found to be Mn^{2+} concentration dependent and shows usual behaviour. Three structural phase transitions are found to occur at 272 K, 203 K and 103 K. The first two are second order transitions.

The angle of rotation of the principal z-axis (order parameter) and the D parameter have been determined experimentally for the phases below these two transition temperatures and are found to conform with the theories available for the second order phase transition. A first order phase transition occurs at 103 K and the spectrum becomes very much complex below this temperature.

The crystal structure of $Zn(ClO_4)_2.6H_2O$ is essentially the same as that of $Mg(ClO_4)_2.6H_2O$ and the EPR study of this crystals doped with Mn^{2+} is presented in Chapter IV. A 30-line hyperfine spectrum for H parallel to c-axis, hyperfine forbidden transitions for H oriented away from c-axis and concentration dependent linewidths are observed in this system also. Line shape distortions with temperature variation were used for proposing a probable structural phase transition at 284 K.

EPR of Mn^{2+}:$Cd(ClO_4)_2.6H_2O$ is presented in Chapter V. A 30-line hyperfine spectrum at room temperature for H along c-axis was recorded as expected. Three phase transitions occur at 272 K, 259 K and 115.5 K. Those occurring at 272 K and 259 K are of the second order whereas the one at 115.5 K is of the first order. The variation of D parameter found experimentally conforms to the theoretical expressions available.

The room temperature EPR study of Mn^{2+} doped $Fe(ClO_4)_2.6H_2O$, $Co(ClO_4)_2.6H_2O$ and $Ni(ClO_4)_2.6H_2O$ crystals alongwith its temperature dependence is described in Chapter VI. The spectra in these systems are not well resolved and do not show thirty lines clearly as the lines are broad. From temperature variation study, one probable structural phase transition is indicated in $Co(ClO_4)_2.6H_2O$ at 245 K, and in $Ni(ClO_4)_2.6H_2O$ at 247 K in addition to the ones already reported (at 154.5 K and 225 K respectively) by Mössbauer studies and susceptibility measurements. The principal axes are found to change their orientations after the phase transition at 237 K in $Fe(ClO_4)_2.6H_2O$ and at 154.5 K in $Co(ClO_4)_2.6H_2O$ but not in $Ni(ClO_4)_2.6H_2O$.

The present study shows interesting results in diamagnetic systems : two new phase transitions have been found in $Mg(ClO_4)_2.6H_2O$, the phase transitions in $Zn(ClO_4)_2.6H_2O$ and $Cd(ClO_4)_2.6H_2O$ have been recorded for the first time. However, paramagnetic systems did not yield quantitative results accurately because of the larger linewidths. Specific heat measurement may confirm new phase transition temperatures and low temperature x-ray study may help in understanding the mechanisms of the phase transitions in these systems.

CHAPTER I

INTRODUCTION

Abstract

A brief description of the phenomenon of electron paramagnetic resonance is given in this chapter. Various systems which can be studied and the types of information which can be obtained, are indicated.

Paramagnetism occurs whenever a system of charges possesses a resultant angular momentum. The momentum arising due to electronic motion gives rise to electronic paramagnetism. Such paramagnetism is found in a large number of systems: free atoms and ions with an odd number of electrons e.g. atomic sodium, chlorine and silicon; free molecules with an odd number of electrons such as NO, NO_2 and also with even number of electrons but ground state with partially filled molecular shells e.g. O_2; free molecular radicals like $\dot{C}H_3$; larger molecules and ions such as triphenyl methyl, $\dot{C}(C_6H_5)_3$ and D.P.P.H.; point defects in solids formed by the impurities of transition and rare-earth group ions, e.g. Mn^{2+} in MgO; donor and acceptor impurities in semiconductors, e.g. phosphorous in silicon; electron and hole traps in photoconductors like Fe^{3+} in CdS; activators and coactivators in phosphors such as self-activated ZnS; colour centres in insulators e.g. F centres in KCl; radiation damage centres e.g. Si vacancy in Si crystal; conduction electrons in metals having unfilled energy bands and excited triplet states of molecules such as in ultraviolet light irradiated naphthalene.

In all these systems, Zeeman levels can be produced by an external magnetic field and transitions between these levels can be studied. Such a study is made by electron paramagnetic resonance, a brief introduction of which is given below.

An intrinsic spin angular momentum (p_s) and a permanent magnetic moment(μ_s) are associated with a free electron and are given by the expressions

Spin angular momentum $\quad \vec{p}_s = \hbar\vec{S}$

Magnetic moment $\quad \vec{\mu}_s = -\left(\frac{e\hbar}{2mc}\right)\vec{S} = -g\,\beta\,\vec{S}$

where e is the electronic charge, m is the mass of the electron, c is the velocity of light, $S = \frac{1}{2}$, β is the Bohr Magneton, g is the Lande's splitting factor and its value for an electron is 2.0023, and $h = h/2\pi$, h being the Planck's constant.

In a static magnetic field this tiny magnet aligns itself either parallel or antiparallel to the field. The parallel position with magnetic spin quantum number $m_s = -\frac{1}{2}$ has lower energy and the antiparallel position with $m_s = +\frac{1}{2}$ has higher energy. The energy of interaction of the electron with the static magnetic field H is given by

$$\begin{aligned} E_{m_s} &= -\vec{\mu}.\vec{H} \\ &= -(-g\,\beta\,\vec{S}).\vec{H} \\ &= g\,\beta\,\vec{S}.\vec{H} \\ &= g\,\beta\,H\,m_s \\ &= \pm\tfrac{1}{2}\,g\,\beta\,H \end{aligned} \qquad (1.1)$$

Equation 1.1 shows that the separation between levels depends on the strength of the magnetic field H, other

factors being constant. The level variation with H is shown in Fig. 1.1. It is possible to induce electronic transition between these levels by the interaction of electromagnetic radiation of appropriate frequency ν such that resonance condition

$$E_{\frac{1}{2}} - E_{-\frac{1}{2}} = h\nu = g\,\beta\,H \qquad (1.2)$$

is satisfied. For maximum absorption, the oscillating magnetic field component of the radiation is kept perpendicular to H. Since the energy difference between the levels for a magnetic field of the order of few kilogauss is very small, the quantum of energy $h\nu$ is obtained from microwave source.

A continuous resonance absorption of microwave radiation is possible only if the lower of the two levels is always more populated than the higher one. If there are N electrons distributed among these two levels, then the number of electrons in the upper level, N_+, is lower than the number of electrons in the lower level, N_-, and the condition for resonance absorption is satisfied. According to Boltzmann distribution law

$$\frac{N_+}{N_-} = \exp\,(-g\,\beta H/kT) = \exp\,(-h\nu\,/kT) \qquad (1.3)$$

where k is Boltzmann's constant and T is the absolute temperature. The net absorption would be larger if the energy separation is higher and the temperature is smaller.

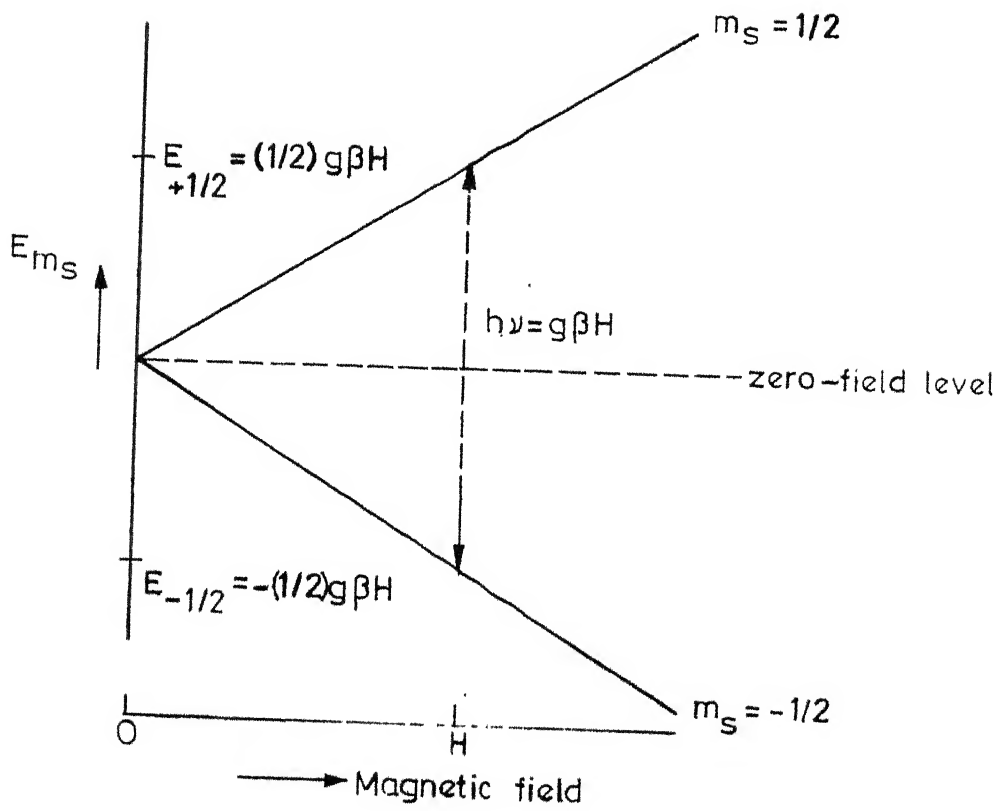

Fig. 1.1 Energy level splitting for single electron (s=1/2) in a static magnetic field.

The electrons transferred to the upper level by absorbing radiation must be brought back to the lower level. This is accomplished by relaxation processes and the absorption continues. This resonance absorption of microwave radiation (usually between the ground state energy levels of an electronic system under the action of an applied static magnetic field) is called Electron Paramagnetic Resonance.

Next, let us consider a free ion of resultant angular momentum J placed in the static magnetic field H. The magnetic moment associated with it is $\vec{\mu} = - g \beta \vec{J}$. The ion would have the energy levels in the magnetic field as given by

$$E_{M_J} = (- g \beta \vec{J}). \vec{H} = g \beta H M_J \qquad (1.4)$$

where $M_J = J, J-1 \ldots\ldots - (J-1), - J$

Thus there are 2J+1 equally spaced levels which are generally called as Zeeman levels. Here Lande's splitting factor g is given by

$$g = 1 + \frac{J(J+1) + S(S+1) - L(L+1)}{2J\ (J+1)} \qquad (1.5)$$

where L and S are orbital angular momentum and spin angular momentum respectively and L-S coupling holds.

For $J = 5/2$, the energy levels are as shown in Fig. 1.2. The alternating microwave field of frequency ν perpendicular

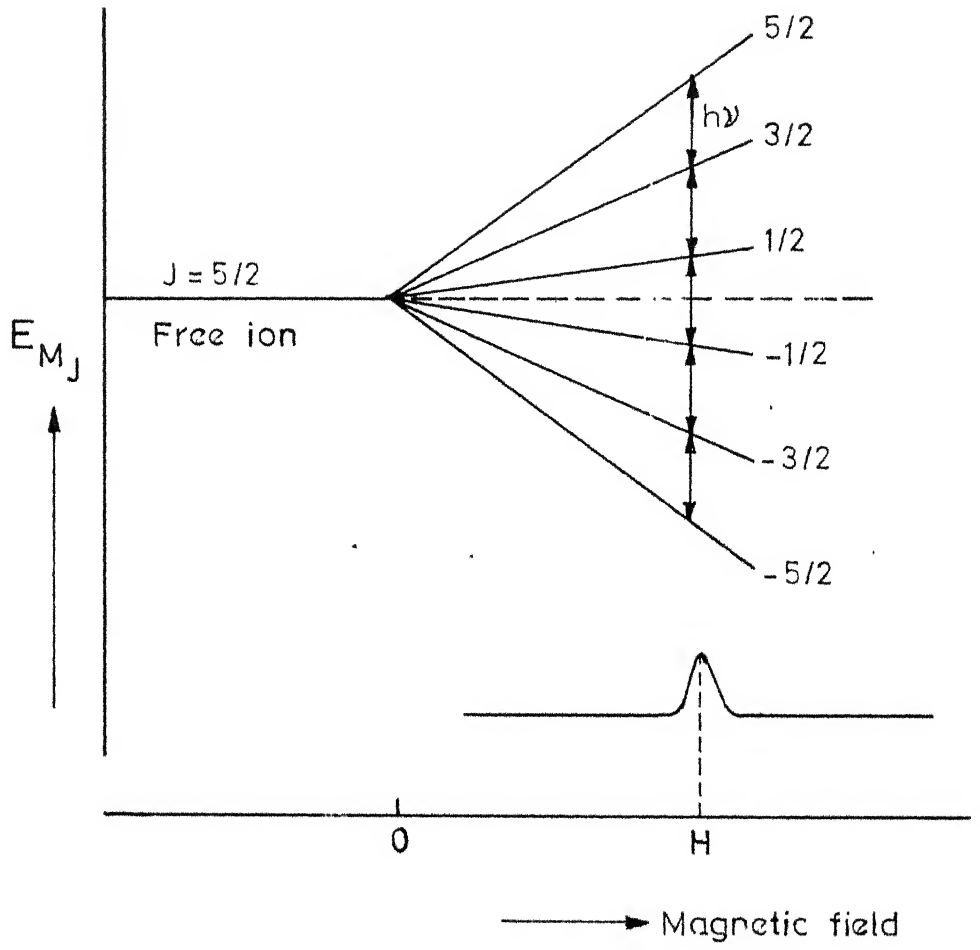

Fig.1.2 Splitting of energy levels and the allowed transitions of a free ion with J=5/2 in a static magnetic field.

to H induces magnetic dipole transitions $\Delta M = \pm 1$. Five possible transitions occur superimposed on each other at a single frequency.

When a paramagnetic ion is placed in a crystalline solid, it experiences the effect of its environment. Firstly, it interacts with the ions of the same kind present in the solid. Secondly, the solid lattice interacts with the paramagnetic ion through its ligands which are charged ions or neutral molecules. The solid lattice, usually diamagnetic, and the paramagnetic ion may interact to give some useful information about the ion as well as the lattice but the interaction between paramagnetic dipoles may not serve any purpose. By keeping the concentration of paramagnetic ions in the diamagnetic lattice small (about 1 ppm), the interaction between magnetic dipoles is greatly reduced.

The ligands interact with the ion either through the electrostatic field produced by charges or by covalent bonding. The energy levels of the paramagnetic ion are affected in the same manner by either process[1]. They split the ground state as well as excited states into a number of components. This splitting is called crystal field or ligand field splitting and is similar to Stark effect. Symmetry of the ligand field and its strength determines the number of split

components and the amount of splitting. A splitting as shown in Fig. 1.3 may occur for the ion with $J = 5/2$ doped in a solid when placed in a magnetic field. Five possible transitions may be observed separately at five different frequencies if the frequency is varied and at five different field strengths if H is varied. In practice, H is varied and ν is held constant. The 'g' factor is now defined by equation 1.2.

In the earlier experiments on magnetic resonance in solids, Zavoisky[2] observed strong electron paramagnetic resonance absorption in the $Mn\ SO_4$ at 298 K and 2.75 GHz. Since then the electron paramagnetic resonance has become a useful tool in solid state physics. It gives the most direct and accurate description of the ground state under the crystalline environment. Symmetry of the crystal field and the strength of the interactions are also reflected in EPR spectrum. It enables one to determine the crystal field parameters and the symmetry of the site at which doped paramagnetic ion is sitting in the crystal. The changes in the crystal structure with temperature produce corresponding changes in the EPR spectrum and therefore phase transitions occuring in the crystals can be detected. Thus the information about the doped paramagnetic ion as well as the crystal structure may be obtained.

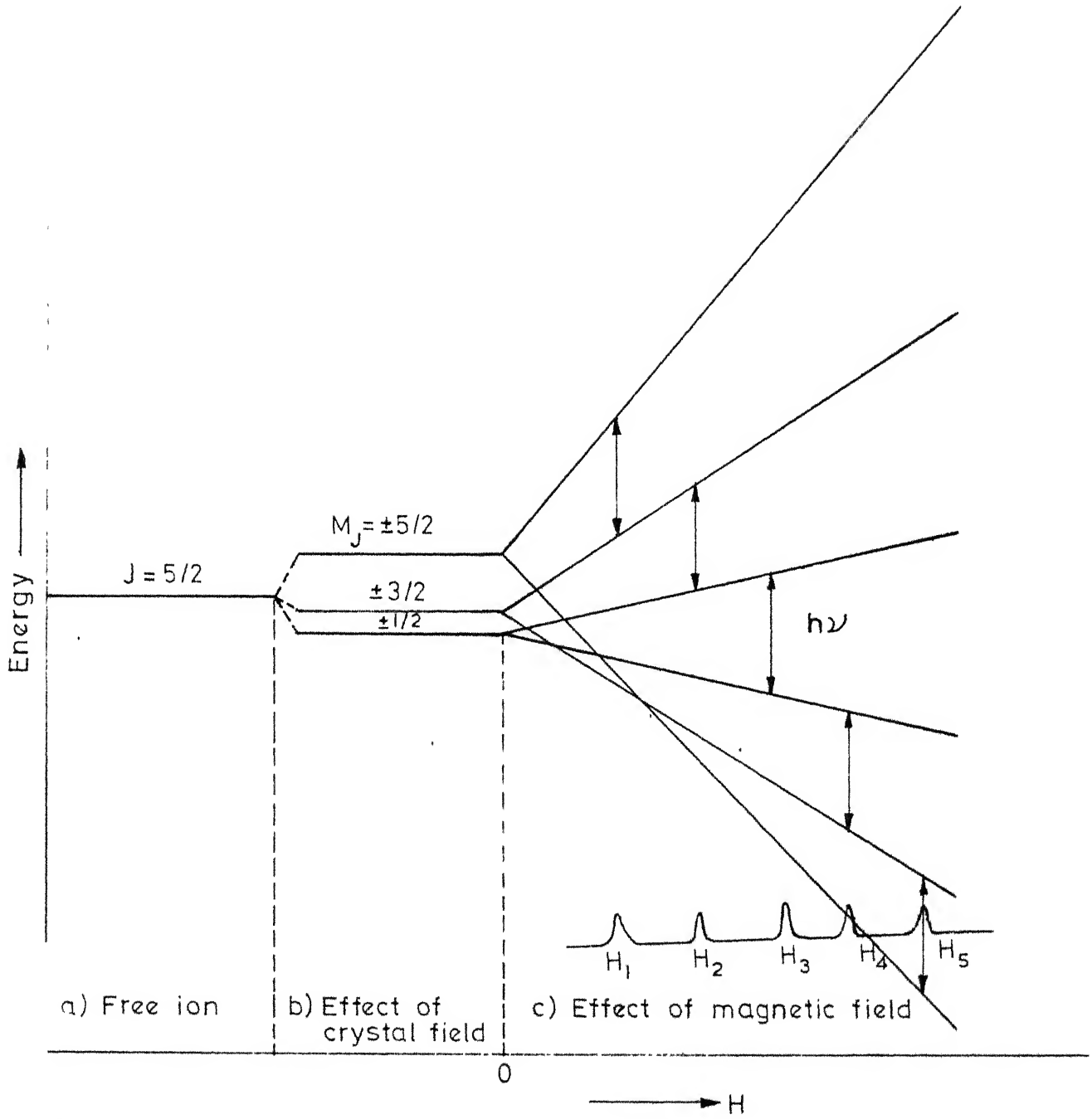

Fig.1.3 Energy level splitting in a crystal field and a magnetic field for an ion (J=5/2) doped in a crystal Allowed transitions are indicated.

In addition, the paramagnetic resonance has been used to determine the free radical concentration, molecular structure and character of bonds. It helps in detecting the association or dissociation of radicals and measuring equilibrium constants. The species of free-radicals can be detected and identified. Changes occuring in radical concentration with time, chemical treatment or irradiation can be studied by electron paramagnetic resonance. Measurement of relaxation time , magnetic susceptibility and electronegativity can be done. Zero-field splittings, free-radical mobilities and intermolecular electron changes are well investigated by EPR. Some typical applications are mentioned below.

Among analytical problems, the crystal field parameter in inorganic materials were investigated by Carrington et al[3]. A study of the effects in thermoelectricity was made by Bennett et al[4]. Analysis of semiquinones and polynuclear hydrocarbons was carried out by Venkataraman and others[5].

Libby and workers[6] used EPR to study the degree of the organic free radical production by gamma - radiation. Phosphorescent naphthalene having molecules in their first excited state, was studied by Hutchinson and Mangum[7].

Enzyme interactions[8], free radicals in living tissues[9], anomalous magnetic properties of nucleic acids[10]

and effects of x-irradiation on biological materials[11] are some of the biological and medical problems studied by EPR.

Irradiation effects in solids[12], conduction band and trapped electrons in metals[13], radiation damage[14] and cyclotron resonance[15] etc. are various physical and solid state problems investigated by EPR.

REFERENCES

1. Griffith, J.S., J. Chem. Phys. 41, 576 (1964).
2. Zavoisky E., J. Phys. USSR 9, 211, 245, 447 (1945).
3. Carrington A., and Longuet-Higgins H.C., Quart. Rev. Chem. Soc. Lond. 14, 427 (1960).
4. Bennett J.E., Ingram D.J.E., and Tapley J.G., J. Chem. Phys. 23, 215 (1955).
5. Venkataraman B., Segal B.G., and Fraenkel G.K., J. Chem. Phys. 30, 1006 (1959).
6. Libby D., Ormerod M.G., and Charlesby A., Polymer I, 212 (1960).
7. Hutchinson C.A., and Mangum B.W., J.Chem. Phys. 34, 908 (1961).
8. Gibson J.F., Ingram D.J.E., and Nicholls P., Nature (London) 181, 1398 (1958).
9. Commoner B., Townsend J., and Pake G.E., Ibid. 174, 689 (1954).
10. Blumenfel'd L.A., and Bendorskii V.A., Doklady Akad. Nauk SSSR 113, 1481 (1960).
11. Gordy W., Ard W.B., and Shields H., Proc. Nat. Acad. Sci. 41, 983 (1955).
12. Griffiths J.H.E., Owen J., and Ward I.M., Report on the Conference on Defects in Crystalline Solids, p. 81, Lond. Phys. Soc. (1955).
13. Owen J., Browne M., Knight W.D. and Kittel C., Phys. Rev. 102, 1501 (1956).
14. Anderson J.H., and Weil J.A., J. Chem. Phys. 31, 427 (1959).
15. Ingram D.J.E., J. Brit. IRE 19, 357 (1959).

GENERAL REFERENCES

1. Low W., Paramagnetic Resonances in Solids (Suppl.2, Solid State Physics) Academic Press, N.Y. (1960).
2. Assenheim H.M., Introduction to Electron Spin Resonance, Hilger and Watts Ltd., London (1966).
3. Carrington A., and Mclachlan A.D., Introduction to Magnetic Resonance, Harper and Row, N.Y. (1967).
4. Sorin L.A., and Vlasova M.V., Electron Spin Resonance of Paramagnetic Crystals (Translated from Russian by Gluck P.) Plenum Press, N.Y. (1973).
5. Pake G.E., and Estle T.L., The Physical Principles of Electron Paramagnetic Resonance (2nd Ed.), W.A. Benjamin, Inc., London (1973).

CHAPTER II

THEORY OF ELECTRON PARAMAGNETIC RESONANCE AND STRUCTURAL PHASE TRANSITION

Abstract

This chapter presents a brief theory of electron paramagnetic resonance and structural phase transition. The Hamiltonian of a free ion and the effect of the crystal field have been discussed. The spin Hamiltonian, its parameters, selection rules, relaxation processes and zero-field splitting mechanisms for the Mn^{2+} have been described. The theory of structural phase transition has been given in brief. The advantages of the study of the phase transition by electron paramagnetic resonance are indicated.

HAMILTONIAN OF A FREE ION

The Hamiltonian of a free ion may be considered as the sum of energy contributions from various interactions present within the ion. Some of these interactions may be considerably strong while the others could be negligible. Different terms of the Hamiltonian and their relative magnitudes are considered below.

Coulomb Interaction: This is the most dominant term of the Hamiltonian. The interaction of electrons with effective nuclear charge Ze and the mutual repulsion of electrons constitute this term. Without relativistic corrections, it is written as

$$H_c = \sum_{k=1}^{N} \frac{p_k^2}{2m} - \sum_{k} \frac{Z_k e^2}{r_k} + \sum_{k>j=1} \frac{e^2}{r_{kj}} \qquad (2.1)$$

where $p_k = i\hbar \nabla_k$ is the linear momentum operator, r_k is the radius vector from nucleus to the k-th electron and m is the mass of the electron. The sum extends over all the N electrons in the ion through the running indices k and j.

Spin-Orbit Interaction: This is the magnetic interaction between electron spins s_k and orbital angular momenta l_k and is expressed as

$$H_{LS} = \sum_{jk} (a_{jk} \vec{l}_j . \vec{s}_k + b_{jk} \vec{l}_j . \vec{l}_k + c_{jk} \vec{s}_j . \vec{s}_k)$$

where a_{jk}, b_{jk} and c_{jk} are constants. For R-S coupling the spin-orbit interaction takes the form

$$H_{LS} = \lambda \vec{L} . \vec{S} . \qquad (2.2)$$

where λ is called spin-orbit coupling constant. It may be positive or negative. Here L and S are total orbital and spin angular momentum operators.

Spin-Spin Interaction: This terms is very small though very important in some transition metal ions such as Mn^{2+}, Fe^{3+} and Cr^{3+}. This mechanism was first suggested by Pryce[1] and represents weak magnetic interaction between electrons in the ion and is given by

$$H_{SS} = \sum_{jk} 4\beta^2 \left[\frac{\vec{s}_j . \vec{s}_k}{r_{jk}^3} - \frac{3(\vec{r}_{jk} . \vec{s}_j)(\vec{r}_{jk} . \vec{s}_k)}{r_{jk}^5} \right] \qquad (2.3)$$

where β is the Bohr magneton.

Hyperfine Interaction: If the nucleus has spin I and magnetic moment μ_n, it may interact with its environment[2] because of the local magnetic field produced by orbital motion of each electron and its spin. The contributions of these two terms to the Hamiltonian are given below. For each

electron from orbital motion, $H_{o,k} = 2\, g_n\, \beta\beta_n\, r_k^{-3}\, \vec{l}_k.\vec{I}$ and from spin, $H_{s,k} = -g_e\, \beta g_n\, \beta_n\, r_k^{-3} \left[\vec{I}.\vec{s}_k - 3\, \frac{(\vec{I}.\vec{r}_k)(\vec{s}_k.\vec{r}_k)}{r_k^2}\right]$

where g_n is the nuclear splitting factor and β_n is the nuclear magneton. There is, however, a third contribution from s electrons due to Fermi contact interaction[3]. At the nucleus, all s electrons have a non-vanishing charge density which is nearly uniform throughout the small volume of the nucleus. The nucleus is thus in a uniformly magnetized medium and has a magnetisation

$$\vec{M} = -g_e\beta\, |\psi(0)|^2\, \vec{s}_k$$

where $|\psi(0)|^2$ represents the charge density. The energy of nuclear magnetic dipole moment μ_n in this field is

$$H_{FC} = -\frac{8\pi}{3}\, \vec{M}.\vec{\mu}_n$$

$$= \frac{8\pi}{3}\, g_e\beta\, g_n\beta_n\, |\psi(0)|^2\, \vec{I}.\vec{s}_k.$$

Adding all the contributions and summing over all the electrons, we get

$$H_N = 2g_n\beta_n\beta \sum_k \left[\frac{(\vec{l}_k - \vec{s}_k).\vec{I}}{r_k^3} + \frac{3(\vec{I}.\vec{r}_k)(\vec{s}_k.\vec{r}_k)}{r_k^5} + \frac{8\pi}{3}\delta(\vec{r}_k)(\vec{s}_k.\vec{I})\right] \qquad (2.4)$$

Nuclear Quadrupole Interaction: This has been discussed in detail by Bleaney[4]. It describes the energy of interaction of electrons with quadrupole moment Q of the nucleus in the form

$$H_Q = \frac{e^2 Q}{2I(2I-1)} \sum_k \left[\frac{I(I+1)}{r_k^3} - \frac{3(\vec{r}_k . \vec{I})^2}{r_k^5} \right] \qquad (2.5)$$

Interaction with external magnetic field: If the free ion is placed in the external static magnetic field H, then the energy of interaction of electrons with this field is

$$H_H = \sum_k \beta \, (\vec{l}_k + 2\vec{s}_k) . \vec{H} . \qquad (2.6)$$

Similarly, the direct interaction of the nucleus with the external magnetic field is

$$H_{HN} = -\gamma\beta_n \, \vec{I} . \vec{H} \qquad (2.7)$$

where γ is nuclear gyromagnetic ratio . Collecting all the terms together, the Hamiltonian of a free ion in a steady magnetic field is written as

$$H = H_c + H_{LS} + H_{SS} + H_N + H_Q + H_H + H_{HN} \qquad (2.8)$$

The magnitudes of these terms are of the following order

$H_c = 10^5$ cm^{-1}, Optical region

$H_{LS} = 10^2$ cm^{-1}, for ion group

10^3 cm^{-1}, for rare earths and uranium group

$H_{SS} = 1$ cm^{-1}

$H_N = 10^{-1} - 10^{-3}$ cm^{-1}

$H_Q = 10^{-3}$ cm^{-1}, Quadrupole energy

$H_H = 1\ cm^{-1}$, Zeeman energy

$H_{HN} = 10^{-3}\ cm^{-1}$, Nuclear spin energy

Effect of Crystal Field: When a paramagnetic ion is placed in a crystal lattice, an additional term is introduced into the Hamiltonian. The effect of crystalline surroundings on the ion may be considered in the form of a crystal field potential. The ion is subjected to electrostatic field created by the ligands, which are considered as point charges[5-7] or dipoles and the type of the potential V follows the symmetry at the site of the ion. This potential satisfies Laplace equation $\nabla^2 V=0$ and therefore can be expressed in terms of spherical harmonics. Thus

$$V = \sum_n \sum_{m=n}^{-n} \sum_k C_n^m r^n Y_n^m (\theta_k, \phi_k)$$

$$= \sum_n \sum_m V_n^m \qquad (2.9)$$

where $Y_n^m = (-1)^m Y_n^{-m}$ and for a real V, $C_n^m = (-1)^n C_n^{-n}$. The sum over k extends over all the electrons of cation. It is assumed that the surrounding ions do not overlap the electron cloud of the paramagnetic ion.

Since V should reflect the symmetry at the magnetic ion site, its form should be such that it should be invariant under the symmetry of the point group to which the magnetic ion site belongs. Further restrictions on the expansion of V refer to the nature of the magnetic ion. The electronic

wavefunctions also can be expanded in spherical harmonics and the matrix elements of V in the basis of free ion wavefunction vanish for $n > 21$, where l is the orbital angular momentum of the electron. For iron group (3d), terms upto $n = 4$, are retained and for rare-earths (4f), terms upto $n = 6$, are needed. Thus, for d electrons in octahedral symmetry, the crystal field potential has the form

$$V = Y_4^0 + \sqrt{\left(\frac{5}{14}\right)} \left(Y_4^{+4} + Y_4^{-4}\right) ,$$

the axis of quantization has been taken along the four-fold axis and the multiplication factor has been left out. In terms of the cartesian co-ordinates, this is expressed in the form

$$V = x^4 + y^4 + z^4 - \frac{3}{5} r^4$$

The contribution to the Hamiltonian due to the crystal field potential is

$$H_{cr} = - eV \qquad (2.10)$$

To find the non-zero matrix elements associated with states having the same J, the method of equivalent operators of Stevens[8-10], Elliott[10] and Judd[11] is usually employed. The set of functions Y_n^m ($m = o, \pm 1, \pm 2, \ldots\ldots \pm n$) forms the basis of an irreducible representation of rotation group of dimensionality $(2n + 1)$. Each of the functions of the electron coordinates ΣV_n^m may be associated with an equivalent

operator i.e. an analogous function of operators of projection of angular momenta J_x, J_y, J_z which have the same transformation properties with proper reference to the commutation relations. By the operator equivalent method, the calculation of matrix elements becomes quite simple and the matrix elements of several $V_n^{m'}$s are tabulated by Low, and Abragam and Bleaney. [See for example, Solid State Physics, Supplement 2, 1960 (Paramagnetic Resonance) by W. Low and Electron Paramagnetic Resonance of Transition Ions, 1970, by A. Abragam and B. Bleaney]. The operator equivalent form of H_{cr} is expressed as follows

$$H_{cr} = \sum_{nm} B_n^m \; O_n^m$$

where coefficients B_n^m depend on crystalline field and O_n^m transform like $V_n^{m'}$s with x, y, z being replaced by L_x, L_y, L_z.

Now the total Hamiltonian for a paramagnetic ion in a given crystal field can be written with proper choice of $V_n^{m'}$s. The terms of the Hamiltonian may be arranged in decreasing order of magnitude. The relative magnitudes of H_{cr} and $\lambda \vec{L}.\vec{S}$ make a considerable difference in the nature of magnetism in solids and following are the examples which have been frequently observed

$H_{cr} < \lambda \vec{L}.\vec{S}$, complexes of the rare-earths

$\lambda \vec{L}.\vec{S} < H_{cr} < \sum_{k>j=1} \frac{e^2}{r_{kj}}$, complexes of iron group

$H_{cr} > \sum_{k>j=1} \frac{e^2}{r_{kj}}$, covalent complexes such as transition metal cyanides.

The situations where H_{cr} is stronger than electron-electron repulsion are referred to as 'low spin' complexes and the situations where H_{cr} is smaller than $\sum_{k>j=1} \frac{e^2}{r_{kj}}$ are referred to as 'high spin'. All systems of present interest belong to the latter category.

In the case of high spin 3d transition metal ions as mentioned above, the crystal field interaction will have to be considered before spin-orbit interaction. This would mean that one has to consider the effect of crystal field of a particular symmetry on the Russel-Saunders states of a free ion from $3d^1$ to $3d^9$. Bethe has worked it out on group theoretical basis and the crystal field splittings under O_h are shown in Table 2.1.

As can be seen from Table 2.1, the crystal field of octahedral symmetry partly lifts the orbital degeneracy of the electronic states and this is what is normally called the 'quenching' of orbital motion in solids. Whenever there is descent in symmetry to axial or lower, the orbital degeneracy will be further lifted. Whenever the symmetry is orthorhombic or lower, the orbital degeneracy will be completely lifted as all the irreducible representations of these point groups are non-degenerate. There are two important theorems

TABLE 2.1: Crystal Field Splittings of the Ground States

Number of electrons	Transition metal ions	Ground term of free ion	Total spin S	Splitting under O_h
$3d^1$	V^{4+}, Ti^{3+}	^2D	1/2	$^2E_g + ^2T_{2g}$
$3d^2$	Cr^{4+}, Ti^{2+}	^3F	1	$^3T_{1g} + ^3T_{2g} + ^3A_{2g}$
$3d^3$	Mn^{4+}, Cr^{3+}, V^{2+}	^4F	3/2	$^4A_{2g} + ^4T_{1g} + ^4T_{2g}$
$3d^4$	Mn^{3+}, Cr^{2+}	^5D	2	$^5E_g + ^5T_{2g}$
$3d^5$	Fe^{3+}, Mn^{2+}, Cr^{+}	^6S	5/2	$^6A_{1g}$
$3d^6$	Co^{3+}, Fe^{2+}, Mn^{+}	^5D	2	$^5E_g + ^5T_{2g}$
$3d^7$	Ni^{3+}, Co^{2+}, Fe^{+}	^4F	3/2	$^4A_{2g} + ^4T_{1g} + ^4T_{2g}$
$3d^8$	Cu^{3+}, Ni^{2+}, Co^{+}	^3F	1	$^3A_{2g} + ^3T_{1g} + ^3T_{2g}$
$3d^9$	Cu^{2+}, Ni^{+}	^2D	1/2	$^2E_g + ^2T_{2g}$

which are of consequence in the removal of degeneracy of electronic levels. They are due to Kramers[12] and Jahn and Teller[13] and are mentioned below.

Kramers' Theorem: This theorem is concerned with the effect of crystal field on the degeneracy of the ground state of a doped paramagnetic ion. It states that in a crystalline field of any symmetry, a system having an odd number of electrons (e.g. Cr^{3+}, Mn^{2+}, Co^{2+}) will always possess at least a two fold degenerate state. Thus a pure electrostatic field acting on the system cannot remove all the degeneracy of the state. This theorem is a consequence of the fact that the Hamiltonians are invariant under time reversal[14] when no magnetic field is present.

It is obvious that for odd electron systems, there are at least two states with the same energy in the crystal field and these are split by the application of a magnetic field, therefore EPR could usually be observed in such systems.

Jahn-Teller Theorem: It states that a symmetrical non-linear molecule or molecular complex having a degenerate electronic energy level does not have stable geometrical configuration of the nuclei and will distort to a nuclear configuration of lower symmetry in such a way that the degeneracy of the electronic state is lifted and only two

fold Kramers' degeneracy, if any, is left. Because of weak interaction between spins and nuclear coordinates, only orbitally degenerate states may be affected.

This theorem holds true for ions in crystal field also where it is assumed that the paramagnetic ion is under the influence of a static crystal field and its symmetry remains unchanged if no charge compensation occurs. The ground or the excited state of the ion may be orbitally degenerate in the crystal field of high symmetry but this degeneracy will not persist as the small displacements of neighbouring atoms lower the symmetry of the crystal field seen by the ion and orbital degeneracy is lifted. Such splittings occur in Cu^{2+} in trigonal field[15-17] and in Fe^{2+} in octahedral field[18-19].

Group theory predicts only the pattern of splittings but it does not tell anything about the order of levels or their relative separations. Quantum mechanical calculations with a reasonably good knowledge of wavefunctions are needed to obtain that information. In the present context, the interest mainly centres around those ions whose crystal field state-that is the lowest electronic state after considering the crystal field interaction is an orbital singlet. In practice, it has been observed that V^{4+}, V^{2+}, Cr^{3+}, Mn^{2+}

and Cu^{2+} are the best candidates to satisfy this requirement. Pryce, and Abragam and Pryce have developed a perturbation approach to analyse the experimental data on EPR of orbital singlets and this has been very widely used to parameterize the EPR data. In this approach, essentially the higher order perturbations in spin-orbit and spin-spin interactions are considered. In what follows, the spin Hamiltonian formalism of Pryce[20], and Abragam and Pryce[21] has been described.

SPIN HAMILTONIAN FORMALISM

In most of the cases, EPR is restricted to the ground states. An effective spin S' is defined such that the total degeneracy of the ground state is (2S' + 1). The Hamiltonian describing such a system is called spin Hamiltonian. Actual and effective spins are same for the orbital singlet states. The effective spin may not be equal to the actual spin of electronic system in other cases. There it is an experimentally determined quantity and it is obtained by equating the number of magnetic dipole transitions to 2S'.

The expressionsobtained in accurate theoretical formulation of the actual interactions of electron spins are quite complicated. A simpler form is obtained by writing the Hamiltonian in terms of actual or effective

spin as has been done by Pryce, and Abragam and Pryce using degenerate perturbation theory. We restrict ourselves to a ground manifold of states with spin S and spin degeneracy (2S+1) but with no orbital degeneracy. The Hamiltonian $\mathcal{H}$ is first solved for $\mathcal{H}_o = \mathcal{H}_c + \mathcal{H}_{cr}$ for the iron group in the ground manifold and other terms are considered as perturbation over this. Thus the Hamiltonian may be expressed as

$$\begin{aligned} \mathcal{H} &= \mathcal{H}_o + \mathcal{H}_1 \\ &= \mathcal{H}_o + \sum_{\alpha} R_\alpha T_\alpha \qquad (2.11) \\ \alpha &= x, y, z \end{aligned}$$

where $\mathcal{H}_1$ may include the remaining terms in the total Hamiltonian, R is an operator operating only on spatial variables and T is the operator that operates only on spin variables. Using perturbation theory, it has been shown[22] that

$$\mathcal{H}_{spin} = \sum_{\alpha} \langle 0| R_\alpha |0\rangle T_\alpha - \sum_{\alpha\alpha'} \sum_{n\neq o} \frac{\langle 0| R_\alpha |n\rangle\langle n| R_{\alpha'} |0\rangle}{E_n - E_o} T_\alpha T_{\alpha'} \qquad (2.12)$$

where E_o and $|0\rangle$ represent unperturbed energy eigenvalue and eigenfunction, E_n is the energy eigenvalue of nth state. $\mathcal{H}_{spin}$ is called the spin Hamiltonian operator. This spin Hamiltonian operator operating on effective spin functions and true Hamiltonian operating on the true eigenfunctions give the same energy eigenvalue.

For the iron group, H_1 may be taken as follows

$$H_1 = \lambda \vec{L}.\vec{S} + \beta\,(\vec{L} + g_e\vec{S}).\,\vec{H}$$

$$\text{or}\quad H_1 = \lambda \sum_\alpha L_\alpha\, S_\alpha + \beta \sum_\alpha L_\alpha\, H_\alpha + g_e\beta \sum_\alpha S_\alpha\, H_\alpha$$

Therefore we obtain

$$\sum_\alpha \langle 0|R_\alpha|0\rangle\, T_\alpha = \lambda \sum_\alpha \langle 0|L_\alpha|0\rangle\, S_\alpha + \beta \sum_\alpha \langle 0|L_\alpha|0\rangle\, H_\alpha + g_e\beta \sum_\alpha \langle 0|S_\alpha|0\rangle\, H_\alpha$$

Since $\langle 0|L_\alpha|0\rangle = 0$,

$$\sum_\alpha \langle 0|R_\alpha|0\rangle\, T_\alpha = g_e\beta \sum_\alpha \langle 0|S_\alpha|0\rangle\, H_\alpha = g_e\beta \vec{S}.\vec{H}.$$

Second order perturbation gives

$$-\sum_{\alpha\alpha'} \sum_{n\neq o} \frac{\langle 0|R_\alpha|n\rangle\langle n|R_{\alpha'}|0\rangle}{E_n - E_o}\, T_\alpha T_{\alpha'} =$$

$$-\sum_{\alpha\alpha'} \sum_{n\neq o} \left[\frac{\lambda^2 \langle 0|L_\alpha|n\rangle\langle n|L_{\alpha'}|0\rangle}{E_n - E_o}\right] S_\alpha S_{\alpha'},$$

$$-\sum_{\alpha\alpha'} \sum_{n\neq o} \left[\frac{\beta^2 \langle 0|L_\alpha|n\rangle\langle n|L_{\alpha'}|0\rangle}{E_n - E_o}\right] H_\alpha H_{\alpha'},$$

$$-\sum_{\alpha\alpha'} \sum_{n\neq o} 2\lambda\beta \left[\frac{\langle 0|L_\alpha|n\rangle\langle n|L_{\alpha'}|0\rangle}{E_n - E_o}\right] H_\alpha S_{\alpha'},$$

Choosing $\Lambda_{\alpha\alpha'} = \sum_{n\neq o} \frac{\langle 0|L_\alpha|n\rangle\langle n|L_{\alpha'}|0\rangle}{E_n - E_o} = \Lambda_{\alpha'\alpha}$, above expression is written as

$$-\sum_{\alpha\alpha'} \sum_{n\neq o} \frac{\langle 0|R_\alpha|n\rangle\langle n|R_{\alpha'}|0\rangle}{E_n - E_o}\, T_\alpha T_{\alpha'} =$$

$$-\sum_{\alpha\alpha'} \lambda^2 \Lambda_{\alpha\alpha'} S_{\alpha\alpha'} - \sum_{\alpha\alpha'} \beta^2 \Lambda_{\alpha\alpha'} H_\alpha H_{\alpha'},$$

$$-\sum_{\alpha\alpha'} 2\lambda\beta\, \Lambda_{\alpha\alpha'} H_\alpha S_{\alpha'},$$

Finally H_{spin} may be expressed as

$$H_{spin} = g_e \beta \vec{S}.\vec{H} - \sum_{\alpha\alpha'} \lambda^2 \Lambda_{\alpha\alpha'} S_\alpha S_{\alpha'} - \sum_{\alpha\alpha'} \beta^2 \Lambda_{\alpha\alpha'} H_\alpha H_{\alpha'} - \sum_{\alpha\alpha'} 2\lambda\beta \Lambda_{\alpha\alpha'} H_\alpha S_{\alpha'}$$

$$= \sum_{\alpha\alpha'} (g_e \delta_{\alpha\alpha'} - 2\lambda\Lambda_{\alpha\alpha'})\beta H_\alpha S_{\alpha'} - \sum_{\alpha\alpha'} \lambda^2 \Lambda_{\alpha\alpha'} S_\alpha S_{\alpha'} - \sum_{\alpha\alpha'} \beta^2 \Lambda_{\alpha\alpha'} H_\alpha H_{\alpha'}$$

$$= \sum_{\alpha\alpha'} g_{\alpha\alpha'} \beta H_\alpha S_{\alpha'} + \sum_{\alpha\alpha'} D_{\alpha\alpha'} S_\alpha S_{\alpha'} - \sum_{\alpha\alpha'} \beta^2 \Lambda_{\alpha\alpha'} H_\alpha H_{\alpha'}$$

If we include spin-spin interaction, hyperfine interaction, quadrupole interaction and nuclear Zeeman terms also in perturbation H_1, then for an orbital singlet ground state, total spin Hamiltonian is

$$H_{spin} = \sum_{\alpha\alpha'} D_{\alpha\alpha'} S_\alpha S_{\alpha'} + \sum_{\alpha\alpha'} g_{\alpha\alpha'} \beta H_\alpha S_{\alpha'} + \sum_{\alpha\alpha'} A_{\alpha\alpha'} S_\alpha I_{\alpha'} + Q_{\alpha\alpha'} I_\alpha I_{\alpha'} - \beta_n g_n \vec{H}.\vec{I}$$

where constant energy terms have been left out. The quantities $D_{\alpha\alpha'}$, $g_{\alpha\alpha'}$, $A_{\alpha\alpha'}$ and $Q_{\alpha\alpha'}$ are tensors of second rank. The above equation is usually expressed in the form

$$H_{spin} = \vec{S}.\vec{\vec{D}}.\vec{S} + \beta \vec{H}.\vec{\vec{g}}.\vec{S}. + \vec{S}.\vec{\vec{A}}.\vec{I} + \vec{I}.\vec{\vec{Q}}.\vec{I}. - \beta_n \vec{H}.\vec{\vec{g}}_n.\vec{I}$$

There are nine components for each tensor. It is possible to choose a system of orthogonal axes by rotation of coordinates such that these tensors are completely

diagonal. This system is called principal axis system. The choice of the principal axis system depends on crystal field symmetry. In the principal axis system ($\alpha = \alpha'$), only single subscripts are needed in place of double subscripts. Thus $g_{\alpha\alpha'}$ is replaced by g_α, $D_{\alpha\alpha'}$ is replaced by D_α, and so on. g_α, D_α, A_α etc. are called spin Hamiltonian constants or parameters and their magnitudes are evaluated in EPR experiments. In general, the principal axis systems of g, D, A etc. are not coincident, and in triclinic symmetry each of them has its own principal axis system and there is no simple relationship among them. In orthorhombic symmetry, three orthogonal directions are determined uniquely and these are principal axis of all the tensors. Once the crystal field symmetry is known, the principal axes are conveniently chosen. The forms of spin Hamiltonian for different symmetries are well known and are given in a number of texts[23]. The spin Hamiltonian for orthorhombic symmetry in the principal axis system is

$$H_{spin}=\beta[g_zH_zS_z+g_xH_xS_x+g_yH_yS_y]+A_zS_zI_z+A_xS_xI_x+A_yS_yI_y$$
$$+D[S_z^2-(1/3)S(S+1)]+E[S_x^2-S_y^2]+Q'[I_z^2-(1/3)I(I+1)]$$
$$+Q''[I_x^2-I_y^2]$$
$$\text{where } D=D_z-(1/2)[D_x+D_y],\quad E=(1/2)[D_x-D_y]$$
$$Q'=Q_z-(1/2)[Q_x+Q_y],\ Q''=(1/2)[Q_x-Q_y] \qquad (2.15)$$

THE SPIN-HAMILTONIAN PARAMETERS

g Tensor: It has been shown in the derivation of Eq. 2.13 that

$$g_{\alpha\alpha'}=g_e\delta_{\alpha\alpha'}-2\lambda \sum_{n\neq o} \frac{\langle 0|L_\alpha|n\rangle\langle n|L_{\alpha'}|0\rangle}{E_n - E_o}$$

In the principal axis system, it can be expressed as

$$g_\alpha = g_e - C_\alpha \left(\frac{\lambda}{\Delta E}\right) \quad , \alpha = x, y, z$$

$$\text{or} \quad g_\alpha = 2.0023 - C_\alpha\left(\frac{\lambda}{\Delta E}\right) \qquad (2.16)$$

where ΔE is the energy separation between the singlet and higher orbital states, λ is the spin-orbit coupling constant and C_α is a constant in the range of 1 to 10. Thus, besides $g_e = 2.0023$, there is a contribution of the admixed higher lying orbital states due to spin-orbit interaction. The g shift $(g-g_e)$ is negative for a paramagnetic ion with unfilled shell less than half full since λ is positive. The shift may be positive for the shell more than half full. Other terms in the spin-Hamiltonian may also contribute to the g factor but spin-orbit interaction is the most important. Now it is clear how the g factor in solids differs from Lande's splitting factor given by Eq. (1.5). In octahedral field, g factor is isotropic with $g_x = g_y = g_z$; in tetragonal, trigonal or hexagonal field, g is anisotropic with $g_z \neq g_x = g_y$ and in orthorhombic field with $g_x \neq g_y \neq g_z$.

In the spin Hamiltonian, the sign of g value is arbitrary and could be reversed by changing the sign of effective spin S. The sign tells the sense of precession of magnetic moment in the external magnetic field. A negative g means that the moment precesses in the direction opposite to that of a free electron spin. The sign of g is mostly positive.

Fine Structure Constants D and E: D is a measure of the splitting of the ground state spin multiplet in an axial crystalline field in the absence of external magnetic field and hyperfine interaction, the splitting being caused by spin-orbit coupling and spin-spin interaction in the second order. Any rhombic component of the field is represented by $E\,(S_x^2 - S_y^2)$.

There exists a relation between g factor and D. The principal values of D, without considering spin-spin interaction are given by

$$D_{\alpha\alpha'} = D_\alpha = -\lambda^2 \sum_{n \neq o} \frac{|\langle o|L\alpha|n\rangle|^2}{E_n - E_o} \qquad (2.17)$$

$$D = -\left(\frac{C_\alpha}{2}\right) \frac{\lambda^2}{\Delta E}$$

the right hand side of which is related to g.

Hyperfine constant A: Hyperfine structure is present because of interactions with nuclear spin. 'A' gives the

separation between the hyperfine levels. It depends on hyperfine interaction, Fermi contact interaction and to some extent on spin-orbit interaction. For orthorhombic symmetry, three principal values are A_x, A_y and A_z and for axial symmetry, $A_z \neq A_x = A_y$.

Q' and Q'': These express the quadrupole interaction and are axial and rhombic parts respectively. The magnitudes of these are very small and are determined from hyperfine forbidden transitions.

Spin Hamiltonian parameters, described above, are experimentally determined from the EPR spectrum. The EPR spectrum is very much dependent on the orientation of principal axes relative to external magnetic field. For determination of spin Hamiltonian parameters the crystal is oriented with one of the principal axis parallel to the magnetic field and the variation of the spectrum in the desired plane is studied. Similar study is made along the other two principal axes also.

SELECTION RULES AND INTENSITY OF MAGNETIC RESONANCE TRANSITIONS

In EPR studies of the paramagnetic ions in solids, a constant magnetic field H removes the degeneracy of the Kramers' doublets and an oscillating magnetic field $H_1 \cos(wt)$

applied perpendicular to it induces the magnetic dipole transition between the Zeeman levels.

The terms involving the magnetic field H in the spin Hamiltonian are $\beta \vec{H}.\ \vec{\vec{g}}.\ \vec{S}$ and $\beta_n \vec{H}.\ \vec{\vec{g}}_n.\ \vec{I}$. Substituting $H_1 \cos(wt)$ for H in these terms, time-dependent perturbation is obtained in the form

$$\mathcal{H}_1' = \beta \vec{H}_1.\ \vec{\vec{g}}.\ \vec{S} - g_n \beta_n \vec{H}_1.\ \vec{I}$$
$$\mathcal{H}_1 = \mathcal{H}_1' \cos(wt) \qquad (2.18)$$

This perturbation results in transition from the state represented by $|i\rangle$ to the state $|j\rangle$ and the intensity of the transition is given by

$$I_{ij} = |\langle j|\mathcal{H}_1'|i\rangle|^2$$
$$= \beta^2 |\langle j|\vec{H}_1.\ \vec{\vec{g}}.\ \vec{S}|i\rangle|^2 + g_n^2 \beta_n^2 |\langle j|\vec{H}_1.\vec{I}|i\rangle|^2$$
$$-2g_n\beta_n\beta\ \mathrm{Re}[\langle j|\vec{H}_1.\vec{\vec{g}}.\vec{S}|i\rangle \langle j|\vec{H}_1.\vec{I}|i\rangle^*]$$

The first term produces the EPR transitions and the second induces NMR transitions. The third term is negligible.

The direction along which the spin is quantized may be chosen parallel to $\vec{H}.\vec{\vec{g}}$ and eigenfunctions can be written in terms of this coordinate system. Then $S_+=(S_x+iS_y)$ and $S_-=(S_x-iS_y)$ always exist in $\beta \vec{H}_1.\vec{\vec{g}}.\ \vec{S}$ except for H_1 parallel to H and these therefore result in electronic transitions for which $\Delta M = \pm 1$, M= S, S-1, ...-S. Thus if $\beta \vec{H}.\vec{\vec{g}}.\vec{S}$ is the dominant term in the spin Hamiltonian and the weak, low frequency NMR transitions caused by the second term are ignored, then the allowed transitions are given by the selection rule,

$\Delta M = \pm 1$, $\Delta n = 0$ $n = I, I-1, \ldots\ldots -I$.

The intensity of allowed transitions[24] is given by

$$I_{ij}=I_{M,M\pm1}= (1/4)\left(\frac{g_t}{g^2}\right)^4 \beta^2 I_1[(S(S+1)-M(M\pm1)] \qquad (2.20)$$

where g_t depends on all other components of g in a complicated way.

Sometimes, weaker transitions not allowed by $\Delta M=\pm1$, $\Delta n=0$ may also occur at low fields when the magnetic field H is off the principal axis. These are called forbidden transitions. The transitions corresponding to $\Delta M=\pm2$, ±3 etc. are called fine forbidden transitions and they occur due to a mixing of $|M\pm1, n\rangle$ and $|M\pm2, n\rangle$ because of the off-diagonal elements produced by D when H is not parallel to the axis of symmetry. If E is also present, fine forbidden transition may occur even for H parallel to the symmetry axis.

Under certain conditions, the nuclear selection rule, $\Delta n = 0$, may also break and $\Delta n = \pm 1$ may become allowed. The transitions thus caused are called hyperfine forbidden transitions and are produced by a mixing of the wavefunctions $|M, n\rangle$ with $|M, n \pm1\rangle$ in second order due to products of the type (DS_+S_z) $(AS_- I_+)$ for axial field[25] when magnetic field H is off the symmetry axis.

RELAXATION PROCESSES

The ground state of the paramagnetic ions in the crystal field forms a multilevel system when an external magnetic field H is applied on it. In EPR transitions, the electrons are transferred to the higher levels from the lower one of this multilevel system and they return to lower levels by relaxation processes so that the absorption of the microwave radiation is continued. There are two types of relaxation processes, the spin-lattice relaxation and spin-spin relaxation. The processes in which the energy flows from the spin system to the lattice are called spin-lattice relaxation processes and those in which the spins exchange energy among themselves are called spin-spin relaxation processes.

Spin-Lattice Relaxation: The spin system is in thermal equilibrium in the absence of resonance absorption or external fields. By absorption of radiation of frequency ν_o at resonance, the thermal equilibrium is disturbed. The spins are now said to be heated. The heated spins return to thermal equilibrium by an exponential process with time constant T_1 which is called longitudinal relaxation time or spin-lattice relaxation time and this process is called

spin-lattice relaxation process. T_1 is a measure of the energy transfer from paramagnetic ions to surroundings.

In the spin-lattice interaction, the crystal field surrounding the paramagnetic ion gets phonon modulated and the relaxation proceeds by three main processes discussed below.

a) Direct Process: This is of importance at low temperatures only and it proceeds by a phonon emission. The phonon will have an energy equal to the difference in the energy of the two states of the paramagnet between which the electron transition occurs. The heated spin-system emits phonons of energy $h\gamma_o$ and these get absorbed directly by the lattice. The temperature dependence of T_1 in this process is expressed by

$\frac{1}{T_1} \alpha T$, where T is the absolute temperature.

b) Raman Process: If the temperatures are higher, there will be phonons with energies greater than the resonance energy and then the relaxation proceeds by multiphonon processes. Of these, the Raman process involving two phonons is most common. In this process, a phonon of energy $h\nu$ gets scattered inelastically by the spin system resulting in creation of another phonon of energy $h\nu_o + h\nu$ where $h\nu_o$ is the energy difference between the two states of a

paramagnetic ion and the electron drops to the lower state. The relaxation time T_1 depends on the temperature in the following manner

$$\frac{1}{T_1} \alpha T^7 \quad \text{for non-Kramers' doublets}$$

$$\alpha T^9 \quad \text{for Kramers' doublets}$$

For paramagnetic ions with several low lying levels, it has been found theoretically[26] as well as experimentally[27-29] that

$$\frac{1}{T_1} \alpha T^5$$

c) Orbach Process: In this process, two successive transitions occur via an intermediate state. Let an electron be transferred from a level i to level f in the ground manifold of states by absorption of $h\nu_o$. Then by stimulated transition, it goes to a level n higher in energy by an amount Δ and not belonging to the ground manifold. A direct spontaneous transition of the electron from level n to i results in a spontaneous emission of a phonon of energy $\Delta + h\nu_o$. The relaxation rate is given by

$$\frac{1}{T_1} \alpha e^{-\Delta/kT}$$

where k is Boltzmann constant. Low lying excited states like m are found in rare-earth impurities doped in the crystals.

Spin-Spin Relaxation: This mechanism involves dipoles close enough so that they experience various local fields resulting from the dipolar fields of their neighbours. Identical spins precess at the same frequency in external magnetic field and the oscillatory field created by precessing component of one magnetic dipole produces magnetic resonance transitions in another dipole and their spin orientations change . Thus the quanta are exchanged among neighbouring ions by mutual spin flip and spins are in thermal equilibrium amongst themselves. If this equilibrium is disturbed, it is re-established exponentially with time constant T_2 which is called spin-spin relaxation time.

Exchange Interaction: The identical spins interact electrostatically also through a short range interaction which is called exchange interaction. This results in a change in width of absorption lines in EPR spectrum different from the magnetic dipole -dipole interaction.

ZERO-FIELD SPLITTING IN Mn^{2+}

The paramagnetism of this ion arises from unpaired $3d^5$ electrons. The ground state is orbital singlet $^6S_{5/2}$

(L=0). The resultant orbital angular momentum being zero, one does not expect the splitting of the ground state under crystalline field which acts only on orbital motion, but small splittings do take place and these have been explained to be due to various mechanisms[30-31]. In hydrated salts, this ion is surrounded by six water molecules forming an octahedron which gives rise to an octahedral crystalline field of intermediate strength. If the octahedron is distorted, tetragonal or trigonal symmetry may result. In the octahedral field, the ground state $^6S_{5/2}$ is designated as $^6A_1$. The splitting of $^6A_1$ is produced by the effect of spin-orbit coupling and any other noncubic part of the crystal field due a distortion of water octahedron. When there is only spin degeneracy, the splittings are of the order of 1 cm^{-1} and finally, there are left only three Kramer's doublets.

In the presence of a steady magnetic field, three Kramers' doublets further split into six levels. When the nuclear spin of Mn^{55} (I=5/2) couples with the electronic spin, each level splits further into six hyperfine levels. Electronic transitions between these hyperfine levels are given by $\Delta M=\pm 1$, $\Delta m=0$ and these are shown in Fig. 2.1.

Splitting Mechanisms: $^6S_{5/2}$ ground state of Mn^{2+} remains degenerate ($^6A_1$) in the presence of a cubic field alone. The effect of perturbing potential due to spin-orbit coupling

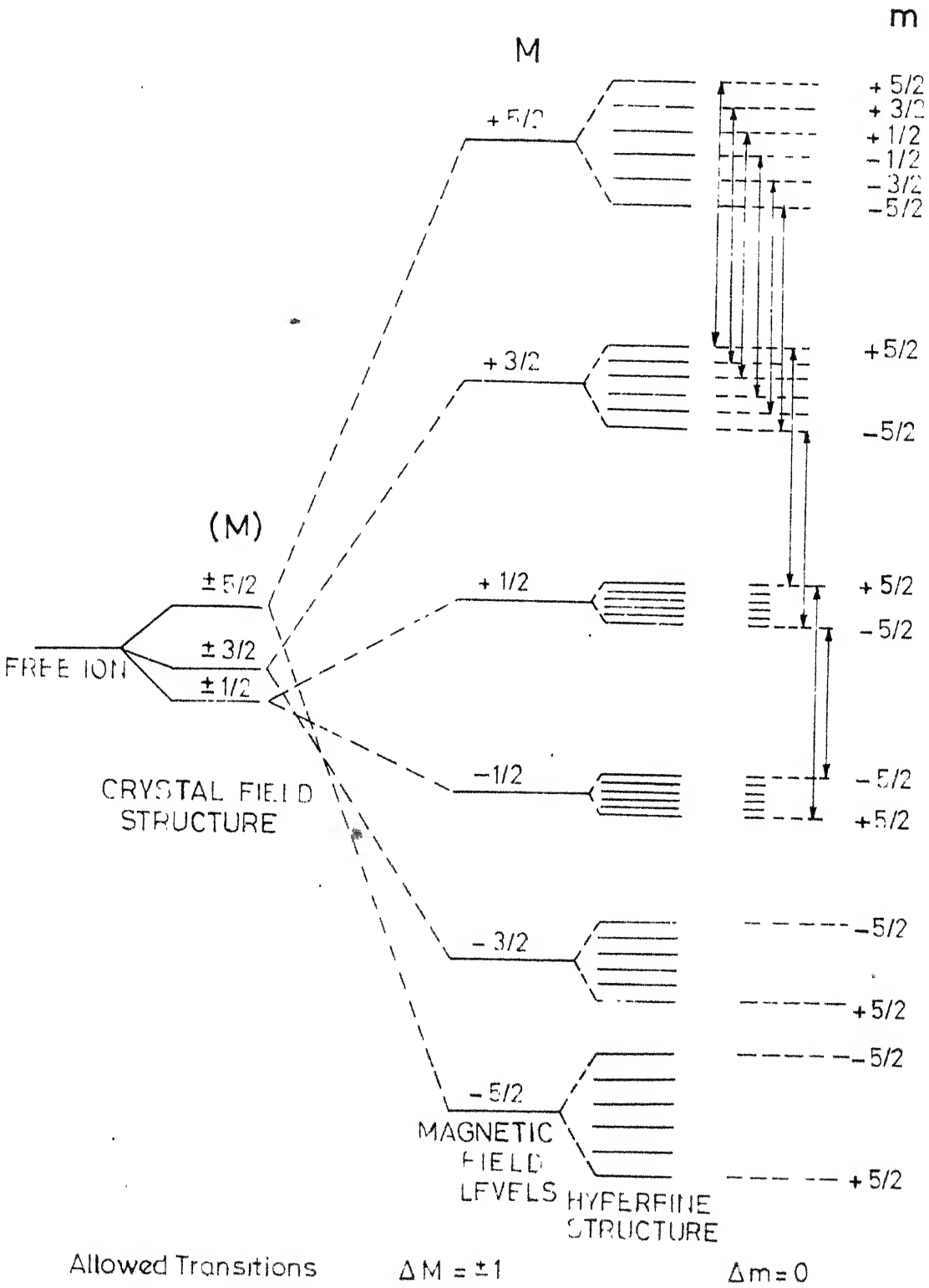

Fig.2.1 Energy level splittings of the ground state of Mn^{2+} ($6S_{5/2}$)

and non-cubic components of the crystal field has to be considered for the splitting of this state. Different mechanisms have been suggested for the splitting and these may be classified into three groups:

a) The mechanisms linear in spin-orbit interaction such as Relativistic mechanism[32].

b) The mechanisms quadratic in spin-orbit interaction such as Blume-Orbach mechanism[33], Watanabe mechanism[34-36] and Lowther-Wyk mechanism[30].

c) The mechanisms cubic in spin-orbit interaction such as Hutchinson, Judd and Pope mechanism[37] (H.J.P. mechanism).

The spin-orbit coupling operator produces a weak admixture of the excited $^4T_1$ cubic states into $^6A_1$ ground state and a perturbed eigenfunction for $^6A_1$ state is obtained. This is used to calculate perturbation energy. In a pure cubic crystal field, the state $^6A_1$ splits into a doubly degenerate state and a quadruply degenerate state which further splits by an axial component of the field.

For the splitting of $^6A_1$ of Mn^{2+} in the crystals having an axial or orthorhombic distortions from octahedral symmetry, relativistic mechanism has been found dominant[38-40] while Blume-Orbach (B-O) mechanism is second in order of magnitude. H.J.P. and Watanabe mechanisms are equal in order of magnitude, but both are smaller than relativistic or B-O mechanism . However, none of the mechanisms has been found satisfactory so far and further theoretical calculations are necessary to explain the splitting of the ground state in Mn^{2+}.

STRUCTURAL PHASE TRANSITION IN CRYSTALS

Different crystal modifications of a substance have different internal symmetry[41]. There exists only one symmetry in one phase of the crystal. The transition between two phases of different symmetry may occur abruptly by means of a phase transition in which a sudden rearrangement of the crystal lattice takes place. Such a transition is called the phase transition of first order. There are no symmetry requirements for this to occur, only the free energies of the two phases should be same at the transition temperature.

It is also possible that the arrangement of atoms in a crystal may change gradually and a small displacement of the atoms from their original symmetry positions may change the symmetry of the lattice. The transition resulting from such a continuous modification of the crystal lattice from one phase to the other is a phase transition of second order. At the transition point, the symmetry of the crystal contains the symmetry elements of boththe phases. The symmetry of one phase is higher than that of the other and there exists only one phase at any temperature.

The change in symmetry in a phase transition may also result from a change in ordering of the crystal. The

change from an ordered to disordered crystal is a first order phase transition if on increasing the temperature, the degree of ordering becomes zero discontinuously. But if the degree of ordering becomes zero continuously, the phase transition is of the second order.

In Landau's theory of phase transition[41-42], a function $\rho(\vec{r})$ such as electron density, changes with temperature and the free energy F of the system depends on $\rho(\vec{r})$. The conditions for the first and second order phase transitions and for the change in symmetry in the second order have been derived from the dependence of F on $\rho(\vec{r})$.

Landau's theory has been extended to 'soft mode' theory[43.b,44-47] in which a second order displacive structural phase transition is shown to be associated with a low frequency unstable optic mode. This mode becomes soft (zero frequency) as the transition temperature approaches. A soft mode is a dynamical aspect signifying the structural instability. (A first order transition involves only one mode whose frequency falls considerably but not to zero. Sometimes, several fairly low frequency modes may also be involved in first order phase transitions). It has been found that the second order phase transition

occurs at a temperature $T = T_c$ with order parameter ξ(a displacive parameter, depending on displacement vectors or angle of rotation or ordering) given by

$$\xi \alpha (T_c - T)^{\eta} \qquad \eta = 1/2, \text{ for } T < T_c$$

where T_c is the transition temperature.

In addition, the dynamical mechanism of structural phase transition has been considered in microscopic theories with mean field approximation[48-52] and the same result is obtained for the order parameter ξ. The temperature behaviour of ξ with $\eta = 1/2$ is called Landau behaviour.

In the critical region $T \simeq T_c$, it has been found experimentally[53] that the critical behaviour of ξ is expressed by

$$\xi \alpha (T_c - T)^{\eta}, \quad \eta = 1/3$$

This is in contrast to the meanfield theory value for η as 1/2. Thus this theory fails in the critical region. In a recent paper, the modifications made by Beck[54] in dynamical meanfield theory are inadequate and further improvements in this theoretical approach are needed to explain the critical behaviour. However, there exist

other theoretical approaches in which the critical behaviour has been explained (X Y model, $\eta = 0.33$; Ising model, $\eta = 0.312$).

In addition to the value of the exponent η, the observation of a central phonon peak near T_c in several experiments[55-58] is also a problem of critical region[54-59].

A considerable number of experimental studies using EPR, first order Raman scattering, elastic and inelastic neutron scattering, ultrasound, x-rays etc.[60-64] have been made on structural phase transitions in single crystals such as $SrTiO_3$, $LaAlO_3$ etc. It has been found that though for explaining the experimental results in critical region further developments in meanfield theory are required, yet the soft mode concept[43.a] has proved to be very useful in describing the gross features of the experimental results correctly and it is not restricted to ferroelectrics only.

The dynamics of some particular type of coordinates of crystal lattice such as the rotations of O_6 octahedron in perovskites and of H_4 tetrahedron in CH_4 and NH_4X, displacement of Ti ions relative to the O_6 octahedron in $BaTiO_3$ and proton motions in the hydrogen-bonded

ferro-electrics, is associated with the phase transitions occuring in the crystal and order parameter ξ is related to these coordinates. The experimental measurements can be related to ξ .

Structural Phase Transition Study using EPR: Methodological aspects of the study of structural phase transition using EPR have been discussed by Müller[65]. The choice of the ion for such studies, the spin-Hamiltonian formalism to describe the spectra, the importance of fourth order terms for local symmetry, confirmation of the space group of the crystal, criteria for the determination of the site of impurity ion, the senstivity, precision and limitations of the method have been described by him.

The EPR spectrum reflects the point symmetry of the crystal field to which an impurity ion is exposed. The paramagnetic impurities whose free ion ground states are $^2S_{1/2}$, are insensitive to details of their environment partly because S = 1/2 and partly because there is very little orbital contribution to the magnetic moment . On the other hand, the free ions with ground state $^6S_{5/2}$ such as half filled d shell ions Cr^+, Fe^{3+}, Mn^{2+} ($3d^5$, S= 5/2) and and those with ground state $^8S_{7/2}$ such as Eu^{2+}, Gd^{3+}, Tb^{4+}

(half filled f shell S = 7/2, $4f^7$) are quite sensitive to their crystalline environment because S > 1/2, resulting in fine structure. The use of such ions is preferred for the following reasons

i) If the ground state of the impurity ion is orbitally degenerate (L ≠ 0), it would introduce additional distortions into the lattice as a result of Jahn - Teller effect but in the orbital singlet (L = 0) ground state, no such distortions would occur. Thus the EPR spectra of $3d^5$ ions would reflect the true point symmetry.

ii) Since S > 3/2 for these ions, the splittings obtained make EPR superior to other methods for determining symmetry.

iii) These ions have first excited state away from the ground state and nearly vanishing orbital angular momentum in the ground state. Therefore, spin-lattice relaxation times are longer at high temperatures. At lower temperatures also, these are reasonable. Thus studies can be made for a large range of temperatures upto 1000K or above.

The EPR method has an advantage over x-ray and neutron-diffraction methods for phase transition study because in these methods, on lowering symmetry only special

reflection spots split or become allowed, while in EPR all lines shift in first order for half integral effective spin ground states.

To use paramagnetic ions for the phase transition study and site-symmetry determination, one has to look for an ion that matches the valency and size of the site of interest in the crystal. Moreover, the concentration of the ion in the crystal has to be kept low so that EPR lines are sharp. For large concentrations, the lines become broad due to dipolar interaction and accurate line positions cannot be determined. Lines should also remain sharp over a wide range of temperature. The EPR method has been very promising for investigation of phase transitions in perovskites like $SrTiO_3$, $LaAlO_3$ and many other ferroelectric crystals.

Structural Phase Transition Parameters: The parameters measured in EPR study are, the angle of rotation ϕ of the symmetry axis of the spectrum and the axial field splitting parameter D. Fourth order cubic field parameter 'a' is necessary for site-symmetry determination. The temperature variations of ϕ and D are given by Müller[66] as

$$\phi \alpha (T_c - T)^{1/2}$$

$$D \alpha (T_c - T)$$

REFERENCES

1. Pryce M.H.L., Phys. Rev. 80, 1107 (1950).
2. Bleaney B. (First article) and Geschwind S. (Sixth article), Hyperfine Interactions (Eds. Freeman A.J. and Frankel R.B., Academic Press, N.Y.) (1967).
3. Fermi E., Z. Physik, 60, 320 (1930).
4. Bleaney B., Hyperfine Interactions, page 14 (1967).
5. Van Vleck J.H., Phys. Rev. 41, 208 (1932).
6. Penney W.G. and Schlapp R., Phys. Rev. 41, 194 (1932).
7. Schlapp R. and Penney W.G., Phys. Rev. 42, 666 (1932).
8. Bleaney B. and Stevens K.W.H., Rept. Progr. Phys. 16 108 (1953).
9. Stevens K.W.H., Proc. Phys. Soc. A65, 209 (1952).
10. Elliott R.J. and Stevens K.W.H., Proc. Roy Soc. A218, 553 (1953).
11. Judd B.R., Proc. Roy. Soc. A227, 552 (1955).
12. Kramers H.A., Proc. Amsterdam Acad. Sci. 33, 959 (1930).
13. Jahn H.A. and Teller E., Proc. Roy. Soc. A161, 220 (1937).
14. Wigner E., Nachr. Akad. Wiss. Gottingen Math-Physik Kl. IIa, 546 (1932).
15. Bleaney B. and Bowers K.D., Proc. Phys. Soc. A65, 667 (1952).
16. Bijl D. and Rose-Innes A.C., ibid. A66, 954 (1953).
17. Bleaney B., Bowers K.D. and Trenam R.S., Proc. Roy. Soc. A228, 157 (1955).
18. Low W., Ann. New York Acad. Sci. 72, 69 (1958).

19. Low W., Phys. Rev. 101, 1827 (1956).

20. Pryce M.H.L., Proc. Phys. Soc. (London) A63, 25 (1950).

21. Abragam A. and Pryce M.H.L., Proc. Roy. Soc. (London) A205, 135 (1951).

22. Pake G.E. and Estle T.L., The Physical Principles of Electron Paramagnetic Resonance, W.A. Benjamin, Inc. Chapt. 4 (1973).

23. See General References given in Chapter I.

24. Pake, G.E. and Estle T.L., The Physical Principles of Electron Paramagnetic Resonance, W.A. Benjamin, Inc. Chapt. 5 (1973).

25. Bleaney B. and Ingram D.J.E., Proc. Roy. Soc. (London), A205, 336 (1951).

26. Orbach R., and Blume M., Phys. Rev. Letters 8, 478(1962).

27. Bierig R.W., Weber M.J. and Warshaw S.I., Phys. Rev. 134, A1504 (1964).

28. Chao-Yuan Huang, Phys. Rev. 139, A241 (1965).

29. Horak J.B. and Nolle A.W., Phys. Rev. 153, 372 (1967).

30. Lowther J.E.,Van Wyk J.A., J. Mag. Res. 13, 328 (1974).

31. Newman D.J. and Urban W., Adv. Phys. 24, 793 (1975).

32. Van Heuvelen A., J. Chem. Phys. 46, 4903 (1967).

33. Blume M. and Orbach R., Phys. Rev. 127, 1587 (1962).

34. Sharma R.R., Das T.P. and Orbach R., Phys. Rev. 149, 257 (1966).

35. Sharma R.R., Das T.P. and Orbach R., ibid.155, 338 (1966).

36. Sharma R.R., Das T.P. and Orbach R., ibid. 177, 378 (1968).

37. Hutchinson C.A., Judd B.R., Pope D.F., Proc. Phys. Soc. B.70, 514 (1957).

38. Hagston W.E and Lowther J.E., J. Phys. Chem. Solids, 34, 1773 (1973).

39. Schlottmann P. and Passeggi M.C.G., Phys. Stat. Sol. B52, K. 107 (1972).

40. Chatterjee R. and Van Ormondt D., Phys. Letters, A33, 147 (1970).

41. Landau L.D. and Lifshitz E.M., Statistical Physics, Pergamon Press, Chap. 13 and 14 (1970).

42. Landau L.D., Physik Z. Sowjetunion II, 26 (1937).

43. (a) Cochran W., Adv. Phys. 9, 387 (1960).
ibid 10, 401 (1961).

(b) Cochran W., Structural Phase Transition and Softmodes, (Ed., E.J. Samuelsen, E. Anderson and J. Feder), Universitetsforlaget, Oslo p.1 (1971).

44. Thomas H. and Müller K.A., Phys. Rev. Lett. 21, 1256 (1968).

45. Slouczewski J.C. and Thomas H., Phys. Rev. B1, 3599 (1970).

46. Slouczewski J.C., Phys. Rev. B2, 4646 (1970).

47. Thomas H., Structural Phase Transition and Softmodes p. 15 (1971).

48. Pytte E. and Feder J., Phys. Rev. 187, 1077 (1969).

49. Pytte E., Phys. Rev. B1, 924 (1970).

50. Feder J. and Pytte E., Phys. Rev. B1, 4803 (1970).

51. Pytte E., Structural Phase Transition and Softmode, p. 133 (1971).

52. Feder J., ibid., p. 171 (1971).

53. Müller K.A. and Berlinger W., Phys. Rev. Lett. 26, 13 (1971).

54. Beck H., J. Phys. C : Solid State Physics, 9, 33 (1976).

55. Riste T., Samuelsen E.J., Osnes K. and Feder J. Solid State Comm. 9, 1455 (1971).

56. Shapiro S.M., Axe J.D., Shirane G. and Riste T., Phys. Rev. B6, 4332 (1972).

57. Müller K.A., Berlinger W., West C. and Heller P., Phys. Rev. Lett. 32, 160 (1974).

58. Shirane G., Axe J.D., Phys. Rev. Lett. 27, 1803 (1971).

59. Szabo N., J. Phys. C : Solid State Phys. 9, 259 (1976).

60. Müller K.A. Berlinger W. and Waldner F., Phys. Rev. Lett. 21, 814 (1968).

61. Fleury P.A., Scott J.F. and Worlock J.M., Phys. Rev. Lett. 21, 16 (1968).

62. Shirane G. and Yamada Y., Phys. Rev. 177, 858 (1969).

63. Cowley R.A., Buyers W.J.L. and Dolling G., Solid State Comm. 7, 181 (1969).

64. Survey papers in Structural Phase Transition and Softmodes (1971).

65. Müller K.A., Structural Phase Transition and Softmodes p. 61 (1971).

66. Müller K.A., ibid. p. 73 (1971).

CHAPTER III

ELECTRON PARAMAGNETIC RESONANCE STUDY OF Mn^{2+} DOPED MAGNESIUM PERCHLORATE HEXAHYDRATE

Abstract

A description of crystal structure and crystal growing method for $Mg(ClO_4)_2.6H_2O$ is given. The EPR apparatus and the accessories used are mentioned. Electron paramagnetic resonance of Mn^{2+} doped $Mg(ClO_4)_2.6H_2O$ crystal has been studied from room temperature to liquid nitrogen temperature. Mn^{2+} substitutes for Mg^{2+} at sites of trigonal symmetry and exhibits a 30 line hyperfine spectrum at room temperature for the axis of trigonal symmetry (c-axis) parallel to the static magnetic field. The spin Hamiltonian necessary to analyse this spectrum is described and the equations used for calculations are given. The angular variation of the spectrum shows that there exist three slightly inequivalent sites for Mn^{2+} in $Mg(ClO_4)_2.6H_2O$ lattice. Hyperfine forbidden transitions ($\Delta M=\pm1$, $\Delta m=\pm1$) are observed when the magnetic field is off the c-axis. The observed linewidths show normal variation with impurity concentration.

Three structural phase transitions have been observed at temperatures 272 ± 1K, 203 ± 1K, and 103 ± 1K respectively, the

last of which could be identified with that detected earlier through Mössbauer study. The transitions occurring at 272±1K and 203±10K appear to be of the second order. The order parameter (which is the angle of rotation of the principal z-axis) and the D parameter have been interpreted in terms of the theories of second order phase transition. The transition occurring at 103K is of the first order.

Introduction:

Electron paramagnetic resonance studies of divalent manganese have been made in a large number of hosts,[1-4] in the crystal fields of different symmetries and with surrounding ligands of different types. When the surrounding ligands are six water molecules, and they form a distorted or undistored octahedron around the paramagnetic ion then the crystal field at the site of the ion is of intermediate strength[1]. Divalent manganese in such a surrounding has been studied by EPR in Tutton's salts[5-9], double nitrates[10-11], fluosilicates[7-8,12], sulphates[8,13-14], bromates[1] etc. Typical interionic distances (paramagnetic ion to ligand ion) are of the order of 2 Å when the ligand is O^{2-} ion (of H_2O) in the hydrated salts.

Metal perchlorate hexahydrates, $M(ClO_4)_2.6H_2O$(M=Mg, Zn, Cd, Hg, Fe, Co, Ni, Mn) form a serie of isostructural compounds. Manganese perchlorate hexahydrate is also a member of this series. It has been reported[15] that Mn^{2+} substitutes for Zn^{2+} in $Zn(ClO_4)_2.6H_2O$ crystal and is surrounded by a trigonally distorted water octahedron. Mn^{2+} may also substitute similarly in other perchlorates of the series. No EPR studies seem to have been made for this

series of crystals except for Mn^{2+} doped $Zn(ClO_4)_2.6H_2O$. The present chapter deals with the EPR study of Mn^{2} doped magnesium perchlorate hexahydrate, $Mg(ClO_4)_2.6H_2O$. This to our knowledge, is the first EPR report on this system.

Crystal Structure:

The crystal structure of $Mg(ClO_4)_2.6H_2O$ (henceforth to be referred to as MgPH) and its isomorphs was determined by West[16] in 1935 from x-ray studies of needle shaped twinned hexagonal crystals and its structure is taken as standard for other isomorphs. He used Laue, oscillation and powder methods with Mo-radiation to work out the structure which has been found to be orthorhombic pseudo-hexagonal with a bimolecular unit cell in the space group C_{2v}^{7} (Pmn), the needle axis being crystallographic c-axis. This structure is the result of combination of a body centred orthorhombic metal lattice (M-lattice) and a base centred hexagonal water perchlorate lattice (P-lattice). The M-lattice has to get twinned along a three fold vertical twinning axis so as to get the hexagonal structure. The term hermaphrodite has been used by West for this type of twinning. Such a twinning may be called repeated twinning, mimetic twinning or growth twinning. It has been discussed

by Battey in the structure of aragonite[17]. The twinning is shown in Fig. 3.1. Because of three fold twinning, in the resulting hexagonal crystal, lattice parameters a and b may be chosen in three equivalent ways. The structure as a whole is thus not twinned in the usual sense. The dimensions of the orthorhombic unit cell for MgPH are

$$a = 7.76\text{Å} \; ; \; b = 13.46\text{Å}; \; c = 5.26\text{Å} \text{ and } b = a\sqrt{3}$$

The projection of the unit cell chosen by West, in a b plane is shown in Fig. 3.2. The general positions for the atoms and molecules in the space group C_{2v}^{7} given by Wyckoff[18] are

(2a) o u v; 1/2, $\bar{u}$, v + 1/2

(4b) x y z; $\bar{x}$ y z; 1/2 - x,$\bar{y}$,z +1/2; x+1/2, $\bar{y}$,z+1/2

The positions of the atoms and molecules are given in Table 3.1 and the unit cell described by West is obtained by changing $x \rightarrow x + 1/4$ and $y \rightarrow y + 1$ in this table.

The six nearest neighbours of the magnesium ions are water molecules and the Mg - $(H_2O)_6$ octahedra have Mg-H_2O distances as 2.14 Å. The ClO_4 tetrahedra are further away from the Mg ions and have Cl-O distance as 1.50 Å. All the octahedron edges are unshared and are nearly equal. Each water oxygen is bonded to Mg ion. Water molecules forming

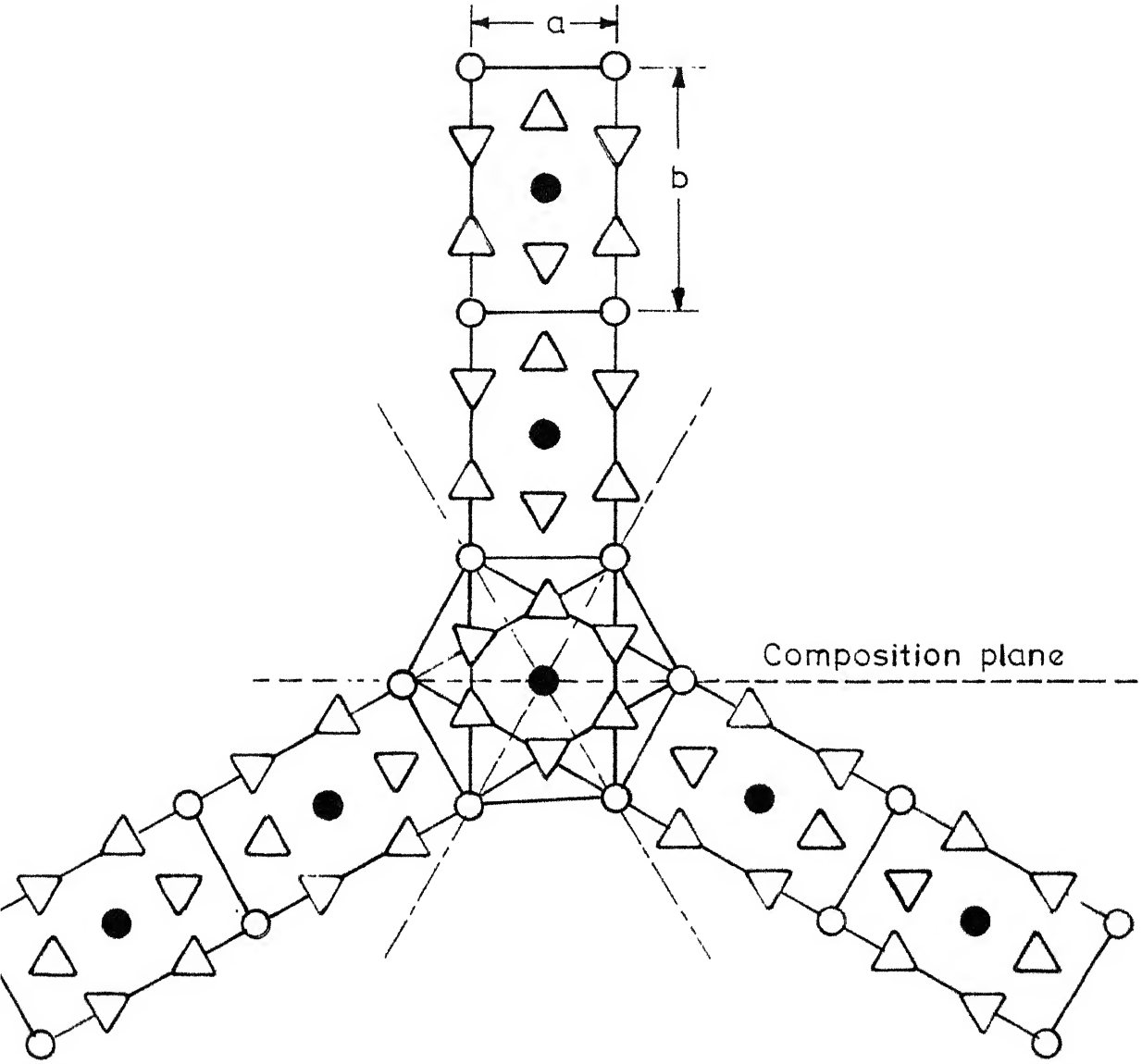

Fig. 3.1 Three fold vertical twinning of Mg lattice. Two types of circles are Mg atoms in two different layers c/2 apart. Triangles in two different orientations are ClO_4 tetrahedrons at two different heights.

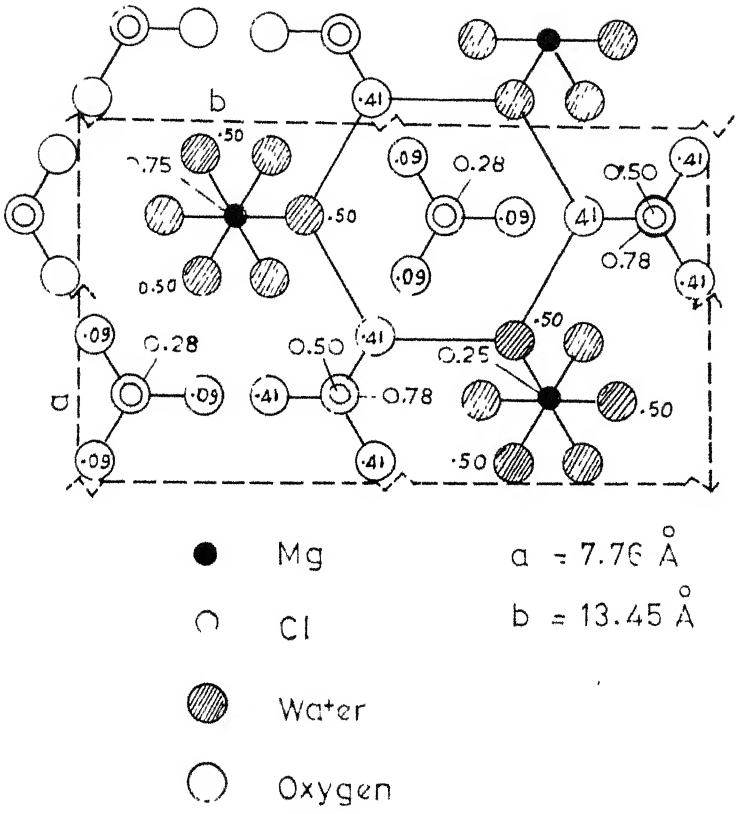

Fig. 3.2 Orthorhombic unit cell of $Mg(ClO_4)_2\ 6H_2O$. A six-ring of three waters and three perchlorate oxygens is outlined.

Table 3.1 Positions of the Atoms and Molecules in $Mg(ClO_4)_2.6H_2O$; $C_{2v}^7(Pmn)$

Atom	Position	x	y	z
Mg	(2a)	0	0.250	0.750
Cl(1)	(2a)	0	-0.083	0.500
Cl(2)	(2a)	0	0.583	0.000
O(1)	(2a)	0	-0.083	0.778
O(2)	(2a)	0	0.583	0.273
O(3)	(2a)	0	-0.189	0.408
O(4)	(2a)	0	0.699	-0.092
O(5)	(4b)	-0.158	-0.031	0.408
O(6)	(4b)	-0.158	0.531	-0.092
$H_2O(1)$	(2a)	0	0.125	0
$H_2O(2)$	(2a)	0	0.375	0.500
$H_2O(3)$	(4b)	-0.187	0.187	0.500
$H_2O(4)$	(4b)	-0.187	0.313	0.000

octahedron are situated at the faces of a cube which is elongated along its body diagonal. The body diagonal is parallel to the crystallographic c-axis which is the axis of hexagonal needle also. The Mg ion site has trigonal symmetry with three-fold axis parallel to c. The configuration about the second Mg ion site in the unit cell is obtained from the first by a rotation of 60^{o} about the c-axis.

Experimental:

Magnesium perchlorate is prepared by dissolving magnesium carbonate in dilute perchloric acid. The excess carbonate is filtered and the solution so obtained is made saturated. It is then crystallized by slow evaportion at a constant temperature in a desiccator containing concentrated sulphuric acid. Crystalline solid is separated and again a saturated solution is prepared with desired impurity added to it. Recrystallization is done in the previous manner. For getting good crystals, growth aid Cr^{3+} or Cu^{2+} is added in very small amount to the solution. The crystallization is done in 100 c.c. beakers which are covered with perforated paper. The crystals of MgPH grow in the form of slender hexagonal prisms (10 $\bar{1}$ 0) which are terminated irregularly and the end faces are not identifiable. Growth axis is crystallographic c-axis. The

crystals of appropriate size are obtained by cutting the long needles (with clear faces) perpendicular to the growth axis. The crystals are hygroscopic and are coated with 1:1 mixture of pertroleum jelly and paraffin oil to prevent absorption of moisture. External morphology of the crystal is used to align the crystal in the magnetic field with desired plane.

For EPR studies of these crystals, a Varian-4502 EPR spectrometer with 100KHz field modulation and control unit V-4560 and 9-inch magnet is used. The spectra are recorded with a G-14 strip chart recorder. DPPH is used as a field marker. The resonance magnetic field for DPPH line is calculated by measuring the frequency with Hewlett Packard frequency meter X-532B and the other field measurements are done with reference to it. Angular variation is studied by a Varian E-229 goniometer and V-4531 cavity.

The temperature variation studies are made by using a Varian-4540 temperature controller which regulates the temperatures from 550K to nearly liquid nitrogen temperatures. A copper-constantan thermocouple placed at the surface of the crystal and Leeds and Northrup Standard potentiometer is used to measure the temperature within an accuracy of

± 1K. The temperature is varied in steps of 5K and sufficient time is given at each interval to assure that the crystal attains uniform temperature. The changes in EPR spectra are first observed on the oscilloscope and then the recording of the spectra is done at various intervals of temperature. Near the phase transition, the temperature is varied in steps of 2K. Angular variation is also done for each phase to determine the principal axes. For the angular variation of the EPR spectrum in the a c plane, at room temperature, the crystals are mounted with the b axis perpendicular to external magnetic field H; and can be rotated in the a c plane. For angular variation study in the a b plane, the needle axis is kept perpendicular to the magnetic field and the crystal rotated in the a b plane. For temperature variation study, the crystal is mounted with the a-axis perpendicular to H, and can be rotated (if the symmetry becomes tetragonal from the trigonal after a phase transition) in the b c plane which contains one of the H_2O - H_2O tetragonal axis (Fig. 3.3).

Results and Discussion:

At room temperature, the EPR spectrum of Mn^{2+} in MgPH for the steady magnetic field H parallel to the crystallographic c axis consists of 30 lines of the allowed transitions

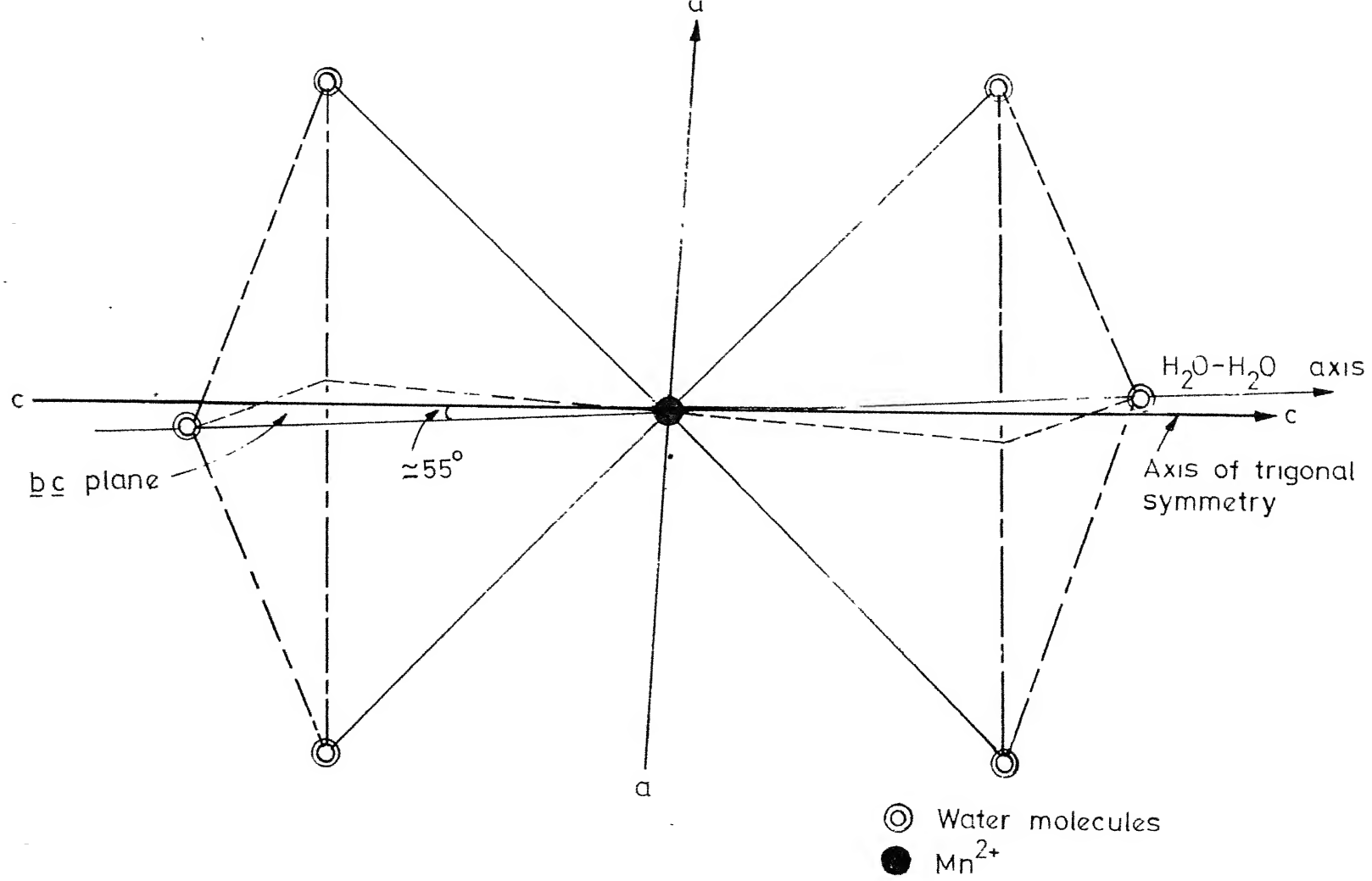

Fig.3.3 Water-octahedron surrounding Mn^{2+}

$\Delta M = \pm 1$, $\Delta m = 0$, as shown in Fig. 3.4. There is overlapping of some hyperfine lines because of smaller spread. As the crystal is rotated such that the c-axis is away from the magnetic field in the a c plane, the spectrum shows a decrease in spread which becomes minimum and attains a secondary maximum for H perpendicular to c. The angular variation of the fine structure transitions is shown in Fig. 3.5 in which the experimental points are plotted alongwith the theoretical curves.

The angular variation in the a c plane also shows the splitting of hyperfine lines for angle θ between the magnetic field and the c-axis more than 10°. As the angle θ increases the splitting of extreme groups of lines becomes more clear and at about 40° off the c-axis there are three components of nearly equal intensity for each line. Fig. 3.6 shows the splitting of some low field lines of the first group. These lines merge again for H perpendicular to c.

The study made in the a b plane shows very small splittings in the h.f.lines with angular variation. For the magnetic field H parallel to a, the lines are merged and this feature is repeated for each possible choice of

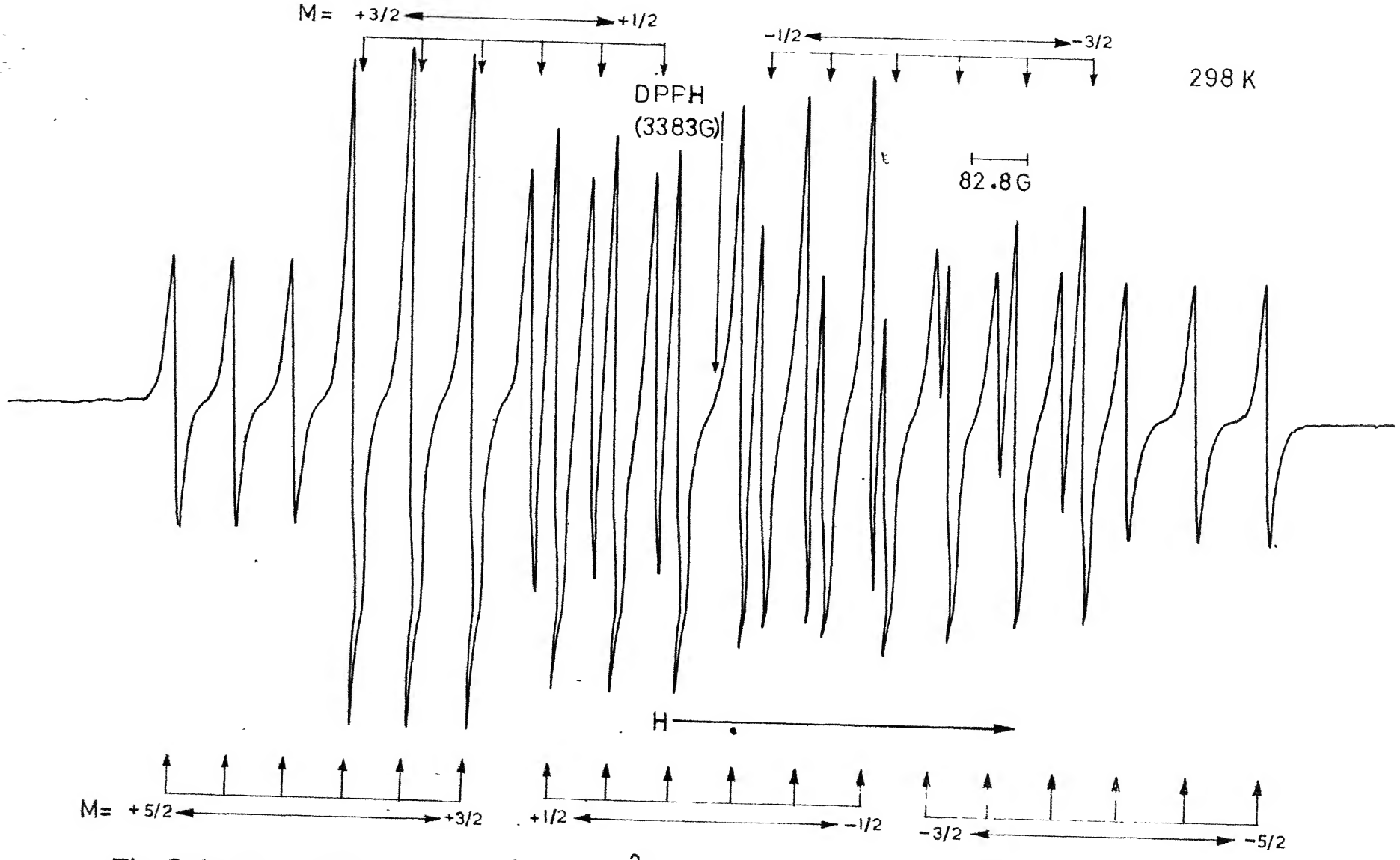

Fig.3.4 The EPR spectrum of Mn^{2+} in $Mg(ClO_4)_2 \cdot 6H_2O$ with magnetic field H parallel to crystallographic axis c at room temperature.

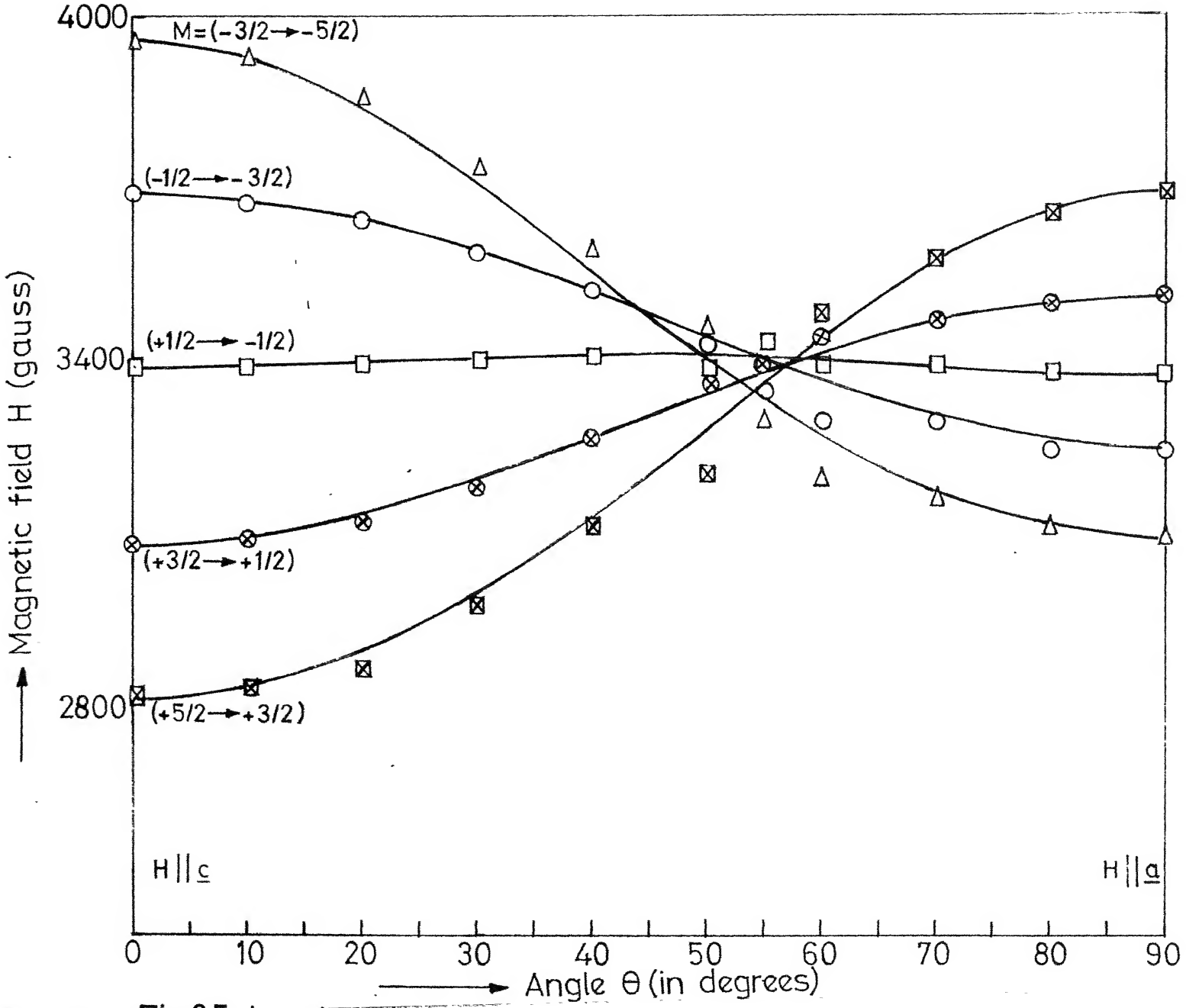
4000
3400
2800
M=(-3/2→-5/2)
(-1/2→-3/2)
(+1/2→-1/2)
(+3/2→+1/2)
(+5/2→+3/2)
Magnetic field H (gauss)
H||c
H||a
0
10
20
30
40
50
60
70
80
90
Angle θ (in degrees)

a i.e. the spectrum repeats itself after each interval of 60^{o}. However, the lines are also found merged for each 30^{o} rotation from a but the sense of merging is different from that of H parallel to a.

From the above observations, it is concluded that at the room temperature, there exist for Mn^{2+} complex three slightly inequivalent sites whose principal z-axes are parallel to a common axis which is the crystallographic c-axis and the axial crystal field splitting parameter D is nearly same for the three sites.

Inequivalent sites may result due to two reasons There may be a small mismatch[17] of the three twinning orthorhombic Mg lattices along the composition planes. Thi mismatch will give rise to only a line broadening and will not produce three sites because the water-perchlorate latt and the three twinning components initially slightly misma will have more and more mismatch for the points away from the composition planes. Next we may consider the effect of the arrangement of the neighbours beyond water-perchlorate surroundings. These are Mg^{2+} ions and due to these one may easily see (Fig. 3.7) that there are only three different possible surroundings for each Mn^{2+} ion. Mn^{2+} going in th

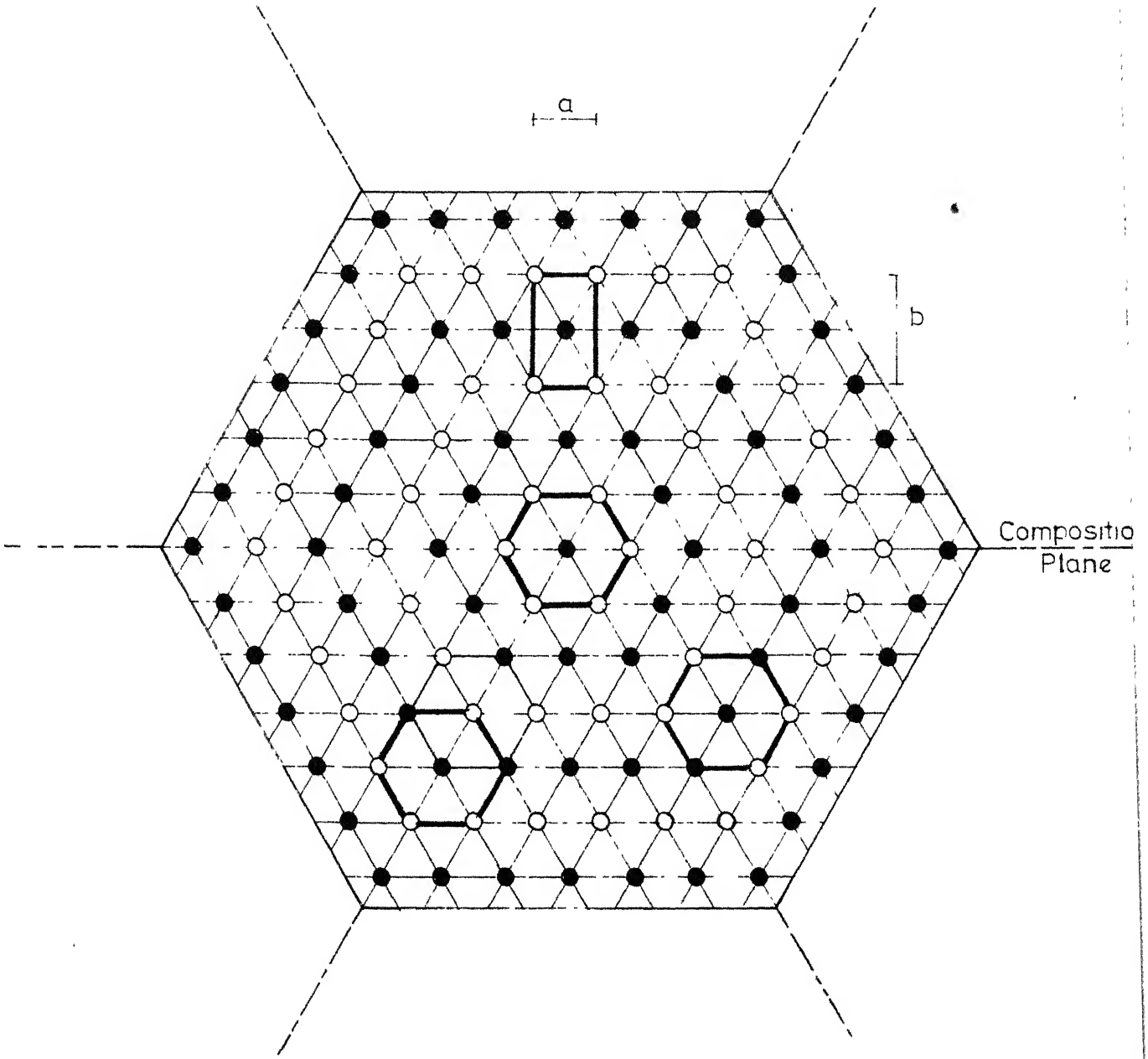

Fig. 3.7 Twinned Mg lattice. Twinning orthorhombic unit and three different environments for Mn^{2+} are indicated by thick lines. Two type of circles are Mg atoms in two different layers c/2 apart.

three different sites will result in three different spectra with very small difference in D. Crystallographic c-axis remains a common symmetry axis for the three spectra. The two sites of Mg^{2+} in a unit cell are identical as far as EPR is concerned. The Mn^{2+} substitutes for Mg^{2+} in a trigonal site formed by an octahedron of water molecules slightly elongated along c-axis and exhibits a 30-line spectrum for H parallel to c.

The spin Hamiltonian necessary to analyse the spectrum of $Mn^{2+}(3d^5, 6S_{5/2}, S=5/2, I=5/2)$ in a trigonal site is written as[19-22]

$$H=g_{\parallel}\beta H_z S_z+g_{\perp}\beta (H_x S_x+H_y S_y)+D(S_z^2-\frac{35}{12})-\frac{7}{36}(a-F)$$

$$X[S_z^4-\frac{95}{14}S_z^2+\frac{81}{16}]+AS_zI_z+(1/2)B[S_+I_-+S_-I_+]$$

$$+Q'[I_z^2-\frac{35}{12}]-g_n\beta_n H_z I_z-g_n\beta_n[H_x I_x+H_y I_y] \qquad (3.1)$$

where g is the splitting factor, β is the Bohr magneton, S is the spin angular momentum operator and $S_{\pm} = [S_x \pm iS_y]$, 'a' is the cubic field parameter, D and F are axial field parameters or fine structure constants with second and fourth degree terms, A and B are hyperfine constants, Q' is quadrupole interaction parameter, g_n, β_n and I are nuclear

splitting factor, nuclear magneton and nuclear spin operator respectively and $I_{\pm} = [I_x \pm iI_y]$. H is the steady magnetic field applied along an arbitrary direction. z-axis is chosen along the c-axis which is the (111) direction of a cubic coordinate system $\xi\,\eta\zeta$. The fine structure part of this Hamiltonian is

$$H_{f.s.} = g\beta\vec{H}.\vec{S} + D\left[S_z^2 - \frac{35}{12}\right] - \frac{7}{36}(a-F)\left[S_z^4 - \frac{95}{14}S_z^2 + \frac{81}{16}\right] \qquad (3.2)$$

and the magnetic fields at which the allowed fine structure transitions occur are given by[19]

$$M=\pm 5/2 \rightleftharpoons \pm 3/2;\ g\beta H = g\beta H_o \mp [2D(3\cos^2\theta - 1) + 2pa + \tfrac{1}{6}Fq] - 32\delta_1 + 4\delta_2$$

$$M=\pm 3/2 \rightleftharpoons \pm 1/2;\ g\beta H = g\beta H_o \mp [D(3\cos^2\theta - 1) - \tfrac{5}{2}pa - \tfrac{5}{24}Fq] + 4\delta_1 - 5\delta_2$$

$$M=+1/2 \rightleftharpoons -1/2;\ g\beta H = g\beta H_o + 16\,\delta_1 - 8\,\delta_2 \qquad (3.3)$$

where H is the field at which a transition is observed for a fixed frequency of the applied microwave radiation and H_o is the field at which it would have occurred if all fine structure terms had been zero. H makes an angle θ with the trigonal axis and

$p = 1 - 5(l^2m^2 + m^2n^2 + n^2l^2)$ l,m,n are direction cosines of H with respect to cubic axis.

$$q = (35\cos^4\theta - 30\cos^2\theta + 3)$$

$$\delta_1 = \left(\frac{D^2}{g\beta H_o}\right)\cos^2\theta \sin^2\theta$$

$$\delta_2 = \left(\frac{D^2}{4g\beta H_o}\right)\sin^4\theta$$

For $\theta = 0^{\circ}$, H is parallel to $\underline{c}$ and the following equations are obtained for resonance fields

$$\begin{aligned} H_{+5/2 \rightleftharpoons +3/2} &= H_o - 4D - 2p\,(a-F) \\ H_{+3/2 \rightleftharpoons +\frac{1}{2}} &= H_o - 2D + (5/2)p\,(a-F) \\ H_{+\frac{1}{2} \rightleftharpoons -\frac{1}{2}} &= H_o \\ H_{-\frac{1}{2} \rightleftharpoons -3/2} &= H_o + 2D - (5/2)p\,(a-F) \\ H_{-3/2 \rightleftharpoons -5/2} &= H_o + 4D + 2p\,(a-F) \end{aligned} \qquad (3.4)$$

where $p = -2/3$

If $\theta = 90^{\circ}$, H is perpendicular to $\underline{c}$ and resonance fields are given by

$$\begin{aligned} H_{+5/2 \rightleftharpoons +3/2} &= H_o + 2D - 2p\,(a-F) + (D^2/H_o) \\ H_{+3/2 \rightleftharpoons +\frac{1}{2}} &= H_o + D + (5/2)p\,(a-F) - (5/4)\,(D^2/H_o) \\ H_{+\frac{1}{2} \rightleftharpoons -\frac{1}{2}} &= H_o - (2D^2/H_o) \\ H_{-\frac{1}{2} \rightleftharpoons -3/2} &= H_o - D - (5/2)p\,(a-F) - (5/4)\,(D^2/H_o) \\ H_{-3/2 \rightleftharpoons -5/2} &= H_o - 2D + 2p\,(a-F) + (D^2/H_o) \end{aligned} \qquad (3.5)$$

where $p = -1/4$

Here D and (a-F) are in units of gauss and the Eqs. (3.4) and (3.5) are used to calculate the spin Hamiltonian parameters $g_{||}$, $g_{\perp}$, D and (a-F).

Neglecting the nuclear Zeeman term and quadrupole interaction term of the remaining spin Hamiltonian in Eq.(3.1 the hyperfine part is left as

$$\mathcal{H}_{h.f.s} = A\, S_z\, I_z + (\tfrac{1}{2})B\,(S_+ I_- + S_- I_+) \qquad (3.6)$$

From this, the positions[23-24] of the hyperfine lines due to transitions $\Delta M = \pm 1, \Delta m = 0$ are found by adding the following terms with appropriate value of M to Eqs. (3.3).

$$\mathcal{H}_{h.f.s} = -Km - \frac{B^2}{4g\beta H_o}\left[\frac{A^2+K^2}{K^2}\right]\left[I(I+1)-m^2\right] - \frac{B^2}{2g\beta H_o}\left(\frac{A}{K}\right)(2M-1)m$$

$$- \frac{1}{2g\beta H_o}\left(\frac{A^2-B^2}{K^2}\right)\left(\frac{g_{\parallel} g_{\perp}}{g^2}\right)^2 m^2 \sin^2\theta \cos^2\theta \qquad (3.7)$$

where

$$K^2 g^2 = A^2 g_{\parallel}^2 \cos^2\theta + B^2 g_{\perp} \sin^2\theta$$

For $\theta = 0^\circ$ and A and g nearly isotropic, the expression becomes

$$\mathcal{H}_{h.f.s} = -Am - \frac{B^2}{2g\beta H_o}\left[I(I+1)-m^2+(2M-1)m\right] \qquad (3.8)$$

and for $\theta = 90^\circ$, A is replaced by B in this expression. This equation is used to calculate the values of A and B.

To obtain the spin Hamiltonian parameters, first of all the value of the magnetic field corresponding to the

DPPH line in the spectrum H $\parallel$ c is calculated from the measured frequency and the known values of h, β and g_D. Then the positions of hyperfine lines are measured relative to the DPPH line. Fine structure transition positions*, $H_{M \rightleftharpoons M-1}$ are determined from them and the values of D and (a-F) are calculated in terms of gauss by elimination process using Eqs. (3.4). The same procedure is followed for the spectrum H $\perp$ c but now for D^2/H_o term in it, D is substituted from the first spectrum and H_o is approximately calculated.

The values of A and B are calculated from hyperfine line positions using Eq. (3.8). With these two known, appropriate corrections are applied to the resonance magnetic field values of the fine structure transitions and the final values of D, (a-F) and H_o are calculated. From the values of H_o in two cases, $g_{\parallel}$ and $g_{\perp}$ are determined. The spin Hamiltonian constants for Mn^{2+} in MgPH have been calculated as

$g_{\parallel}$	$= 2.0023 \pm 0.0010$	$g_{\perp}$	$= 2.0012 \pm 0.0010$
D	$= 146.6 \pm 1.0$ G	(a-F)	$= 8.8 \pm 1.0$ G
A	$= -91.8 \pm 1.0$ G	B	$= -94.3 \pm 2.0$ G

where signs of parameters are relative.

*(Given in the text refer to the mid-point field values of the observed hyperfine sextets in the EPR spectrum of Mn^{2+}. Second order corrections are small and have not been added to these values while plotting angular variation.)

Linewidth :

Peak to peak width of the derivative signal is called linewidth. It depends very much on the concentration of the paramagnetic impurity doped in a solid. The effect of increasing the concentration on the appearance of the EPR lines is reflected as their broadening due to magnetic dipole-dipole interaction[25-26] between Mn^{2+} ions. The concentration dependent EPR line broadening has been studied for Mn^{2+} in aqueous solution[27], frozen aqueous solutions[28] and diamagnetic lattices[26,29]. In the present work, the linewidths in one sample of Mn^{2+} doped MgPH crystal are found to be of 19G to 27G while in another crystal with much smaller concentration of Mn^{2+}, the linewidths are 4G to 10G only. Thus the linewidths are found to be very much concentration dependent in this study.

In addition, the linewidths in the group with transition $M = +\frac{1}{2} \rightleftharpoons -\frac{1}{2}$ are smaller than those with the transitions involving larger quantum number M. This is the usual behaviou and has been explained by Vanier[26]. There are statistical fluctuations in the local crystalline field surrounding the paramagnetic ion due to crystalline imperfections. These are reflected by fluctuations in the amplitude of D which in

turn, affects the linewidths. In case of axial symmetry, the magnetic field for resonance at a frequency ν is given by

$$H = Ho + (M - \tfrac{1}{2}) \left(\frac{D}{g\beta}\right) [3\,Cos^2\theta - 1]; \quad Ho = \frac{h\nu}{g\beta}$$

for a fine structure transition, M being the upper magnetic quantum number of a given transition and θ is the angle between the magnetic field and z-axis. For $M = \frac{1}{2}$, the term in D vanishes and $M = +\frac{1}{2} \rightleftharpoons -\frac{1}{2}$ transition is not affected by D. But for M = +5/2, $\pm$3/2, the second term is not zero and produces a shift in the fields for resonance. D in these terms, under the effect of crystalline imperfections contributes to the broadening of lines.

In addition to this, statistical fluctuations of the orientation of the axis of symmetry of the complexes are also important because of the strong angular dependence of the resonance lines associated with larger M values. This is equivalent to fluctuations of θ in the above expression. A resultant broadening is obtained if fluctuations of the relative orientation of the crystalline field are added to the amplitude fluctuations of D.

Hyperfine Forbidden Transitions :

When the magnetic field H is off the c-axis in the a c or the b c plane, five doublets of lines between the allowed hyperfine lines ($\Delta M = \pm 1$), ($\Delta m = o$) of the

electronic transition $M = +\frac{1}{2} \rightleftharpoons -\frac{1}{2}$ are observed in the spectrum of MgPH: Mn^{2+} system. Some lines of the doublets overlap with the allowed hyperfine lines of the other groups (Fig. 3.8). These doublets are due to hyperfine lines of forbidden transitions ($\Delta M = \pm 1, \Delta m = \pm 1$) and have been observed in many systems. Such transitions occur due to a second order mixing of A with a for cubic symmetry[31-33], A with D and a for axial, trigonal, tetragonal or hexagonal symmetry[8,20,22,34-36] and A with D and E for orthohombic symmetry[37]. The relative intensity expression for axial symmetry obtained by Bleaney and Rubins[38] shows that these doublets cannot be observed as long as magnetic field is parallel or perpendicular to the axis of symmetry. The intensity is maximum for $\theta = 45^{\circ}$ and the lines are strongest for the electronic transition $M = +\frac{1}{2} \rightleftharpoons -\frac{1}{2}$.

The separation between the lines of a hyperfine forbidden doublet has been evaluated by several authors and for trigonal symmetry it is given by

$$\Delta H = \frac{17B^2}{H_o} + \left(\frac{2\gamma\beta n}{g\beta}\right) H_o - \left[\left(Q' - \frac{4B^2 D}{H_o^2}\right)(3\cos^2\theta - 1) + \frac{25A^2}{H_o^2}\right](2m + 1) \qquad (3.9)$$

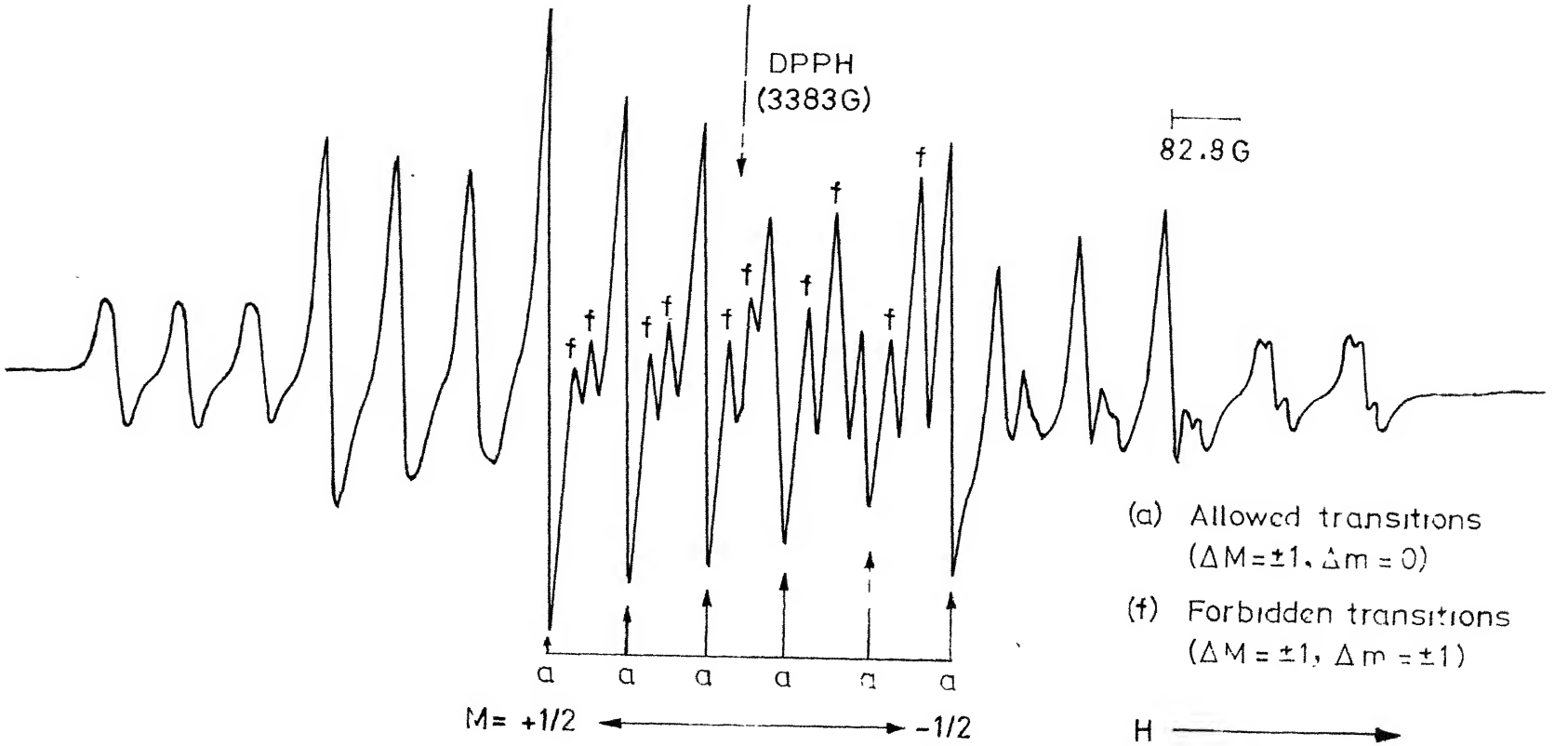

Fig.3.8 Hyperfine-forbidden ($\Delta M = \pm 1, \Delta m = \pm 1$) transitions of the $M = +1/2 \rightleftharpoons -1/2$ for H making an angle 15° from the $\underline{c}$ - axis in the $\underline{a}\,\underline{c}$ plane in $Mg(ClO_4)_2 \cdot 6H_2O : Mn^{2+}$ system.

where γ is the gyromagnetic ratio of the Mn^{55} nucleus, θ is the angle between $\underline{c}$ and H and m = -5/2 for the doublet occurring between m = -5/2 and m = -3/2 allowed transitions. Other terms have their usual meaning.

From the doublet separation in the EPR spectra of Mn^{2+} in MgPH at $\theta = 10^{\circ}$ and $\theta = 20^{\circ}$ from the $\underline{c}$-axis in the $\underline{a}$ $\underline{c}$ plane, the value of Q' and $(\frac{\gamma\beta_n}{g\beta})$ are obtained as

$$Q' = 0.06 \text{ G}$$

$$\frac{\gamma\beta_n}{g\beta} = 0.37 \times 10^{-3}$$

The value of $\gamma\beta n/g\beta$ obtained by other workers[39-41] is 0.3775×10^{-3}.

TEMPERATURE VARIATION AND STRUCTURAL PHASE TRANSITION STUDIES

For temperature variation study the crystal is mounted such that the magnetic field H could be rotated in the $\underline{b}$ $\underline{c}$ plane. This is done for some specific reasons. It has been indicated by Mössbauer studies[42] on $Fe(ClO_4)_2.6H_2O$ that the observed temperature variation of quadrupole splitting may be explained by assuming only axial distortion of water octahedron and a transition from axially compressed (at lower temperature) to axially stretched distortion (at higher temperatures). The susceptibility measurements[43-46] in Fe, Co, Ni, Mn and Cu perchlorates indicate that in these crystals, the trigonal

symmetry due to axial extension of water octahedron at room temperature may change to a tetragonal symmetry due to axial compression of water octahedron after the phase transition. Since these perchlorates are isostructural to MgPH, similar changes may be expected in this crystal also after the phase transition. The b c plane contains one of the three H_2O-H_2O tetragonal axes. After the phase transition this may become one of the principal axes. The spectrum for this direction will show an extremum after the phase transition. This axis is at about 55° from the c-axis in the b c plane (Fig. 3.3). The other two H_2O - H_2O axes will lie in the other two possible b c planes which are oriented at 60° and 120° with respect to this plane.

Spectrum for H || c :

As the temperature is lowered, the hyperfine spread of the spectrum for H || c increases and goes to a maximum at T_a (272.0 ± 1.0K). Below T_a the spread decreases becoming minimum at T_b (about 203.0 ± 10.0 K). From T_b downwards, the spread is found to increase again till T_c (103.0 ± 1.0 K). At T_c the spectrum collapses suddenly and a new spectrum comprising of many more lines appears. Fig. 3.9 shows the changes in the spectrum around T_a. The changes in the spread around T_b are small and these were noted directly from the fine dial

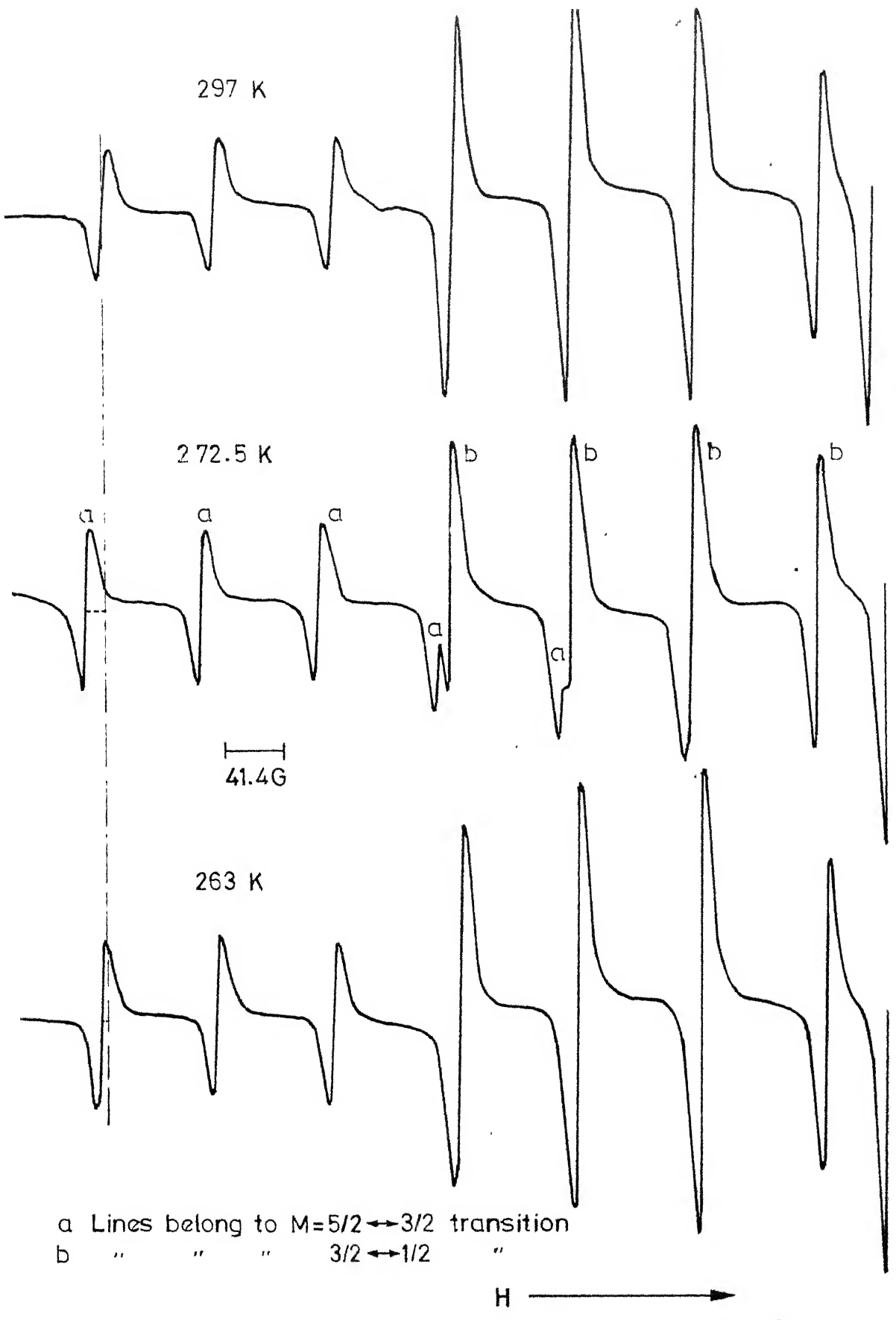

Fig.3.9 A comparision of the EPR spectra of Mn^{2+} in $Mg(ClO_4)_2.6H_2O$ for H||c around T_a (272 K). The increase in spread is marked by the dotted line.

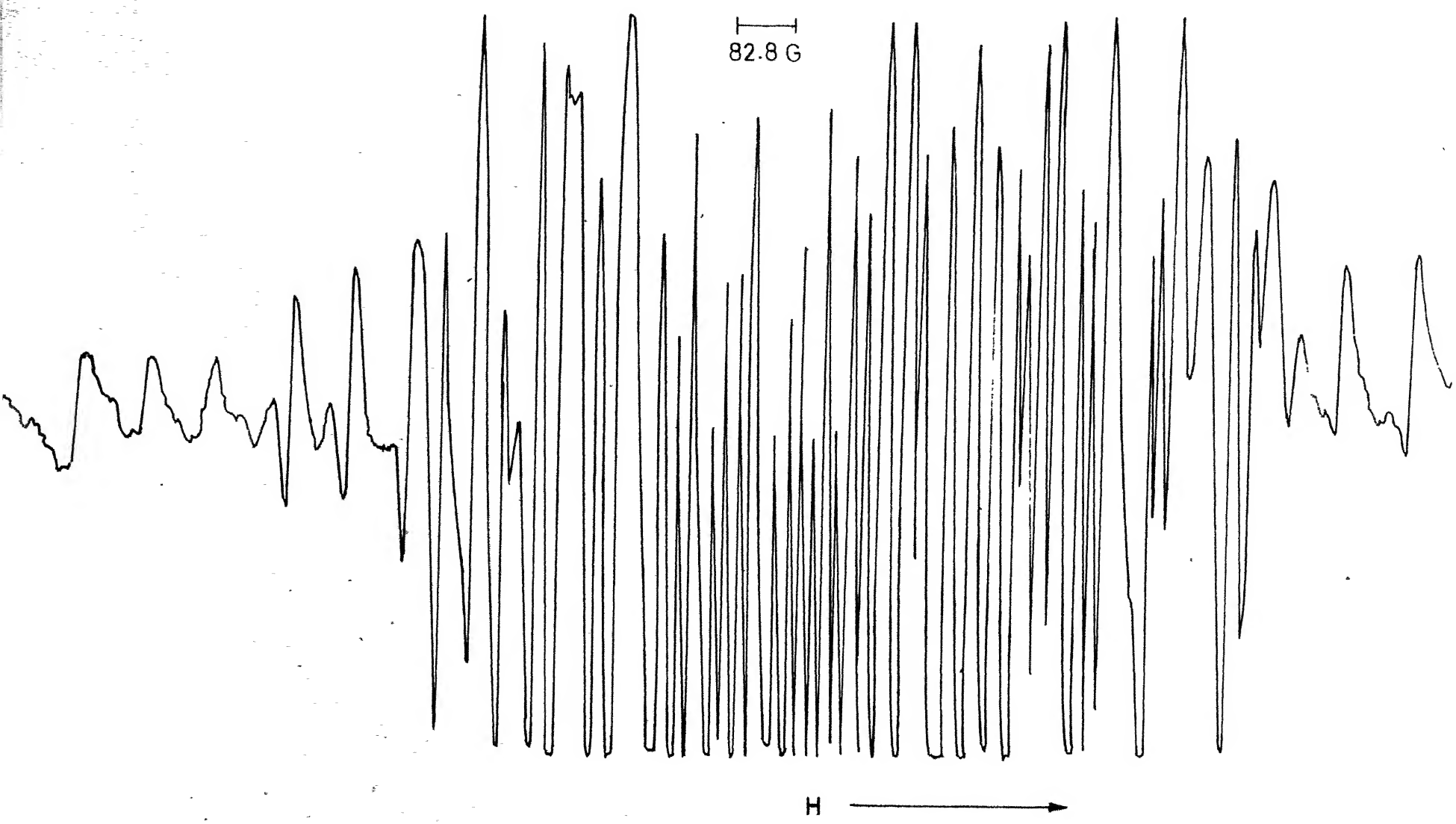

Fig.3.10 The EPR spectrum of Mn^{2+} in $Mg(ClO_4)_2 \cdot 6H_2O$ for H||c at 101 K in phase IV

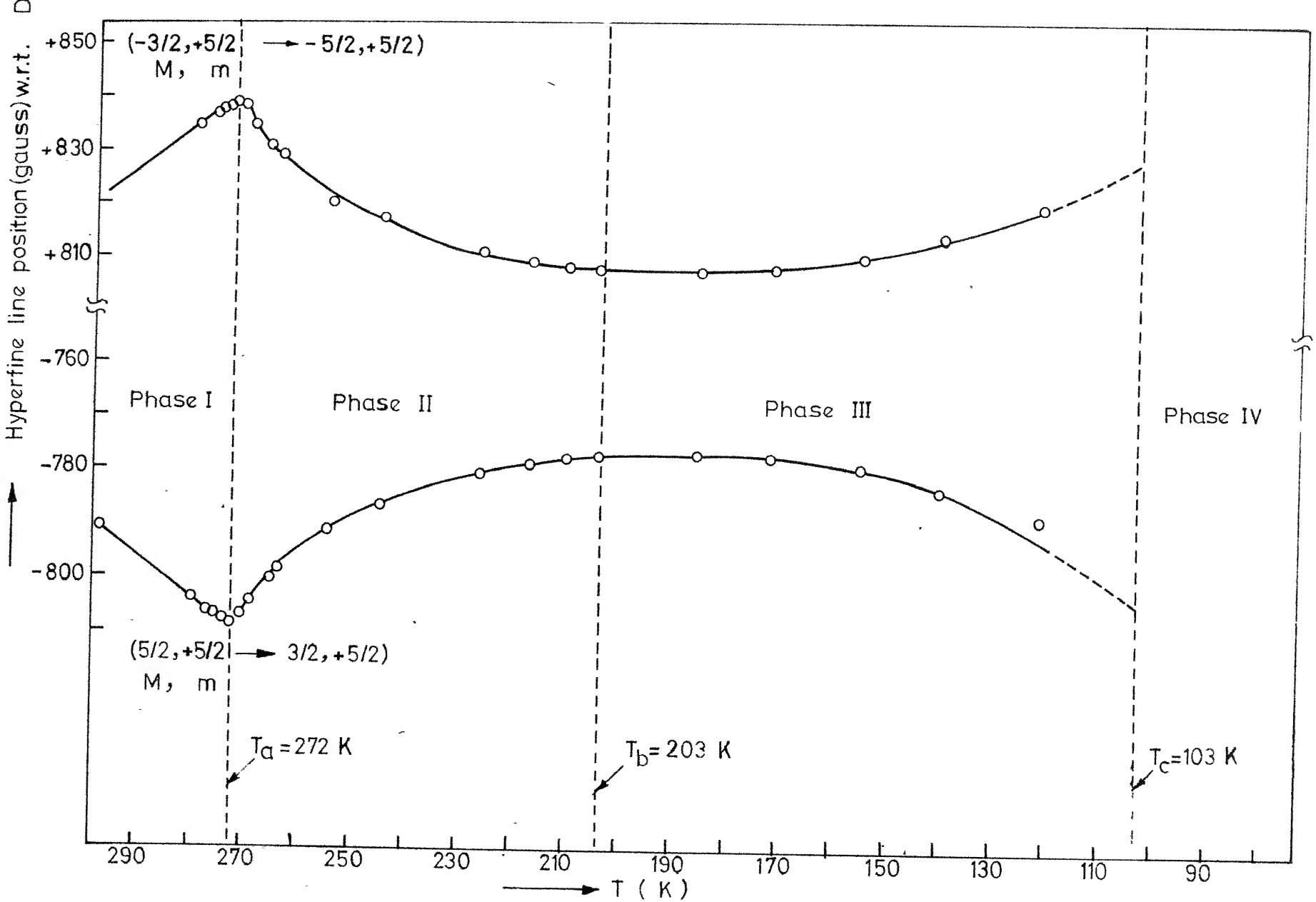

Fig.3.11 Temperature variation of extreme hyperfine line positions in the EPR spectrum of Mn^{2+} in $Mg(ClO_4)_2 \cdot 6H_2O$ for H||c.

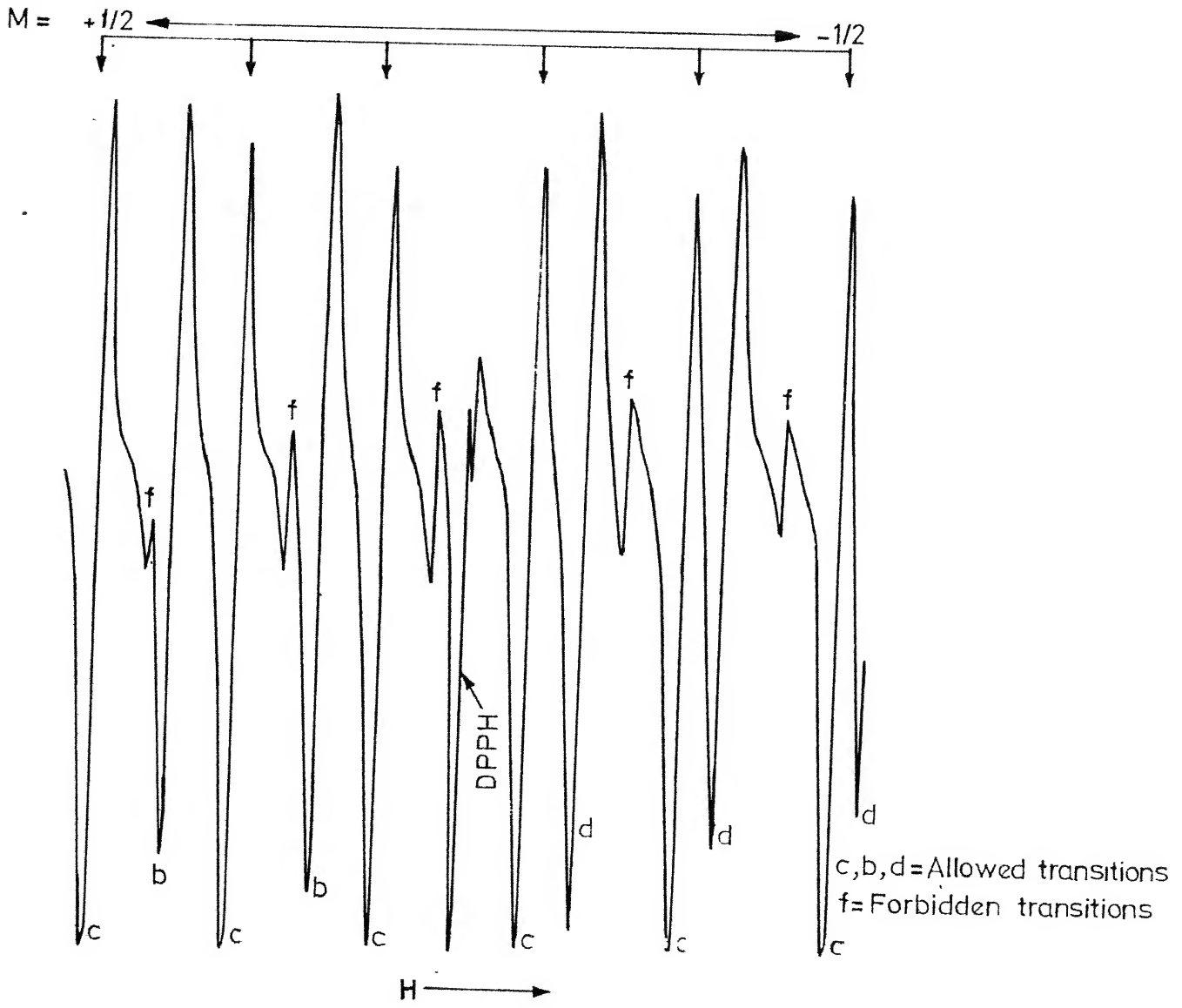

Fig.3.12 The EPR spectrum of Mn^{2+} in $Mg(ClO_4)_2 \cdot 6H_2O$ for $H \| \underline{c}$ at 121.5 K showing hyperfine forbidden lines. One line of each doublet is overlapping with allowed b or d lines.

angular variation, the number of Mn^{2+} complexes and the principal axes remain the same from room temperature to T_a.

Below T_a the maximum spread is not obtained for H parallel to c but at some angle from the c-axis in the b c plane. Thus the principal z-axis does not remain parallel to c. The hyperfine lines are also seen to split in the spectrum along new z-axis. The splitting of the lines is less near T_a but it increases as the temperature decreases and below about 130 K, there are seen six components of each hyperfine line. The z-axis also goes on moving away from c-axis as temperature falls and finally it is about 8^o off the c-axis. Fig. 3.13 shows the splitting of high field lines at 121.5 K. The origin of these sextets appearing below T_a, is different from that of the triplet-splitting at room temperature because triplets start appearing after 10^o or more rotation in the b c plane while the sextets are seen clearly in the new principal z-axis spectrum obtained approximately at 8^o off the c-axis in the same plane. The angular variation study shows that the six split lines show a maximum for H along a direction making an angle ϕ from the c-axis on one side in the b c plane and a similar spectrum is obtained at the same angle ϕ in the same plane on the other side of the c-axis. Thus there are two similar spectra in the b c plane at an angle of 2 ϕ from each

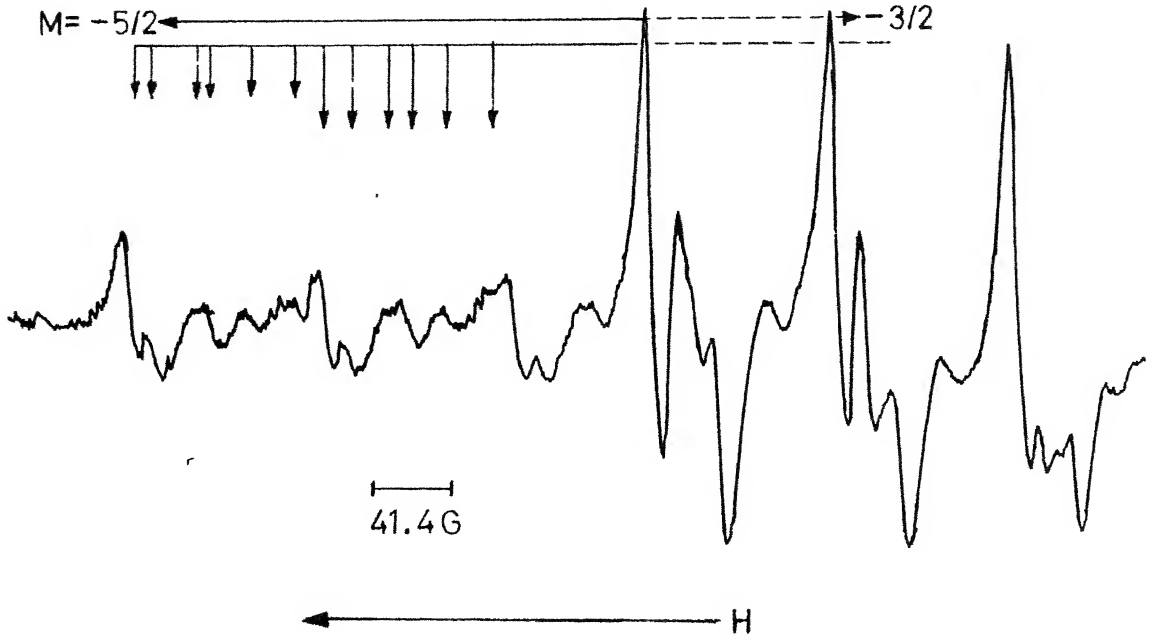

Fig.3.13 Splitting of the lines in the EPR spectrum of Mn^{2+} in $Mg(ClO_4)_2 \cdot 6H_2O$ at 121.5 K for H at 8° from c-axis in the b c plane. Two sextets (M,m = -5/2, 5/2 ⟷ -3/2, 5/2 and -5/2, 3/2 ⟷ -3/2, 3/2) are marked.

other. These are attributed to the two Mn^{2+} complexes having their principal z-axes inclined to the c-axis at angles ϕ and $-\phi$ in the b c plane. Since there is a six-line splitting, there should be six physically inequivalent sites for Mn^{2+} complexes. Such six sites exist in fact due to the crystal structure discussed previously in this chapter. There are three possible b c planes and thus there are six principal z-axis spectra, two in each b c plane. All the six principal axes are equally inclined to the c-axis and each one gives rise to one line in the sextet. It is important to note that for H parallel to c, the six lines merge into one line and a thirty-line spectrum is observed which means that c is a common symmetry axis of all the sites.

New principal z-axis spectrum also appears to have the same behaviour with temperature as the spectrum for H parallel to c. Fig. 3.14 shows the spectra at different temperatures between T_a and T_c, with z-axis tilting continuously away from c-axis. In Fig. 3.15, the fine structure tran. positions of the spectra along the principal z-axes from room temperature to T_c have been plotted against temperature. It may be concluded from all the above data that MgPH exists in four phases from room temperature to liquid nitrogen temperature in the following way

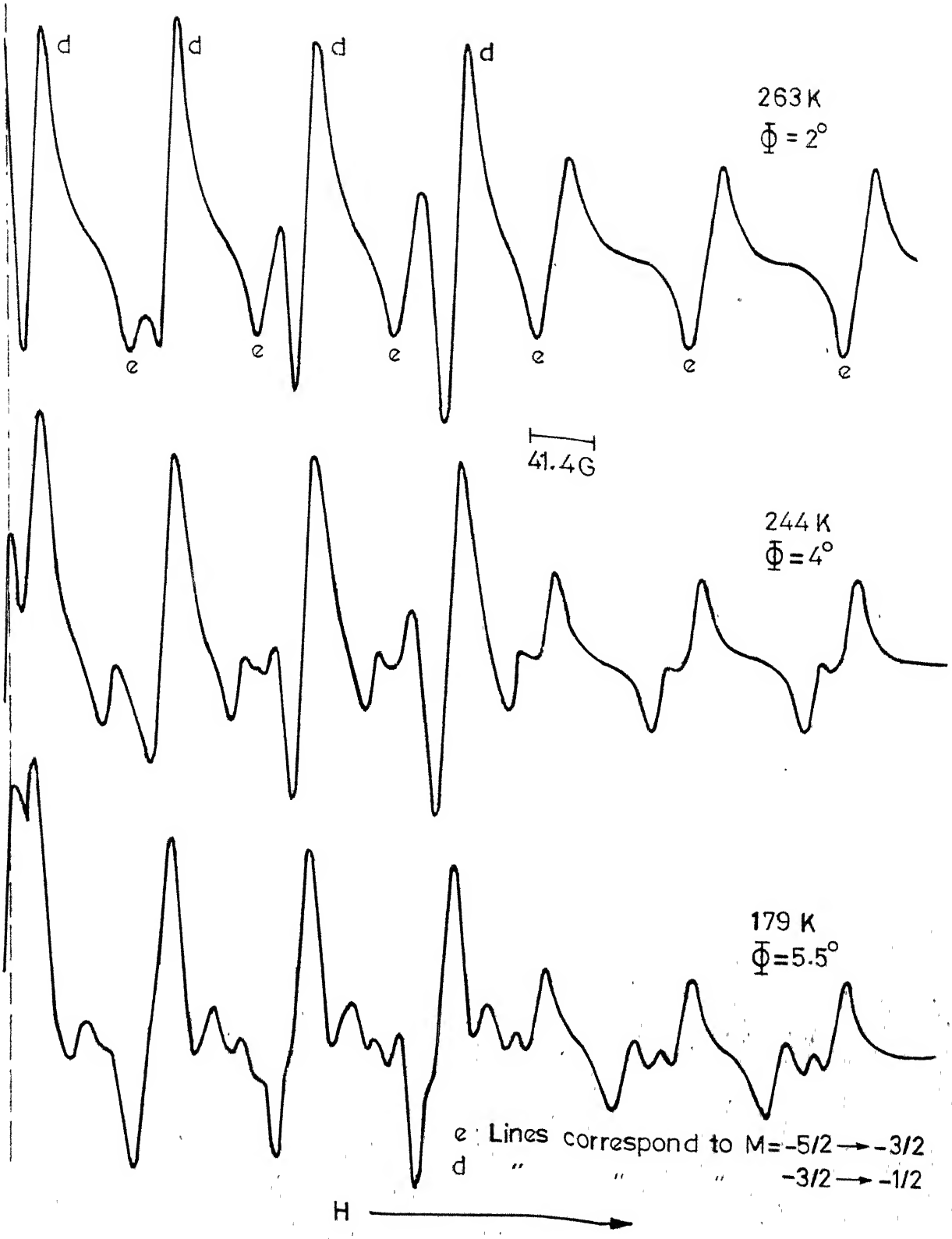

Fig. 3.14 The EPR spectra of Mn^{2+} in $Mg(ClO_4)_2.6H_2O$ for H||z at different temperatures between T_a and T_b. Φ is the angle between c and z in the bc plane.

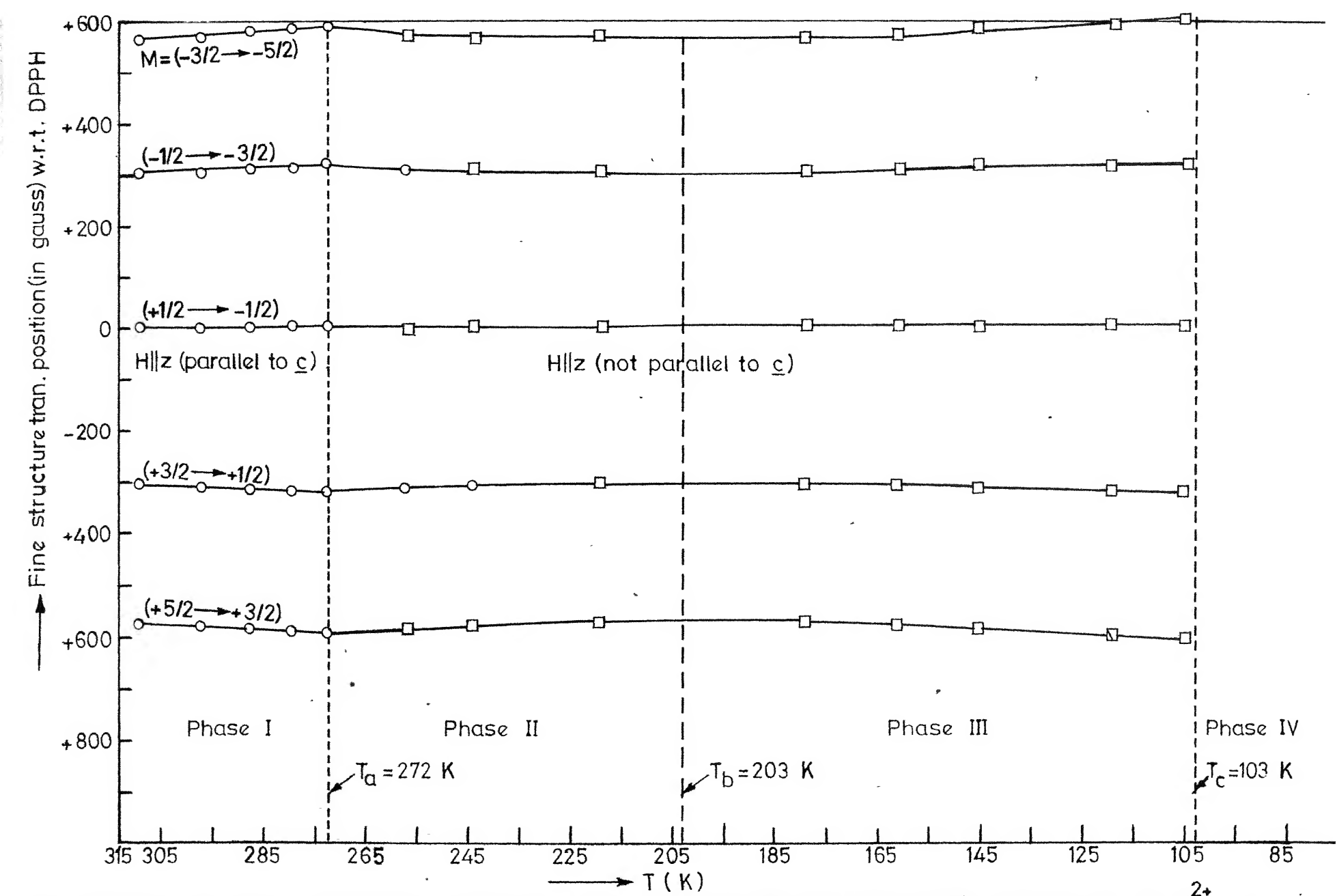

Fig.3.15 Temperature variation of fine structure tran.positions in the EPR spectrum of Mn^{2+} in $Mg(ClO_4)_2 \cdot 6H_2O$.

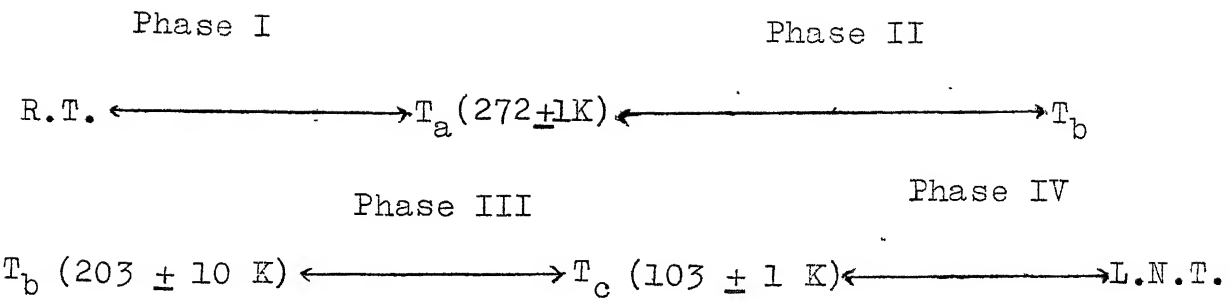

The Mössbauer study of the phase transition in 1.5 atom percent Fe^{57} doped MgPH was first reported by Dézsi and Keszthelyi[42] who found only one phase transition occurring in the range 113 K to 83 K. Thus they could detect roughly, only the third phase transition occuring at T_c in our case. The transitions occuring at T_a and T_b could not be observed by Mössbauer study.

The EPR spectrum in phase IV (Fig. 3.10) is very complex and different lines show extremum for different angles of rotation from the c-axis. For some lines, the spectrum shows extremum at about 55° indicating that some Mn^{2+} centres might have their principal axes parallel to H_2O - H_2O axes.

Rotation of the Principal Axes :

The rotation of the principal z-axis relative to the c-axis in the b c plane is studied from T_a to T_c. The angle of rotation ϕ of the principal z-axis from the c-axis in the b c plane near T_a is approximately 2°. It increases

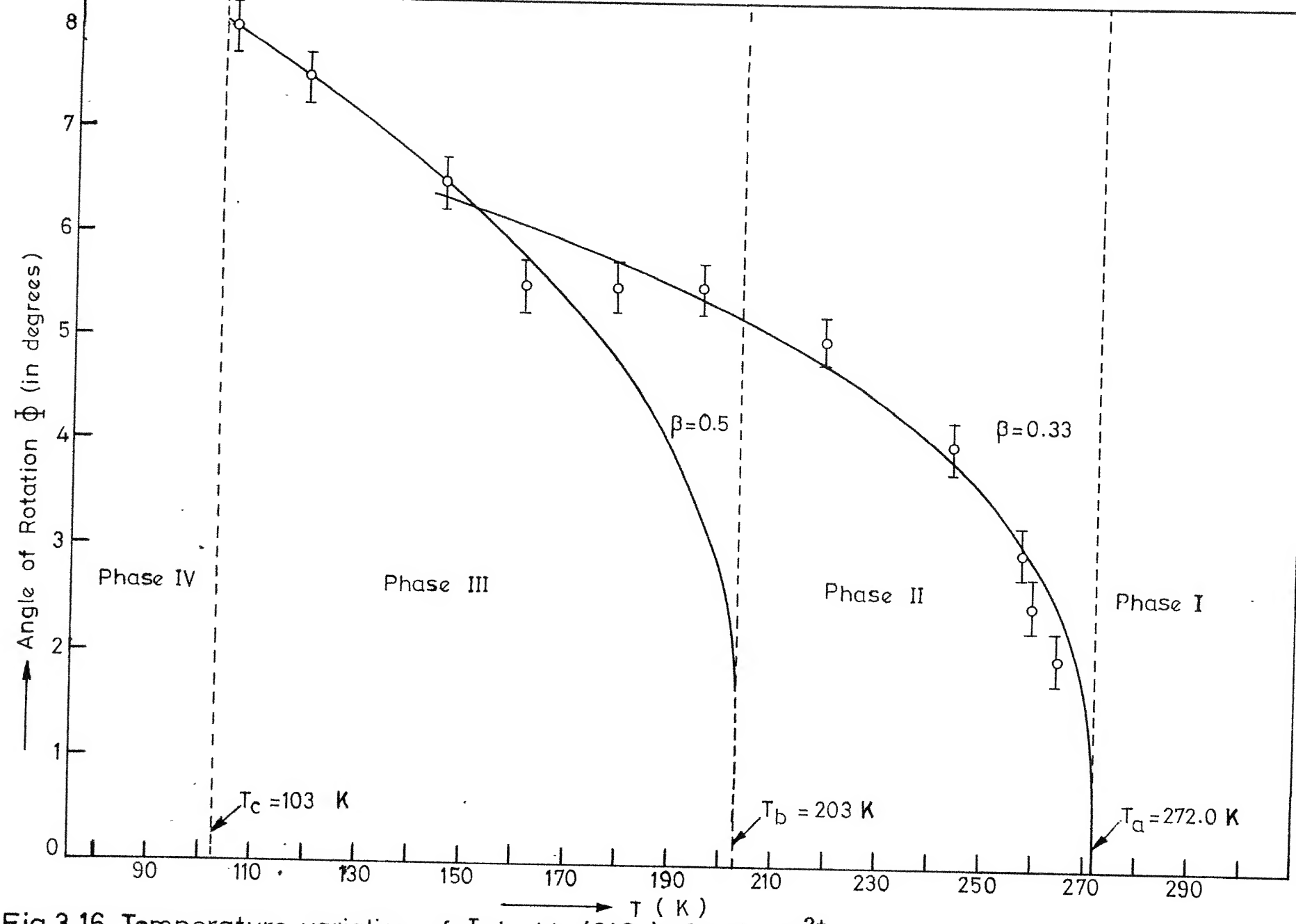

Fig.3.16 Temperature variation of Φ in $Mg(ClO_4)_2 \cdot 6H_2O : Mn^{2+}$ system in phase II and III.

phase III, ϕ shows Landau behaviour[49]

$$\phi = \phi_o + m' (T_b - T)^{\frac{1}{2}} \text{ with } \phi_o = 1.70^o \text{ and } m' = 0.632.$$

Temperature Variation of D :

Fig. 3.17 shows the temperature variation of D from room temperature to near T_c. From room temperature to T_a in the phase I, D shows a variation of the type[50]

$$D = D_o (1 + \alpha T + \beta T^2)$$

with $D_o = 201.40$ G, $\alpha = -9.20 \times 10^{-4}/K$,

$\beta = +7.50 \times 10^{-8}/K^2$

This is due to the trigonal static distortion of $Mn(H_2O)_6^{++}$ complex increasing with the decrease in temperature on accoun of lattice contraction. However, the contribution to D from the lattice vibrations[51] should not be overlooked. It may appear in the form δ coth ($h\omega/k$ T), where δ is a constant and is the frequency of the impurity resonant vibration coupling to D but in the small region of study, it is difficult to access the exact contribution of this term.

In the phase II near T_a, D is found to vary in the following form

$$D = D_a + K_a (T_a - T)^{2/3} \qquad T < T_a$$

where $D_a = 152.50$ G, $K_a = 0.639$, $\eta = 1/3$

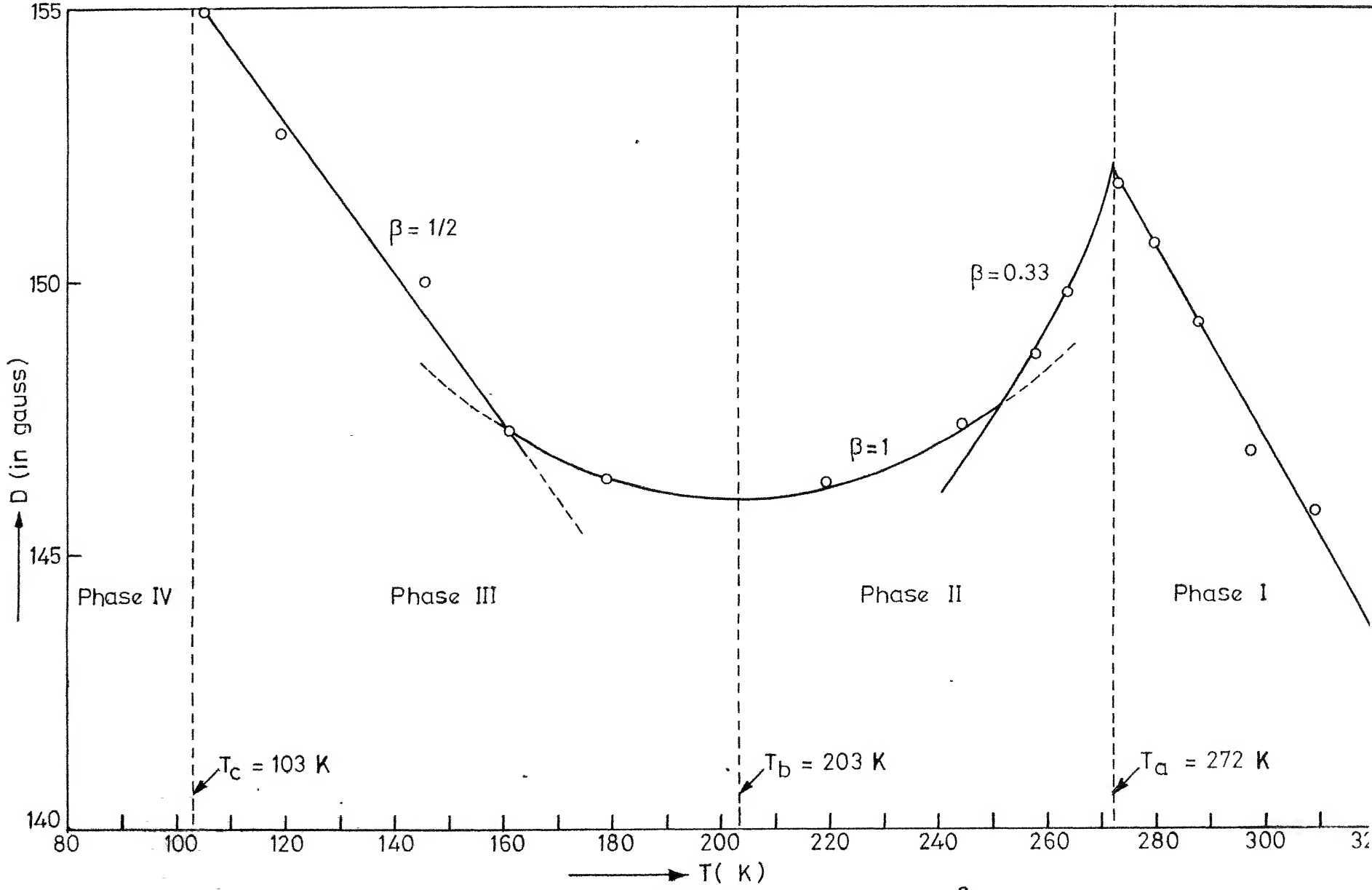

Fig. 3.17 Temperature variation of D in $Mg(ClO_4)_2.6H_2O : Mn^{2+}$ system.

D shows the critical behaviour as expected from the variation of ϕ in this region. ϕ varies as $(T_a - T)^{1/3}$ and D varies[49] as ϕ^2, thus D should vary as $(T_a - T)^{2/3}$.

In the region around T_b, D follows an unexpected behaviour expressed by

$$D = D_b + K_b (T_b - T)^2 \text{ for } T < T_b \text{ as well as for } T > T_b$$

where $D_b = 146.00$ G, $K_b = 7.472 \times 10^{-4}$ $\eta = 1$

This indicates that the variation of ϕ should be linear in this region. More experimental observations are needed to explain the trend of ϕ in the vicinity of T_b.

In the phase III, in the region away from T_b, the variation of D is guessed from the variation of ϕ and it is found to vary as

$$D = D_b' + K_b' (T_b - T) \quad \text{for } T < T_b$$

with constants $D_b' = 141.50$ G, $K_b' = 0.1384$, $\eta = \frac{1}{2}$

Thus it shows Landau behaviour.

The variation of ϕ and D with temperature in the phase III, away from the transition point T_b, fits with soft mode theory or the microscopic theory (for structural phase transition) in the meanfield approximation[52]. In the critical region below T_a also, the fitting is similar to that in $SrTiO_3$ or

$LaAlO_3$. Therefore, it is concluded that the structural phase transitions occuring at T_a and T_b are of the second order type and similar to those occuring in $SrTiO_3$[47,49], $LaAlO_3$[47,49] and fluoperovskites[48]. There may be unstable soft phonon nodes associated with $Mn^{++}(H_2O)_6$ complex that condense at T_a and T_b giving rise to these transitions. Accordingly it may also be assumed that there are rotations of the $Mn^{++}(H_2O)_6$ octahedra in two opposite directions by the same amount about the crystallographic a-axis (Fig. 3.3) in the temperature range T_a to T_c.

It is important to consider the effect of perchlorate ions also on all the above phase transitions. The internal disorder of these ions or the changes in their orientations may change the environment of the Mn^{++} directly or through a rearrangement of water molecules. Such possibilities have been suggested by some workers[53,54].

The present EPR results cannot decide exactly how the environment around Mn^{++} is changing during the temperature variation. It is only after the first order phase transition at T_c that the symmetry of Mn^{++} $(H_2O)_6$ probably becomes tetragonal. Further investigations are needed to determine the site symmetry after each phase transition. X-ray studies as a function of temperature would be of considerable help. The temperature T_b should also be confirmed by specific heat measurements.

REFERENCES

1. Bowers K.D. and Owen J., Reports on Prog. in Phys. 18, 304 (195
2. Orton J.W. ibid. 22, 204 (195
3. Kusha and Rogers, ESR of Ist row transition metal complex io 'Radical Ions', Ed., Kaiser E.T. and Kevan L., John-Wiley)(196
4. Artman J.O., Magnetic Resonance Review 1, 169 (1972).
5. Ingram D.J.E., Proc. Phys. Soc. A66, 412 (1953).
6. Brovetto P., Cin G. and Ferroni S., Nuovo. Cim. 10, 1325 (1953)
7. Hayashi I. and Ono K., J.Phys. Soc. Japan 8, 270 (1953).
8. Bleaney B. and Ingram D.J.E., Proc. Roy. Soc. (London) A205, 336 (1951).
9. Janakiraman R. and Upreti G.C., Chem.Phys. Lett. 4, 550 (1970)
10. Trenam R.S., Proc. Phys. Soc. A66, 118 (1953).
11. Von Ormondt D. and Thalhammer T., Phys. Lett. 14, 169 (1965).
12. Arakawa T., J. Phys. Soc. Japan 9, 790 (1954).
13. Janakiraman R. and Upreti G.C., Phys. Stat. Sol. (b) 47, 679 (1971).
14. Janakiraman R. and Upreti G.C., J.Chem.Phys.54, 2338 (1971).
15. Fritz I.J. and Yarmus L., Phys.Rev.173, 445 (1968).
16. West C.D., Z.Kristall. 91A, 480 (1935).
17. Battey M.H., 'Minerology for students' Ist edition, Oliver and Boyd, Edinburgh, Chap. 2, p. 69 (1972).

18. Wyckoff W.G., Crystal Structure, Vol. 3, 2nd Edition Interscience Publishers, p 814 (1965).

19. Bleaney B. and Trenam R.S., Proc. Roy. Soc. (Lond.) A 223, 1 (1954).

20. Folen V.J., Phys. Rev. 125, 1581 (1962).

21. Brock E.G., Strippe D. and Hornats E.I., J. Chem. Phys. 37, 2735 (1962).

22. Burley S.P., Aust. J. Phys. 17, 537 (1964).

23. Bleaney B., Phil.Mag. 7, 441 (1951).

24. Low W., Paramag. Res. in Solids, (Solid State Phys., Supplement 2, Ed. Seitz and Turnbull), (1960).

25. Van Vleck, Phys. Rev. 74, 1168 (1948).

26. Vanier J., Canad. J. Phys. 42, 494 (1964).

27. Hinckley C.C. and Morgan L.O., J. Chem. Phys. 44, 898 (1966).

28. Ross R.T., J. Chem. Phys. 42, 3919 (1965).

29. Burns G., Phys. Rev. 135, A 479 (1964).

30. Hempstead C.F. and Bowers K.D., Phys. Rev. 118, 131 (1960).

31. Friedman E. and Low W., Phys. Rev. 120, 408 (1960).

32. Drumheller J.E. and Rubins R.S., Phys. Rev. 133, A1099 (1964)

33. Wolga G.J. and Tseng R., Phys. Rev. 133, A1563 (1964).

34. Matarrese L.M., J. Chem. Phys. 34, 306 (1961).

35. Waldner F., Helv. Phys. Acta. 35, 756 (1962).

36. Schneider J. and Sircar S.R., Z. Naturf., 17a, 651 (1962).

37. Folen V.J., Phys. Rev. 139, 6A, A1961 (1965).

38. Bleaney B. and Rubbins R.S., Proc. Roy Soc. (London), 77, 103 (1961).

39. Sheriff R.E. and Williams D., Phys. Rev. 82, 651 (1951).

40. Srivastava K.N. and Venkateswarlu P., Proc. Ind. Acad. Sci. 63, Sec. A, 311 (1966).

41. Upreti G.C., Phys. Stat. Solidi(b) 54, 387 (1972).

42. Dézsi I. and Keszthelyi L., Solid State Comm. 4, 511 (1966

43. Chaudhuri B.K. and Ghosh D., Phys. Stat. Solidi(a) 23, 649 (1974).

44. Chaudhuri B.K., J.Phys. C: Solid State Phys. 7, 3962 (1974

45. Chaudhuri B.K., Ind. J. Pure and Appld. Phys. 13, 363 (1975).

46. Chaudhuri B.K., Solid Stat. Comm. 16, 767 (1975).

47. Müller K.A., Ferroelectric 7, 17 (1974).

48. Rousseau J.J., Rousseau M. and Fayet J.C., Phys. Stat. Solidi(b) 73, 625 (1976).

49. Müller K.A., 'Structural Phase Transition and Softmodes', Universitat forlaget, (Ed., Samnuelsen E.J., Andersen E. and Feder J.), p.73 (1971).

50. Manoogian A. and Leclerc A., J. Chem. Phys. 63, 4450, 4456 (1975).

51. Serway R.A., Phys. Rev. B.3, 608 (1971).

52. References 43 to 52 in Chapter II.

53. Reiff W.M., Frankel R.B. and Abeledo C.R., Chem. Phys. Lett. 22, 124 (1973).

54. Chaudhuri B.K., Ind. J. Pure and Appld. Phys. 14, 525 (1976).

CHAPTER IV

ELECTRON PARAMAGNETIC RESONANCE STUDY OF Mn^{2+} DOPED ZINC PERCHLORATE HEXAHYDRATE

Abstract

An EPR study of Mn^{2+} doped $Zn(ClO_4)_2.6H_2O$ has been made from room temperature to the liquid nitrogen temperature. The crystal structure of this host is similar to that of MgPH at room temperature. We find that Mn^{2+} goes at sites of trigonal symmetry replacing Zn^{2+}. Hyperfine forbidden transitions are observed for H off the crystallographic c-axis. The observed linewidths show normal concentration dependence. The temperature variation study indicates a probable structural phase transition at 284 $\pm$ 2K. No other phase transition seems to occur down to 77K, the lowest temperature attainable in the present study.

Introduction :

The EPR study of $Zn(ClO_4)_2.6H_2O:Mn^{2+}$ system at room temperature was first reported by Fritz and Yarnus[1] in 1968 for the experimental arrangement in which the static magnetic field H was kept parallel to the microwave magnetic field and also for the case in which H was perpendicular to it. Their main interest was to compare the results obtained from these two configurations and to observe the forbidden transitions ($\Delta M = \pm 1$, $\Delta n = \pm 1$) in the parallel field case because the selection rules forbidding these transitions break in this arrangement[2]. In the present work, the forbidden transitions have been observed at room temperature in the perpendicular field case and the EPR study has been extended from room temperature to liquid nitrogen temperature. A probable structural phase transition is suspected in $Zn(ClO_4)_2.6H_2O$ at 284 ± 2K.

Crystal Structure and Crystal Growth :

The crystal structure of $Zn(ClO_4)_2.6H_2O$ (to be called as ZnPH in the following text) is essentially the same as that of $Mg(ClO_4)_2.6H_2O$. The dimensions[3] of the orthorhombic pseudohexagonal unit cell are

$$\underline{a} = 7.76 \text{ Å}, \quad \underline{c} = 5.20 \text{ Å}$$

For the preparation of compound, the crystal growing and the EPR study, the procedure described in Chapter III is followed. The crystals obtained are similar to those of magnesium perchlorate hexahydrate (MgPH).

Results and Discussion :

An allowed ($\Delta M = \pm 1$, $\Delta m = 0$) 30 line EPR spectrum of Mn^{2+} in ZnPH for H parallel to c is observed at room temperature. It is shown in Fig. 4.1. The angular variation of this spectrum in the a c plane is shown in Fig. 4.2 where the fine structure transition positions have been plotted along with the theoretical curves.

The angular variation of the spectrum in the a b plane shows that the spectrum is nearly axially symmetric.

From these observations, it is concluded that as in MgPH, here also the Mn^{2+} substitutes for Zn^{2+} inside a trigonally stretched water octahedron and gives an allowed 30-line spectrum for H along c at room temperature. However, in this system no triplet splittings of the lines are observed in angular variation of the spectrum in the a c plane. Probably the effect of the Zn^{2+} neighbours beyond water-perchlorates is much less compared to that in the MgPH. In MgPH, Mg^{2+} has much smaller ionic radius (0.65 Å) than that of Mn^{2+} (0.80 Å), while in ZnPH, Zn^{2+} has ionic radius (0.74 Å)

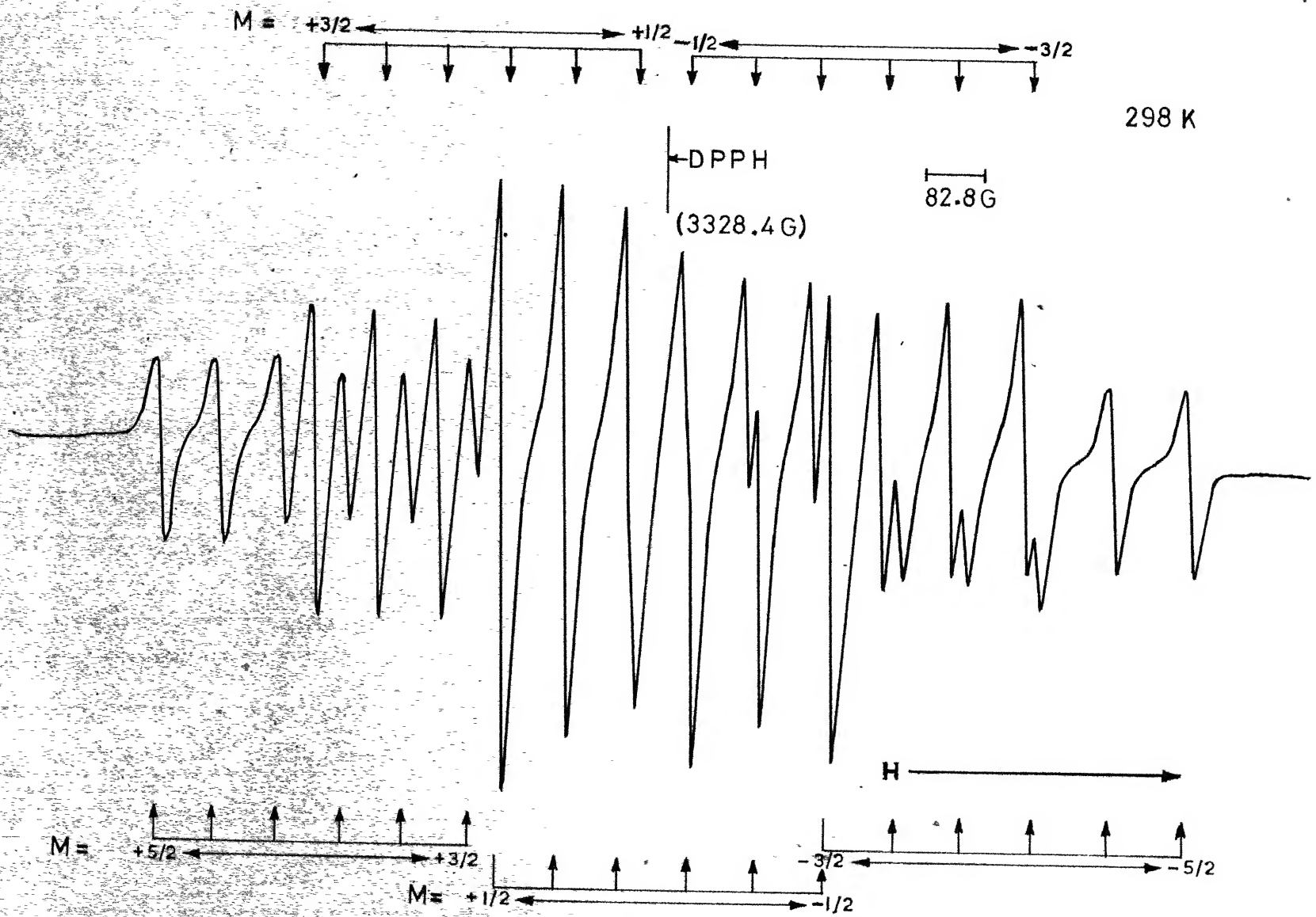

Fig. 4.1 The EPR spectrum of Mn^{2+} in $Zn(ClO_4)_2 \cdot 6H_2O$ crystal with $H \parallel c$ at room temperature.

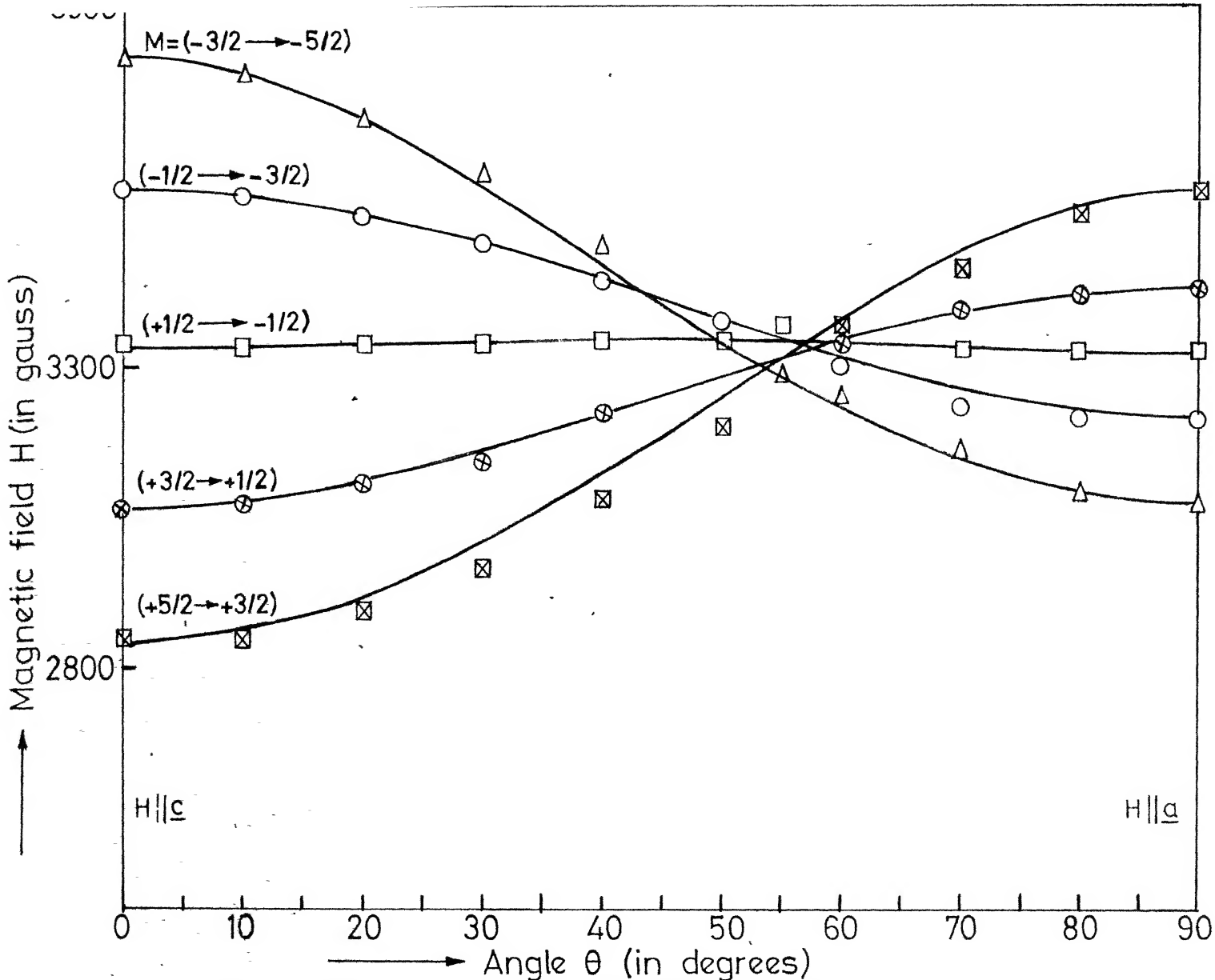

Fig.4.2 Angular variation of fine structure tran. positions in the a c plane in EPR spectrum of Mn^{2+} in $Zn(ClO_4)_2 \cdot 6H_2O$ crystal.

which is not as small as 0.65 Å. Thus, Mn^{2+} in the former case will be more affected by Mg^{2+} ion than Zn^{2+} in the latter case and therefore in the present system three sites will be almost equivalent and the lines do not split. As the angular variation of the spectrum in the a c plane is described by the spin-Hamiltonian given by Eq. 3.1, the spin-Hamiltonian parameters have been calculated using Eqs. 3.4, 3.5 and 3.8 and the values obtained are

$$g_{\parallel} = 2.0026 \pm 0.0010 \qquad g_{\perp} = 2.0005 \pm 0.0010$$

$$D = 125.50 \pm 1.0 \text{ G} \qquad (a-F) = 10.2 \pm 1.0 \text{ G}$$

$$A = 93.30 \pm 1.0 \text{ G} \qquad B = -93.9 \pm 2.0 \text{ G}$$

where the signs of the parameters are relative. These values agree with those obtained by Fritz and Yarmus[1].

Linewidths in the EPR spectrum of Mn^{2+} in the ZnPH for H along c at room temperature are found to increases with the increase in the impurity concentration. Also the EPR lines in the central hyperfine sextet have smaller widths than those of the outer sextets. These observations are similar to those in the MgPH:Mn^{2+} system and thus have an identical explanation.

The hyperfine forbidden transitions are observed between the lines of the central hyperfine sextet when the magnetic field H is off the c-axis. These are shown in Fig. 4.3 for H at 30° from the c-axis in the a c plane and are produced due to a second order mixing of A with D and a. Using Eq. 3.9 and the doublet separation in the spectrum for H at 30° from the c-axis, the value of Q' and $\frac{\gamma\beta}{g\beta}$ are calculated and are found as

$$Q' = - 0.011 \text{ G}$$

$$\frac{\gamma \beta_n}{g\beta} = 0.36 \times 10^{-3}$$

Temperature Variation and Structural Phase Transition Studies :

For the temperature variation study with a view to investigate any possible phase transition in this crystal, the method described in Chapter III is followed. The crystal is mounted such that it can be rotated in the b c plane for the reasons already pointed out in that chapter. The spectrum for H parallel to c has been studied from room temperature to liquid nitrogen temperature. The changes in the spread of the spectrum with the temperature are found to be very small.

As the temperature is lowered, the spread of the hyperfine spectrum increases very slowly and probably some rearrangement takes place at 284.0 ± 2.0K in the lattice because below this temperature, the lineshape distorts. The distortion in

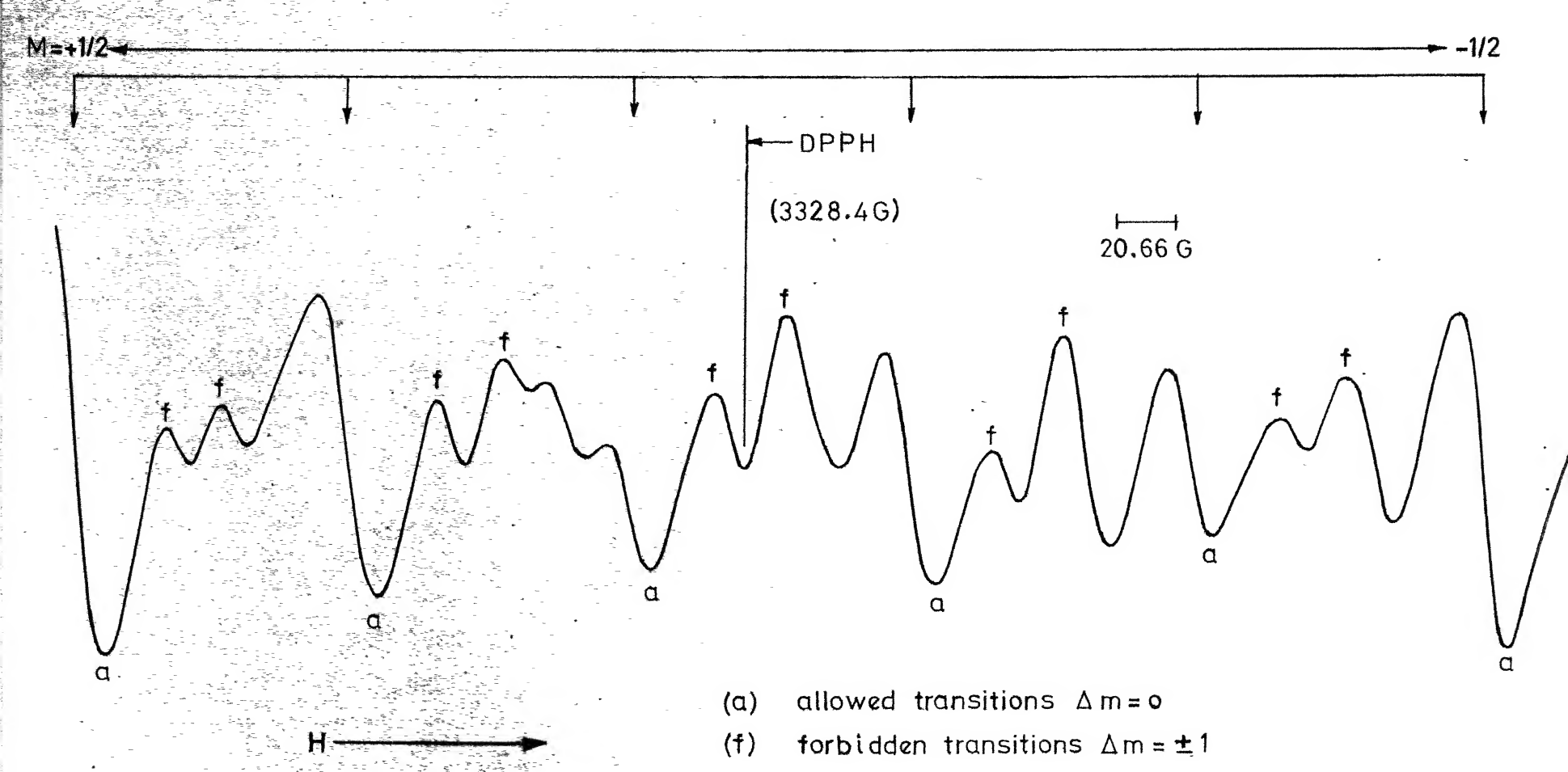

Fig. 4.3 Hyperfine forbidden ($\Delta M = \pm 1$, $\Delta m = \pm 1$) transitions of $M = +1/2 \rightleftharpoons -1/2$ for H making an angle 30° from c-axis in the ac plane in $Zn(ClO_4)_2 \cdot 6H_2O : Mn^{2+}$

the line shape becomes more and more with further decrease in temperature. Fig. 4.4 shows a comparison of the EPR spectra recorded at various temperatures for H parallel to c.

Hyperfine forbidden transitions between the central group of the allowed lines also appear at lower temperatures as seen from Fig. 4.4(d). These also indicate some internal rearrangement in the lattice.

From line shape distortion and appearance of hyperfine forbidden transitions, a probable phase transition seems to occur at 284 ± 2K. No other phase transition has been detected between room temperature to liquid nitrogen temperature. The mechanism of the probable phase transition occuring at 284.0 ± 2.0K in this system cannot be guessed from the present study.

REFERENCES

1. Fritz I.J. and Yarmus L., Phys. Rev. 173, 445 (1968).
2. Smith S.R.P., Auzins P.V. and Wertz J.E., Phys. Rev. 166, 122 (1968). (and references therein).
3. West C.D., Z. Kristall. 91A, 480 (1935).

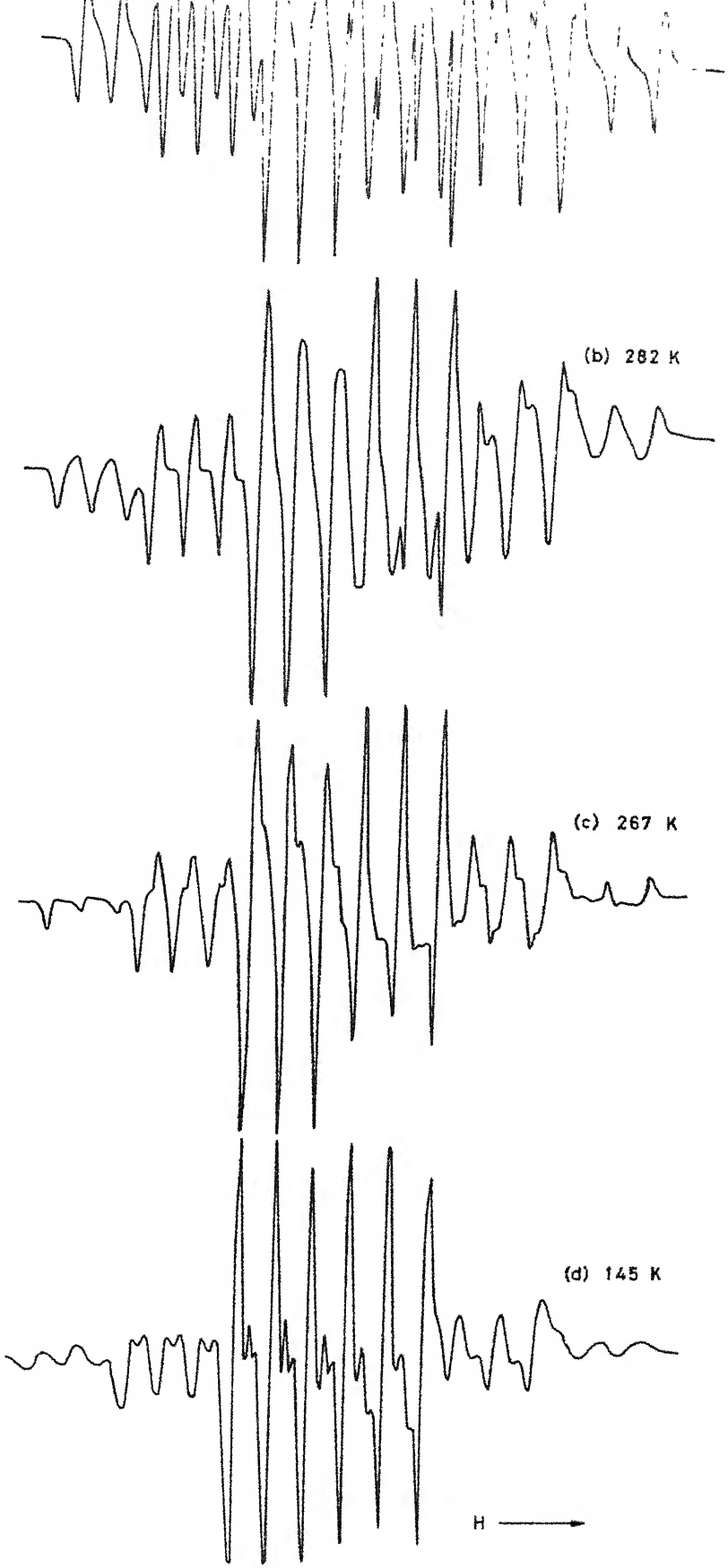

Fig. 4.4 A comparision of the EPR spectra of Mn^{2+} in $Zn(ClO_4)_2 \cdot 6H_2O$ for H||c at different temperatures. Line distortion is clearly seen.

CHAPTER V

ELECTRON PARAMAGNETIC RESONANCE STUDY OF Mn^{2+} DOPED CADMIUM PERCHLORATE HEXAHYDRATE

Abstract

Electron paramagnetic resonance of Mn^{2+} doped in $Cd(ClO_4)_2.6H_2O$ has been studied from room temperature to liquid nitrogen temperature. The site symmetry of Cd^{2+} is trigonal with a water octahedron stretched parallel to crystallographic c-axis. Mn^{2+} substitutes for Cd^{2+} and exhibits characteristic 30-line hyperfine spectrum at room temperature for the magnetic field H along the c-axis. D paramater is small and therefore, there is considerable overlapping of lines in the spectrum. The spectrum is axially symmetric. On lowering the temperature, phase transitions are found to occur at 272 $\pm$ 1K, 259 $\pm$ 2K and 115.5 $\pm$ 1.0K. The transitions occuring at 272 $\pm$ 1K and 259 $\pm$ 2K seem to be of the second order while the one at 115.5 $\pm$ 1.0K is of the first order. The D parameter has been determined experimentally and fitted with theoretical expressions.

Introduction:

The electron paramagnetic resonance study of Mn^{2+} has been made in different compounds of cadmium such as CdS[1], CdTe[2], CdSe[3] etc. but in the literature, there seems to be no information obtained about cadmium perchlorate hexahydrate $Cd(ClO_4)_2.6H_2O$ single crystals by EPR or any other method except the crystal structure determination at room temperature by West in 1935. The EPR study of Mn^{2+} doped $Cd(ClO_4)_2.6H_2O$ is presented for the first time in this work.

Crystal structure:

The crystal structure of $Cd(ClO_4)_2.6H_2O$ [hereafter to be referred as CdPH] was determined by West[4] in 1935 and it is slightly different from the structure of $Mg(ClO_4)_2.6H_2O$ (referred to earlier as MgPH) at room temperature. The atoms in MgPH are arranged in an orthorhombic unit cell with space group C_{2v}^7 but in CdPH they are arranged in a trigonal unit cell with space group C_{3v}^1 as shown in Fig. 5.1. However, hexagonal units of the two structures are related. In Fig. 5.1, the whole of unit shown is hexagonal unit. Each Cd^{2+} is surrounded by a water octahedron stretched

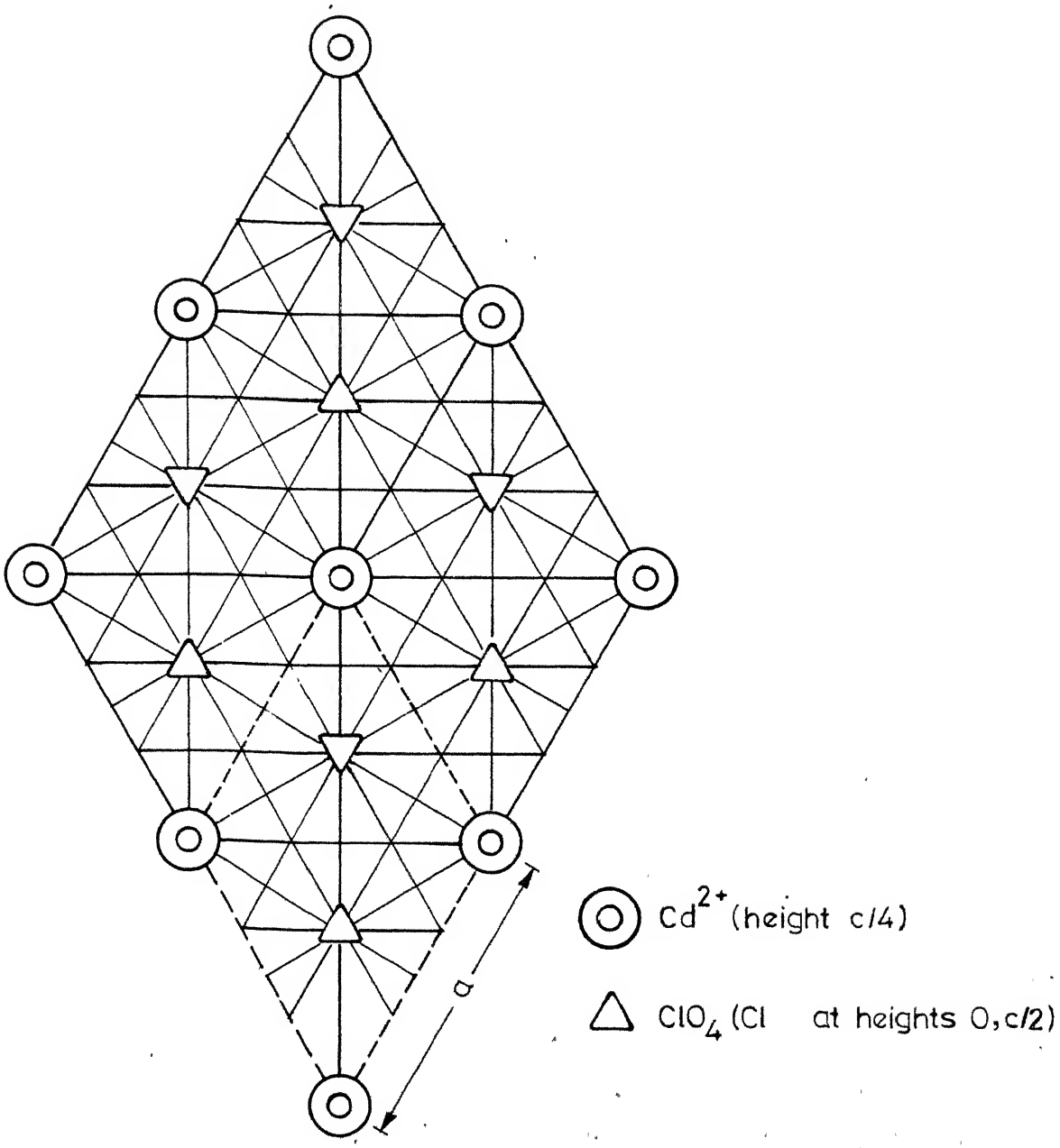

Fig.5.1 Schematic structure of $Cd(ClO_4)_2.6H_2O$, C_{3v}^1 projected on basal plane. Triangles in two different orientations are ClO_4 tetrahedrons at two different heights. Unit cell is outlined by dotted lines. Water molecules are not shown.

along the crystallographic c-axis or the prism axis. The site symmetry is trigonal. The dimensions of the unit cell of CdPH are

$$a = 7.96 \text{ Å}, \qquad c = 5.30 \text{ Å}$$

Experimental :

For the preparation of the compound CdPH, the crystal growing and the EPR study, the procedure followed is the same as in Chapter III. The crystals of CdPH grow in the form of hexagonal prisms with clear end faces, c-axis being the prism axis. The crystals are very hygroscopic and were therefore coated with a mixture of petroleum jelly and paraffin oil before proceeding for the EPR study.

Results and Discussion :

The EPR study of Mn^{2+} doped CdPH at room temperature has been made with H in the a c and a b plane. For the magnetic field H parallel to the prism axis c, this system exhibits a spectrum of 30 allowed ($\Delta M = \pm 1$, $\Delta m = 0$) hyperfine lines, with a considerable overlapping probably due to a smaller value of D. The spectrum is shown in Fig. 5.2.

Angular variation of the spectrum in the a c plane shows that the maximum spread for H parallel to c decreases when H is off from the c-axis on either side and goes to a

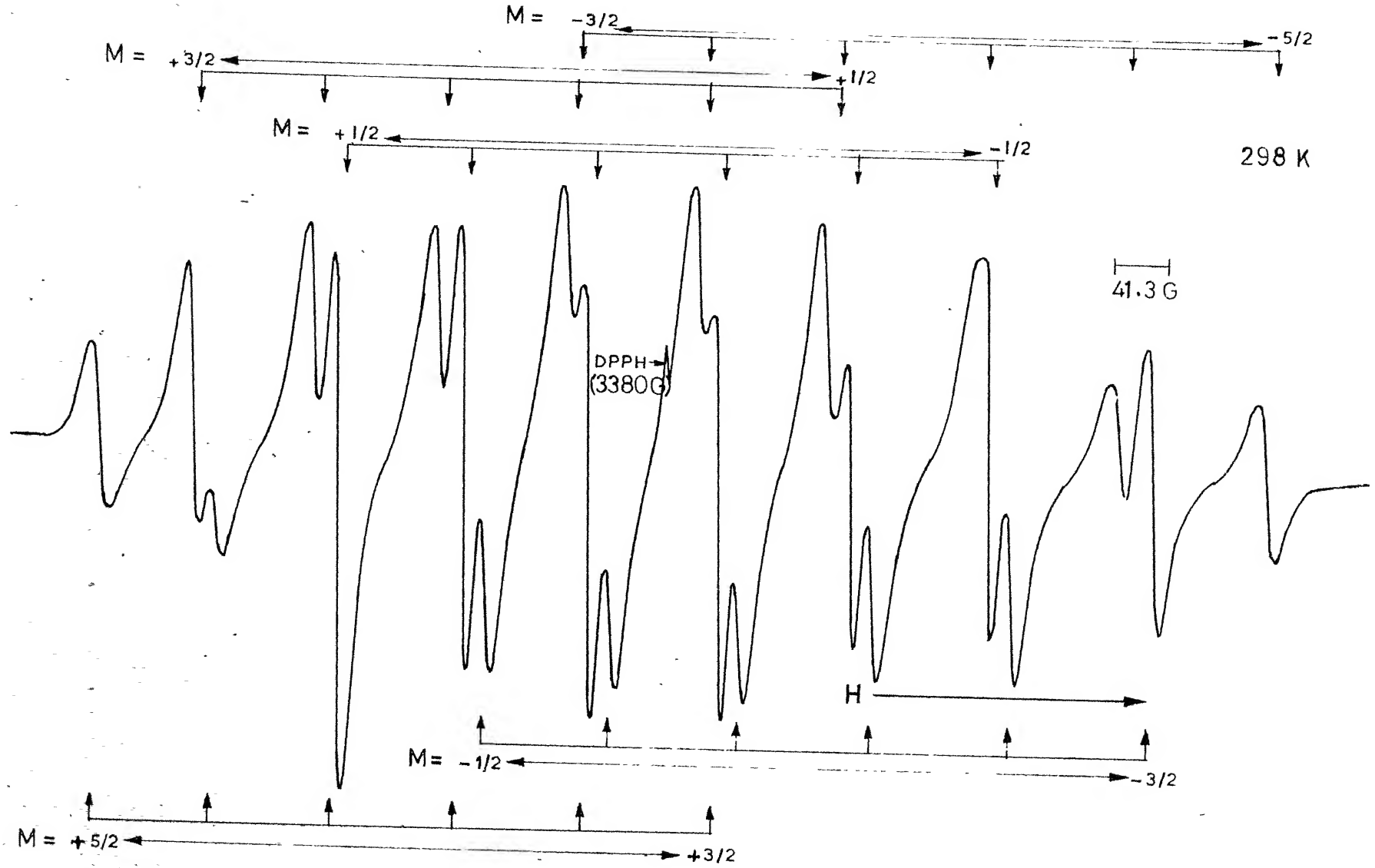

Fig.5.2 The EPR spectrum of Mn^{2+} in $Cd(ClO_4)_2 \cdot 6H_2O$ with $H \| \underline{c}$ at room temperature.

minimum. It attains a secondary maximum again for H perpendicular c i.e. H parallel to a. The angular variation of the fine structure tran. positions is shown in Fig. 5.3 where continuous lines represent the theoretical curves. The angular variation of the spectrum in the a b plane shows no changes in the spectrum and its spread remains constant with in the experimental error.

From the above study, we conclude that Mn^{2+} goes substitutionally replacing Cd^{2+} in the CdPH lattice and thus sits at the site of trigonal symmetry with distorted water octahedron. The principal z-axis is parallel to c. The stretching of the water octahedra is less as compared to that in magnesium and zinc perchlorate hexahydrates. This system may be considered as a good axial system. The angular variation of the spectrum may be represented by the spin-Hamiltonian described in Chapter III (Eq.3.1).

The spin-Hamiltonian parameters have been calculated using Eqs. 3.4, 3.5 and 3.8 of Chapter III and values obtained are

$$g_{||} = 2.0012 \pm 0.0010,\ g_{\perp} = 1.9999 \pm 0.0010;\ D = 47.8 \pm 1.0G$$

$$A = -92.7 \pm 1.0G\ ,\ B = -93.9 \pm 2.0G;\ (a-F) = 6.7 \pm 1.0G$$

Concentration dependent line broadening has been observed in this system also. However, it has not been possible to

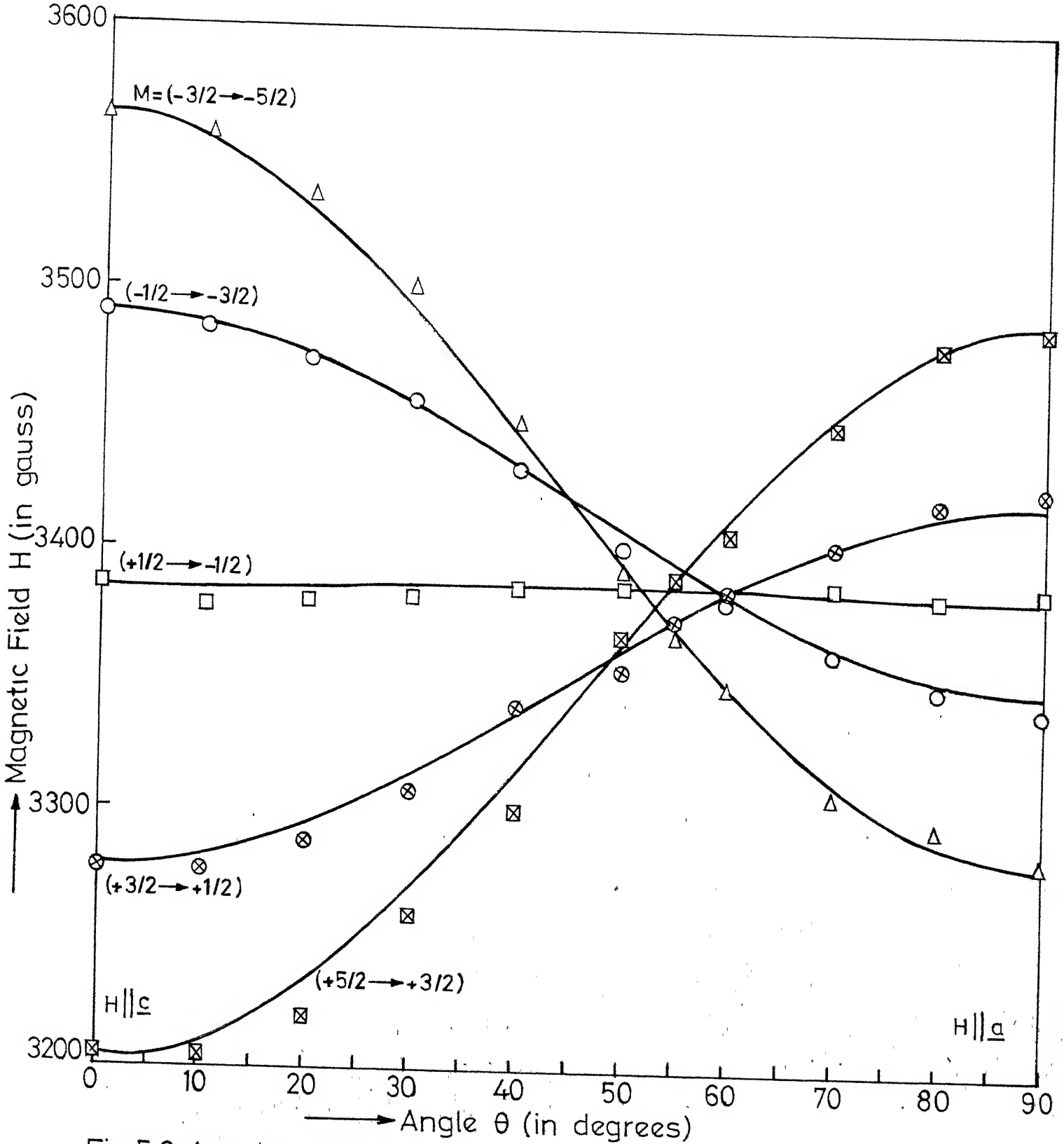

Fig. 5.3 Angular variation of fine structure tran.positions in the ac plane in EPR spectrum of Mn^{2+} in $Cd(ClO_4)_2 \cdot 6H_2O$ crystal.

observe the behaviour of the lines of different hyperfine groups due to overlapping.

TEMPERATURE VARIATION STUDY AND STRUCTURAL PHASE TRANSITIONS

The experimental arrangement is kept such that the magnetic field H is applied in the b c plane of the Mn^{2+} doped CdPH crystal and the crystal is rotated about a-axis. The temperature variation study of the spectrum for H parallel to c is made from 328 K to the liquid nitrogen temperature. The study is also made in the a b plane by keeping the crystal axis perpendicular to the field such that the crystal is rotated about c-axis. If the crystal is dipped in liquid nitrogen it gets completely shattered. Therefore it has to be cooled very slowly during the temperature variation study. As the temperature is lowered, the spread of the spectrum decreases gradually. At the temperature T_a (272 $\pm$ 1 K), a sudden change in the spectrum is observed on the oscilloscope. The spectrum disappears in a short time and a new spectrum with larger spread appears. Disappearance and appearance are clearly observed on the oscilloscope. This indicates that a phase transition has occured at the temperature T_a. After the phase transition is complete, the EPR lines in the spectrum at 271 K are much more resolved as compared to those in the room temperature

spectrum (Fig. 5.2). Fig. 5.4 shows the spectrum at this temperature. The change in the spectrum is not so sudden that it may be considered as due to a first order phase transition.

The angular variation of the spectrum around 271 K in the b c plane shows that this spectrum also has a maximum spread for H parallel to c which means that the principal z-axis is the same after the phase transition. The angular variation study in the a b plane shows that the spectrum is axially symmetric.

After the first transition, the spread of the spectrum increases very slowly in the small temperature range till T_b (259 $\pm$ 2 K). It appears that some sort of rearrangement takes place in the lattice very slowly and it is complete at T_b. Thus T_b may also be called a phase transition temperature, the order of the phase transition being second or higher. The principal axes and sites remain unchanged in this range.

Below T_b, the decrease in temperature results in a decrease of the spread. The spread keeps on decreasing continuously till at T_c (115.5 $\pm$ 1.0 K) a third phase transition occurs. This transition is of the first order. An entirely different spectrum appears after this phase transition. From T_b to T_c,

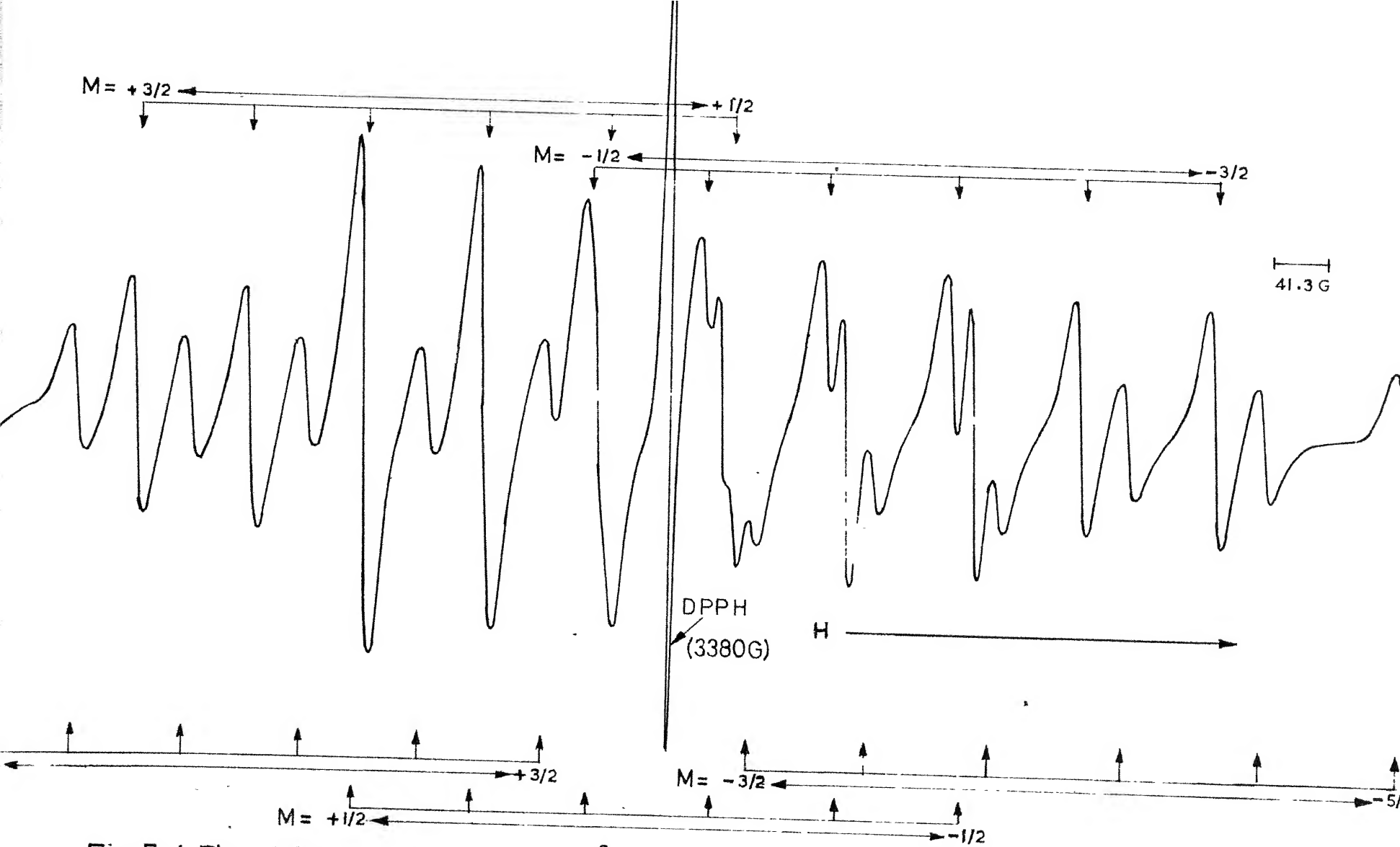

Fig.5.4 The EPR spectrum of Mn^{2+} in $Cd(ClO_4)_2 \cdot 6H_2O$ at 271 K (just after the first phase transition) with H parallel to c-axis.

again the principal z-axis is found to be parallel to c and spectrum remains axially symmetric in the a b plane.

After the third phase transition i.e. below T_c, the angular variation in b c plane shows that there are several extrema. These may correspond to different sites for Mn^{2+} in the lattice. One relatively well resolvedspectrum with extremum is found for H at 11° from the c-axis. It is shown in Fig. 5.5. Another spectrum with extremum is found for H approximately 54° from the c-axis. The spectra are quite complex and indicate that there are several sites for Mn^{2+}. The principal axes of the different sites are oriented in different directions.

Fig. 5.6 shows the variation of fine structure transition positions for H parallel to c with temperature. Three transition temperatures are indicated in the figure. The spectra in the three different phases for H parallel to c are shown in Fig. 5.7 for comparison.

Temperature Variation of D :

From room temperature to liquid nitrogen temperature the CdPH is found to exist in the following phases

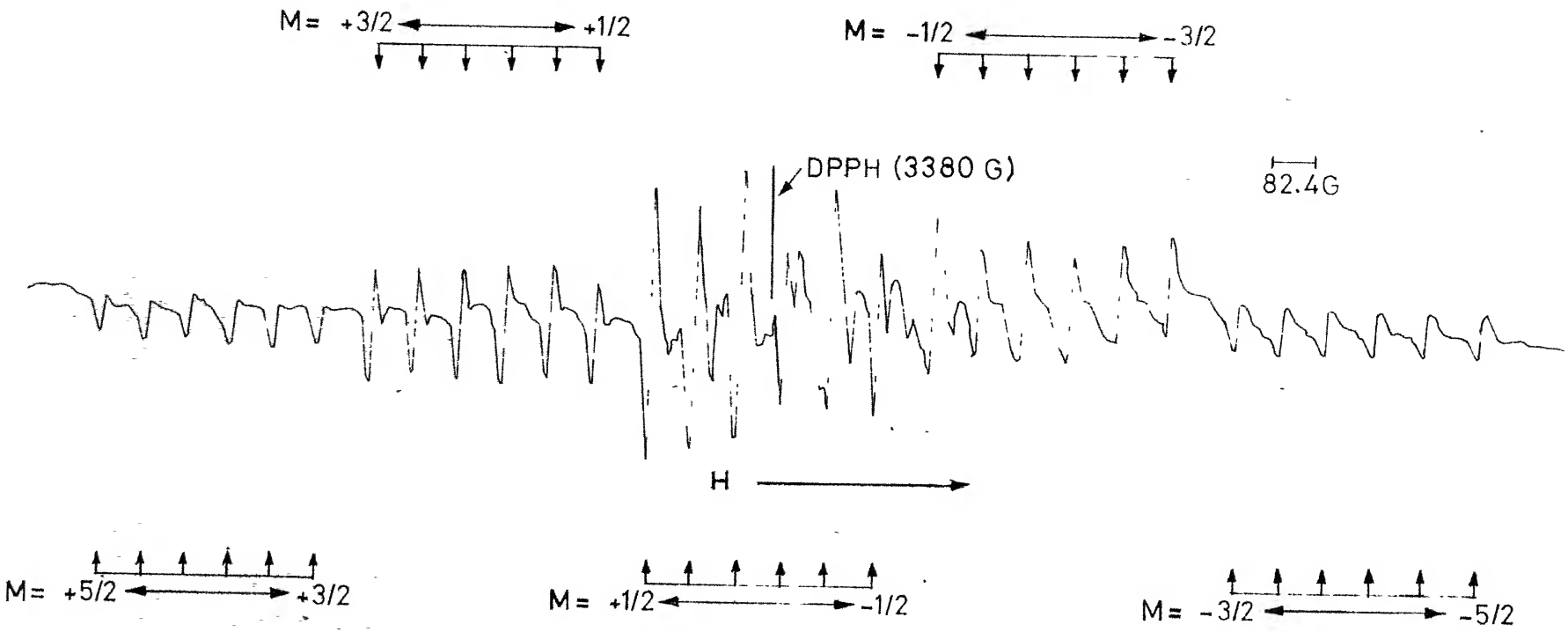

Fig.5.5 The EPR spectrum of Mn^{2+} in $Cd(ClO_4)_2 \cdot 6H_2O$ at 115 K (just after the 3rd. phase transition) with magnetic field H making an angle of 11° with the crystallographic c-axis in the bc plane.

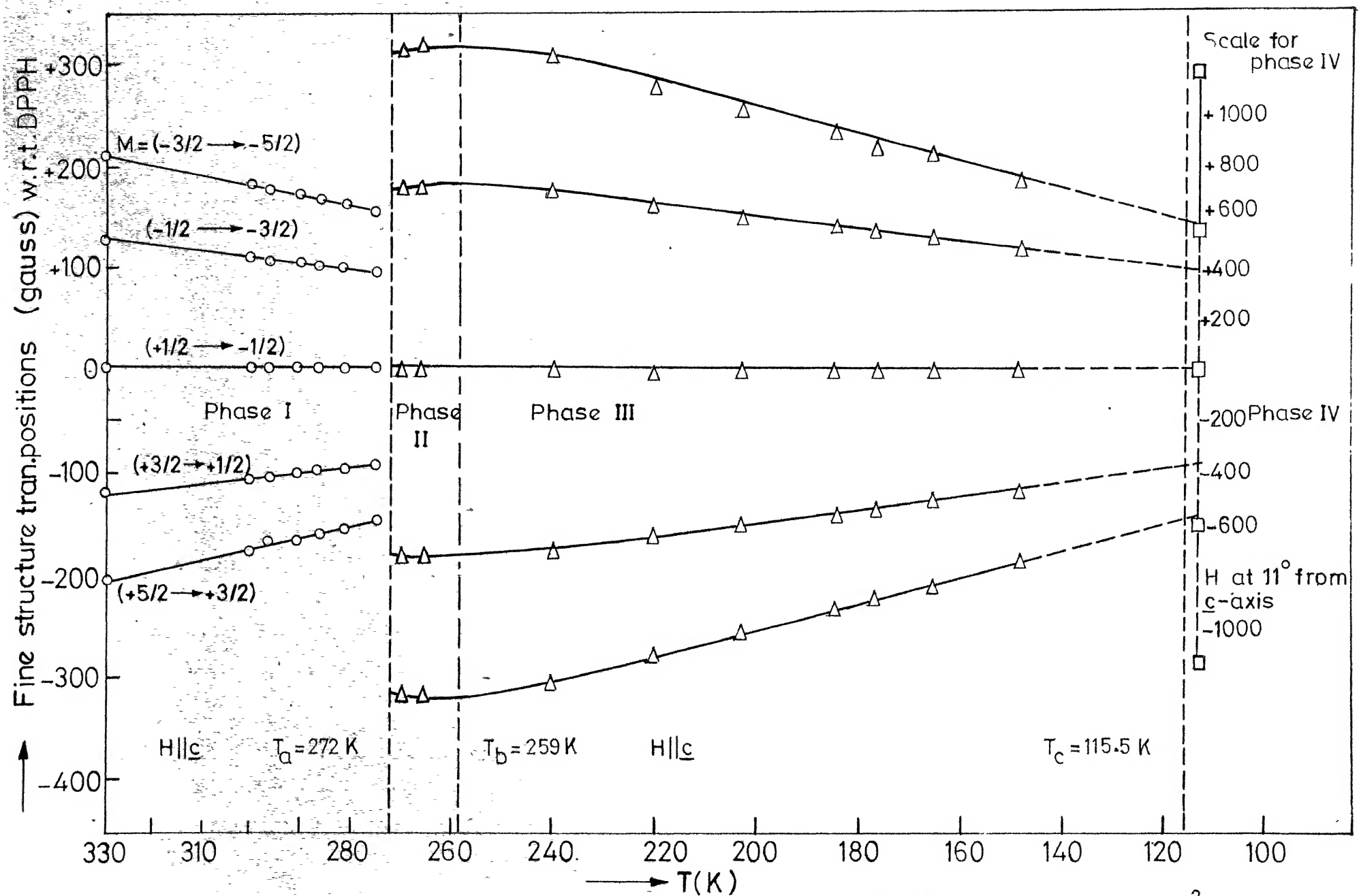

Fig. 5.6 Temperature variation of fine structure tran. positions in the EPR spectrum of Mn^{2+} in $Cd(ClO_4)_2 \cdot 6H_2O$ Crystal.

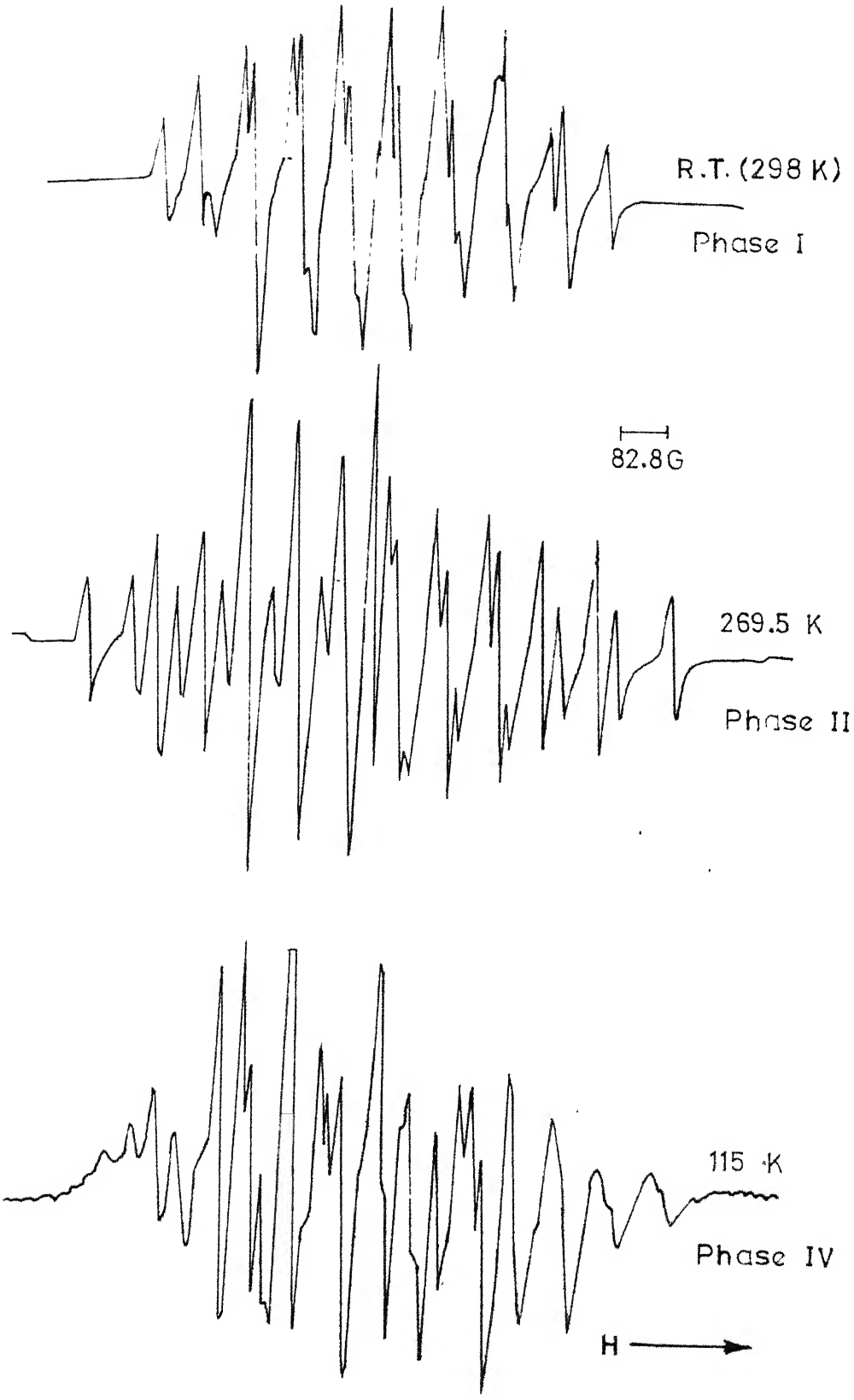

Fig.5.7 EPR spectra of Mn^{2+} in $Cd(ClO_4)_2 \cdot 6H_2O$ with H||c in three different phases.

Phase I — Phase II

R.T. $\longleftrightarrow$ T_a (272 $\pm$ 1 K) $\longleftrightarrow$ T_b

Phase III — Phase IV

T_b(259 $\pm$ 2K) $\longleftrightarrow$ T_c(115.5 $\pm$ 1K) $\longleftrightarrow$ L.N.T.

The variation of D with temperature in the phases I, II and III is shown in Fig. 5.8. In the phase I, the temperature variation of D is fitted to

$$D = D_o (1 + \alpha T + \beta T^2)$$

with values of the constants as $D_o = -36.3$ G, $\alpha = -7.675 \times 10^{-}$ $\beta = + 3.6275 \times 10^{-9}/K^2$, and the continuous line in Fig. 5.8 in phase I represents this fitted curve. This represents the thermal contraction of the lattice in which the distortion changes in such a way that D decreases, the lattice prepares itself slowly for the first phase transition occuring at T_a.

In the small region of phase II, D is seen to increase slowly with temperature till T_b at which the second or highe order transition is already proposed. In this region no theoretical curve fitting is done. In the phase III, however, D fits with the relation

$$D = D_b + m (T_b - T)$$

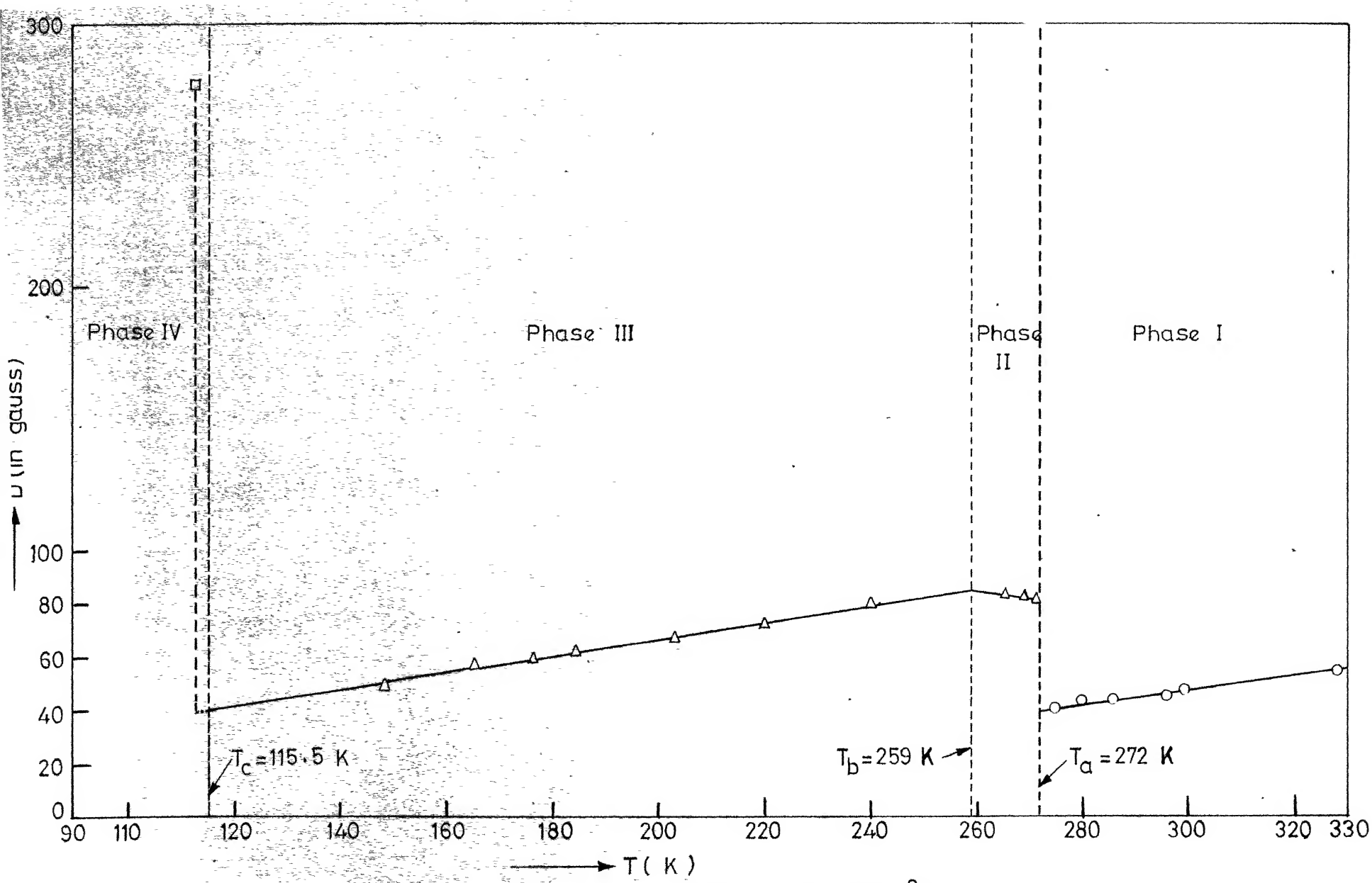

Fig.5.8 Temperature variation of D for $Cd(ClO_4)_2 .6H_2O:Mn^{2+}$ system.

with constants D_b = 84.6 G, m = -3.1235 x 10^{-1} G/K, T_b = 259K. This expresses the Landau bchaviour[5] which indicates that the phase transition at T_b is associated with some order parameter varying as $(T_b - T)^{\frac{1}{2}}$ and representing a second order transition. In phase IV, the D value for the spectrum at 11° off from the c-axis is determined assuming that the spin-Hamiltonian given by Eq. 3.1 holds for this and Eqs. 3.4, 3.5 and 3.8 may be used. It is six times larger than the value at room temperature.

The temperature variation study of the spectrum and the spin-Hamiltonian parameter D, thus show that a first order structural phase transition seems to occur at T_c, a second order phase transition at T_b and another second order phase transition at T_a. In transition from phase I to phase II at T_a, CdPH crystal transforms probably to a symmetry group closely related to C_{3v}^1. Then in the phase II, some slight rearrangement takes place and it is complete at T_b. The resulting symmetry in phase III then continues till T_c where a first order phase transition brings it from phase III to phase IV which has a different symmetry.

The mechanisms of phase transitions in this system are difficult to understand with the present experimental findings. The confirmation of transition temperature T_b is

needed and it may be done by specific heat measurements. The site symmetry determination in different phases needs further experimental study by x-rays.

REFERENCES

1.a) Title R.S., The Physics and Chemistry of II-IV Compounds, (Ed., Aven M. and Prener J.S.), Wiley N.Y., Chap. 6 (1967)

b) Wagner G.R., Murphy J., and Castle J.G., Phys. Rev. B8, 3103 (1973).

c) Kiel A. and Mims W.B., Phys. Rev. B5, 803 (1972).

d) Böttcher R. and Dziesiaty J., Phys. Stat. Solidi 31, K71 (1969).

2.a) Kikuchi G., and Azarbayejani G.H., J. Phys. Soc. Jap. 17, B-I, 453 (1962).

b) Woodbury H.H., and Ludwig G.W., Bull. Am. Phys. Soc. 6, 118 (1961).

3.a) Title R.S., Phys. Rev. 130, 17 (1963).

b) Böttcher R., and Dziesiaty J., Phys. Stat. Solidi 31, K71 (1969).

4. West C.D., Z. Kristall, 91A, 480 (1935).

5. See reference 49 in Chapter III.

CHAPTER VI

ELECTRON PARAMAGNETIC RESONANCE STUDY OF Mn^{2+} DOPED IRON, COBALT AND NICKEL PERCHLORATE HEXAHYDRATES

Abstract

Mn^{2+} doped $Fe(ClO_4)_2.6H_2O$, $Co(ClO_4)_2.6H_2O$ and $Ni(ClO_4)_2.6H_2O$ crystals have been studied by EPR at room temperature. All the crystals have the same structure as that of $Mg(ClO_4)_2.6H_2O$ and Mn^{2+} occupies the site of trigonal symmetry in them. The EPR lines are broad and D parameters are small; so there is overlapping of lines and the spectra are not well resolved. All the three spectra are axially symmetric. A temperature variation study also has been carried out from room temperature to liquid nitrogen temperature. It indicates,in addition to the already observed phase transitions (at 237 $\pm$ 5 K, 154.5 $\pm$ 65 K and 223 $\pm$ 5 K for iron, cobalt and nickel perchlorate hexhydrates respectively), one new probable structural change in $Co(ClO_4)_2.6H_2O$ at 245 $\pm$ 5 K and in $Ni(ClO_4)_2.6H_2O$ at 247 $\pm$ 5 K. The principal axes are found to turn off from the room temperature position after the phase transition at 237 $\pm$ 5 K in iron perchlorate and at 154.5 $\pm$ 6.5 K in cobalt perchlorate hexahydrates. The present study throws some light on the structural changes occuring at phase transitions, but the exact nature of these transitions is not yet fully understood.

Introduction :

The electron paramagnetic resonance study of paramagnetic ions doped as impurity in diamagnetic crystal lattices gives information about the impurity ion as well as about the diamagnetic lattice. It has been possible to obtain the information about some of the paramagnetic crystal lattices also if they are used as hosts in place of diamagnetic ones. The paramagnetic host ions normally have short[1,2] spin-lattice relaxation times at room temperature so that the EPR lines of these ions are too broad to be observed at this temperature and some other paramagnetic impurity doped in such hosts may show its own spectrum. Such host ions are Ti^{3+}, V^{3+}, Fe^{2+}, and Co^{2+} in the iron group and rare earth ions excluding Gd^{3+}, and Eu^{2+}. The paramagnetic host lattices with these ions doped with different impurities have been studied by several workers[3].

In addition, there are other paramagnetic host ions which have large zero field splitting[2] in the ground state and thus the microwave radiation does not produce transitions among the split levels at moderate fields. The crystal lattices of compounds of such ions such as Ni^{2+} are also studied by doping in them some suitable impurity ion as a probe.

The present chapter deals with the EPR study of Mn^{2+} doped single crystals of Fe, Co and Ni perchlorate hexahydrates. The Mn^{2+} acts as a probe to determine the site symmetry, the crystal field strength and phase transition temperatures. The effect of paramagnetic ions of a host on the EPR of Mn^{2+} is reflected in the spectrum. The Mössbauer effect study[4,5] and the susceptibility measurements[6-9] have been made on all these perchlorates.

Crystal Structure :

Iron, cobalt, nickel and manganese perchlorate hexahydrates, (henceforth to be referred to as FePH, CoPH, NiPH and MnPH) are isomorphous to MgPH and thus possess the crystal structure discussed in Chapter III. The dimensions[10] of the orthorhombic pseudohexagonal unit cells are given below in Table 6.1

Table 6.1 Dimensions of Unit Cells.

Crystal Lattice	a (Å)	c (Å)
FePH	7.79	5.24
CoPH	7.76	5.20
NiPH	7.73	5.17
MnPH	7.85	5.30

The ions of Fe^{2+}, Co^{2+}, Ni^{2+} and Mn^{2+} are situated at sites of trigonal symmetry formed by the water octahedra stretched along the crystallographic c-axis. Mn^{2+} easily substitutes for Fe^{2+}, Co^{2+} and Ni^{2+} as impurity in FePH, CoPH and NiPH.

Experimental :

The FePH is prepared by dissolving AR grade iron powder in dilute perchloric acid in vacuum while CoPH, NiPH and MnPH are prepared from their carbonates dissolved in dilute perchloric acid. The crystallization of the compounds in solutions is done at room temperature in a desiccator containing concentrated sulphuric acid. A solution is prepared from the crystalline solid separated after the previous crystallization, and desired impurity (MnPH) is added to it. Recrystallization gives good crystals which grow in the form of hexagonal needles similar to MgPH.

The EPR study and the temperature variation are done in the manner followed in Chapter III. All the crystals are hygroscopic and are protected from air exposure by coating with a 1:1 mixture of petroleum jelly and paraffin oil before mounting them for EPR study.

Results and Discussion :

The EPR study of the crystals of FePH, CoPH and NiPH doped with Mn^{2+} exhibits allowed hyperfine structure for magnetic field H parallel to c at the room temperature. The lines are broad and there is a considerable overlapping, therefore 30 lines of the structure are not well resolved. Figs. 6.1(a), 6.1(b) and 6.1(c) show the spectra of Mn^{2+} in FePH, CoPH and NiPH for the magnetic field H along the c-axis of the crystals.

The angular variation of the spectra in the a c plane shows a behaviour similar to that for Mn^{2+} in MgPH, ZnPH and CdPH reported in earlier chapters, and Figs. 6.2(a), 6.2(b) and 6.2(c) show the angular variation in FePH, CoPH and NiPH hosts at room temperature in the a c plane.

The angular variation in the a b plane shows up almost no appreciable change in the spread of the spectra, and any observed changes are well within the experimental error.

The above observations are consistent with the crystal structure studies for the divalent cation site, hence it can be concluded that Mn^{2+} substitutes for Fe^{2+}, Co^{2+} and Ni^{2+} respectively at the sites of trigonal symmetry and gives rise to the thirty-line spectra.

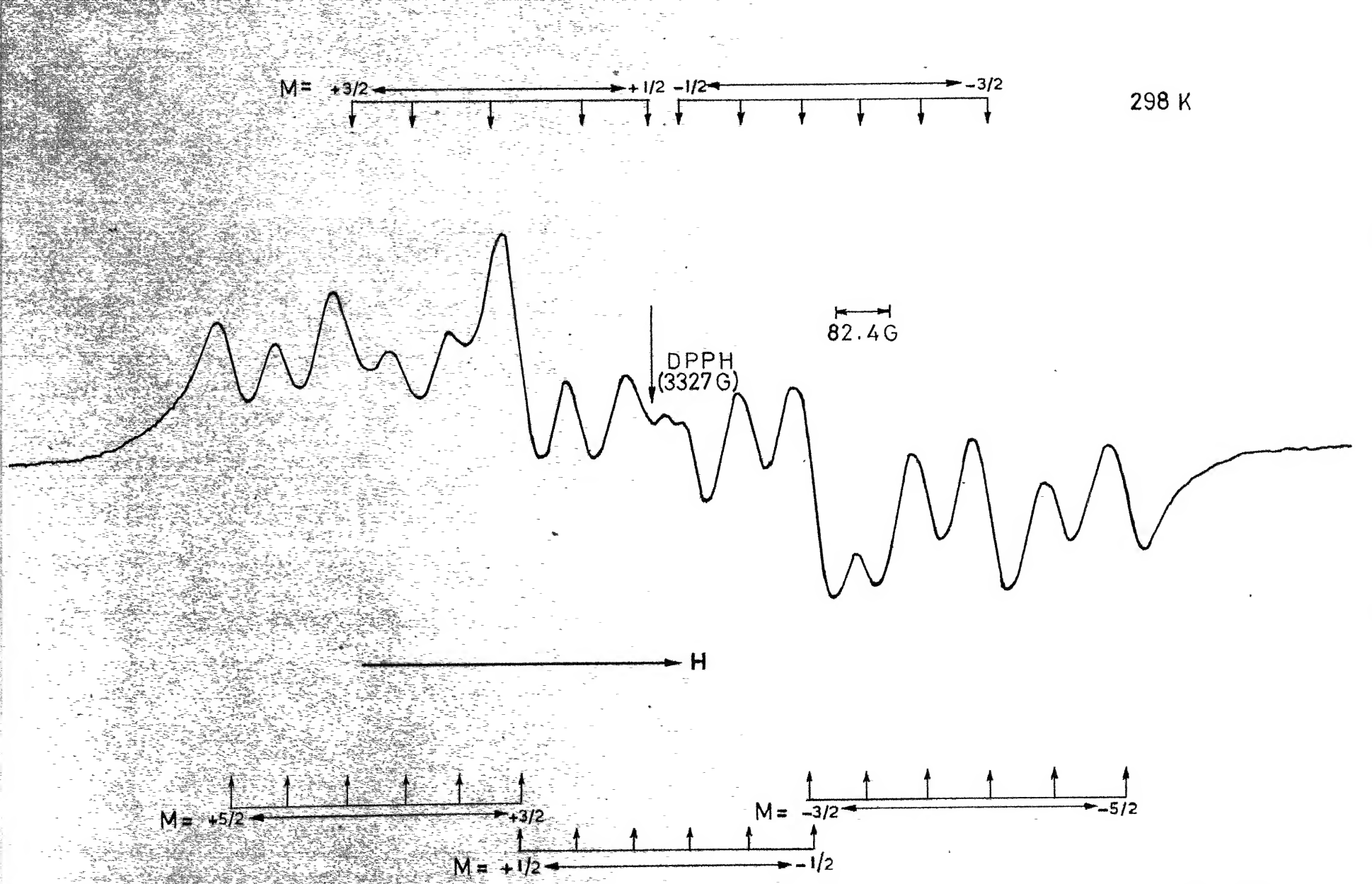

Fig.6.1(a) The EPR spectrum of Mn^{2+} in $Fe(ClO_4)_2 \cdot 6H_2O$ at room temperature with $H \| \underline{c}$.

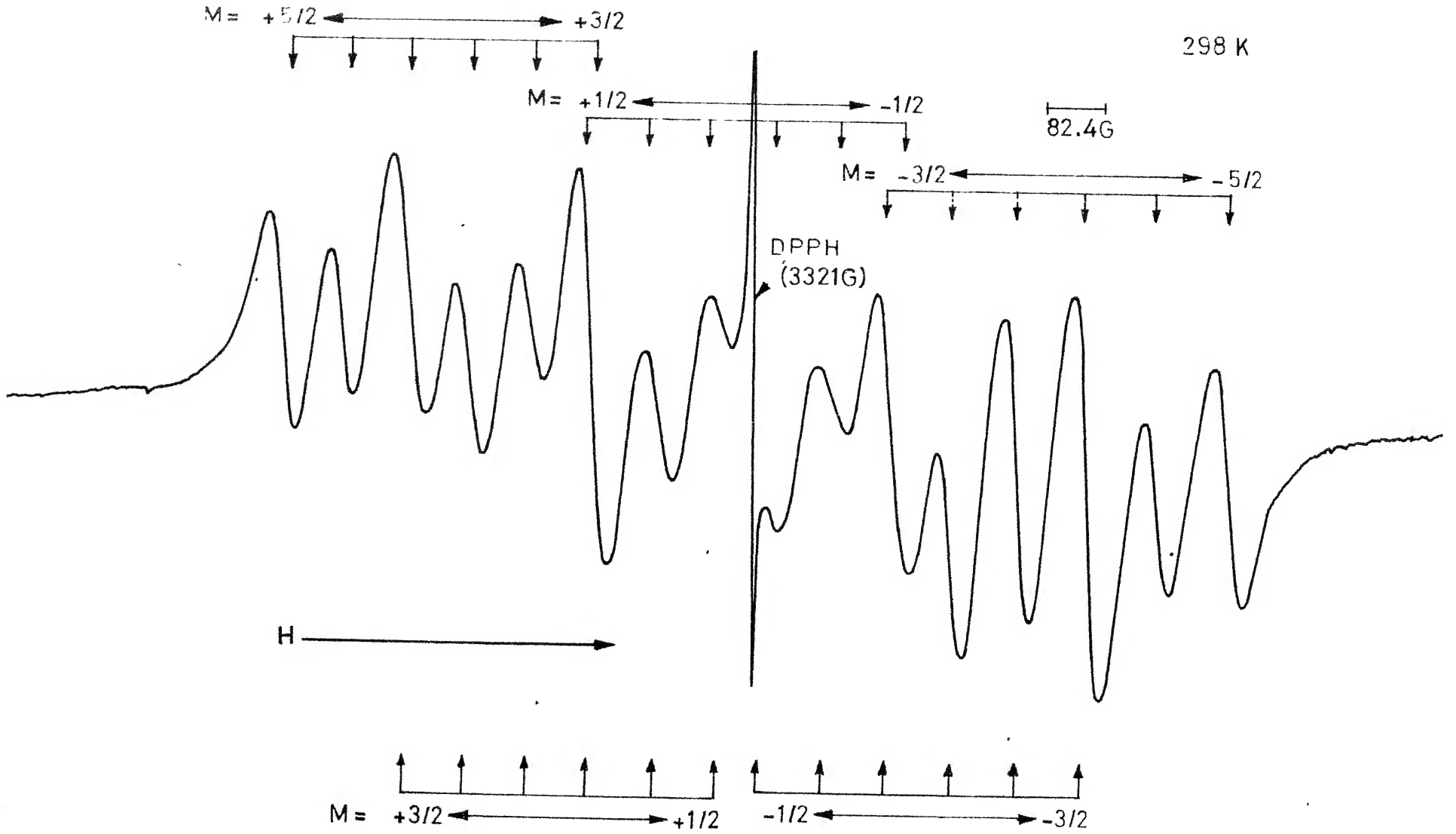

Fig.6.1(b) The EPR spectrum of Mn^{2+} in $Co(ClO_4)_2 \cdot 6H_2O$ at room temperature with H||c.

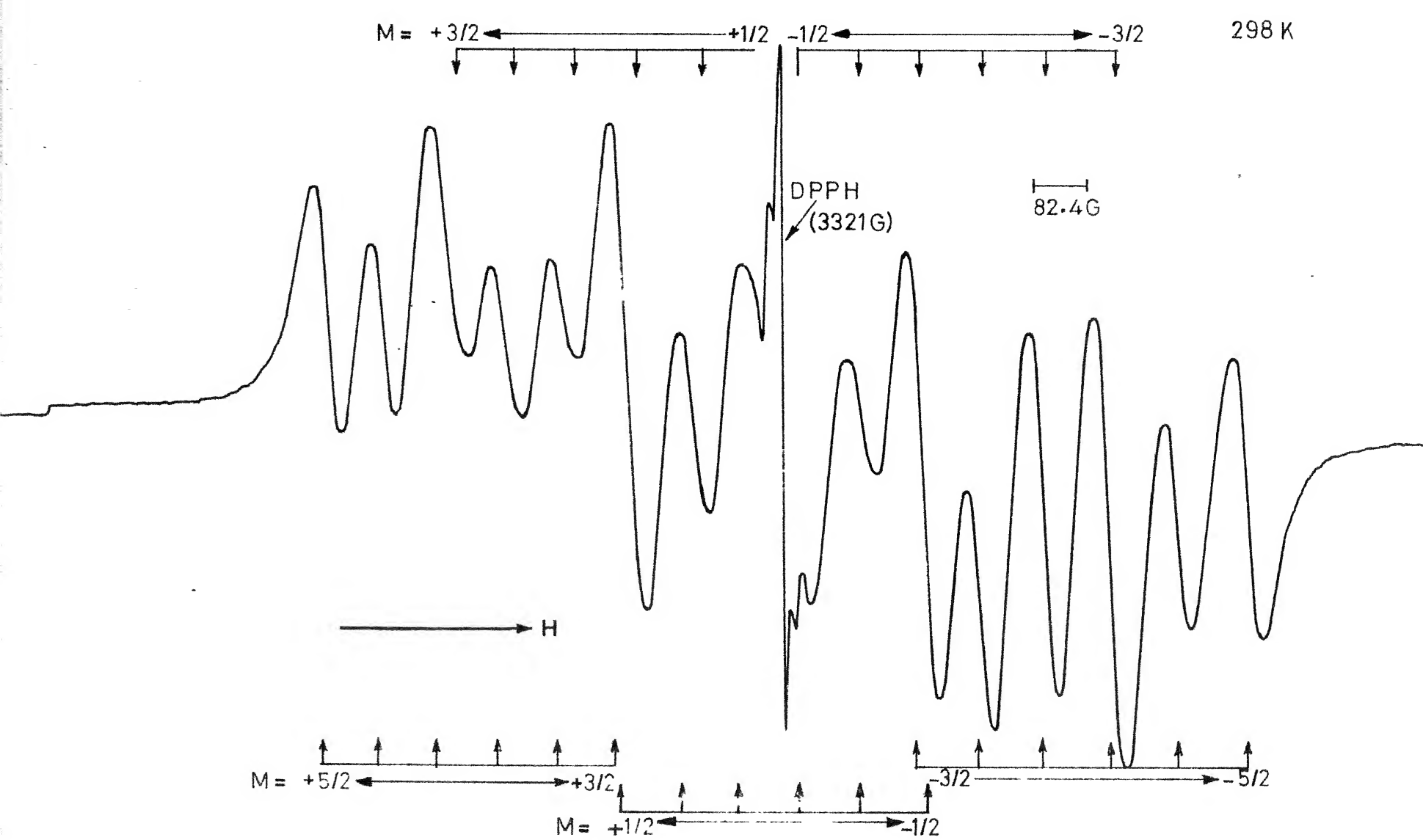

Fig.6.1(c) The EPR spectrum of Mn^{2+} in $Ni(ClO_4)_2 \cdot 6H_2O$ with $H \| \underline{c}$ at room temperature.

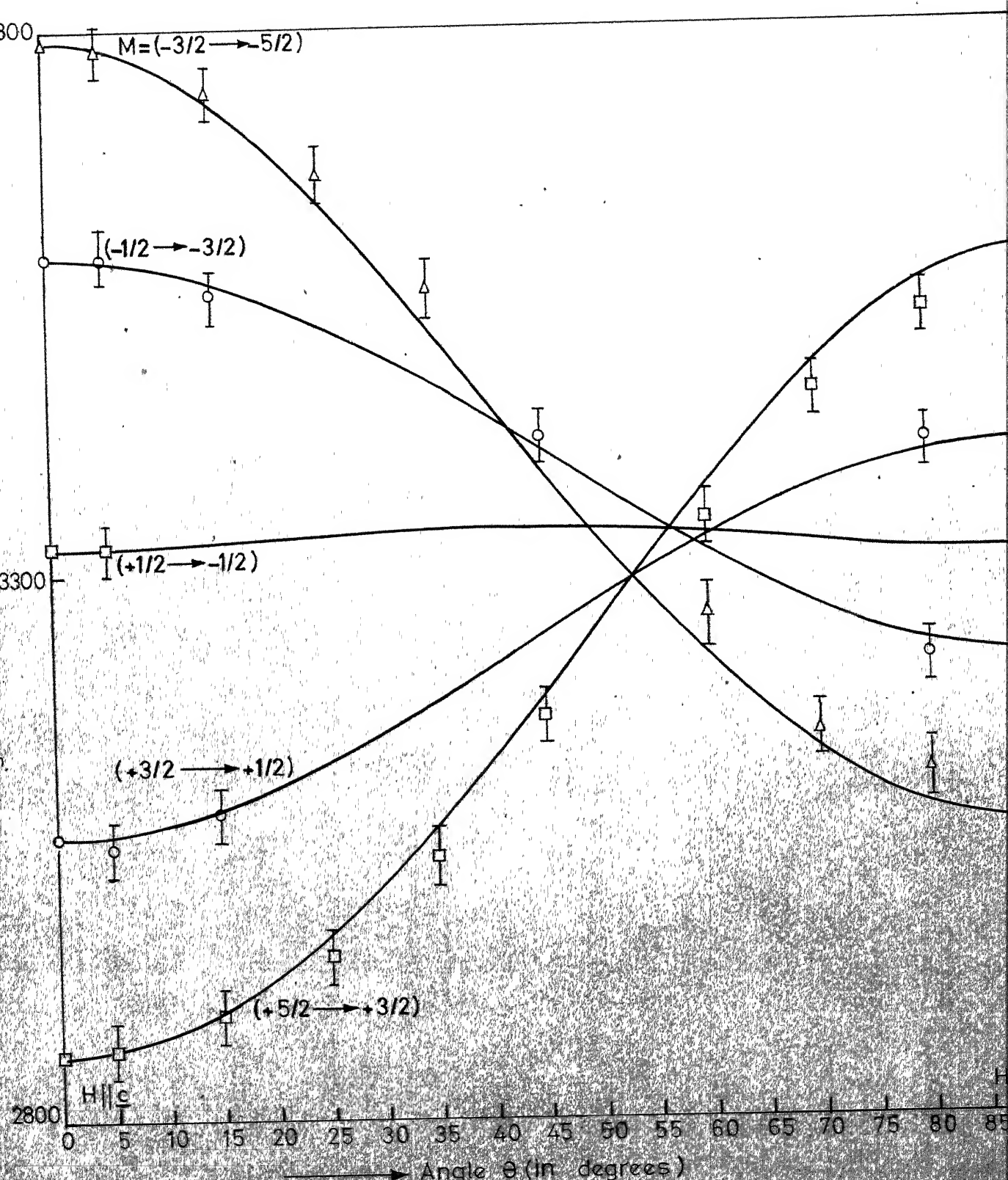

Fig.6.2(a) Angular variation of fine structure tran. positions in a c plane the EPR spectrum of Mn^{2+} in $Fe(ClO_4)_2 \cdot 6H_2O$.

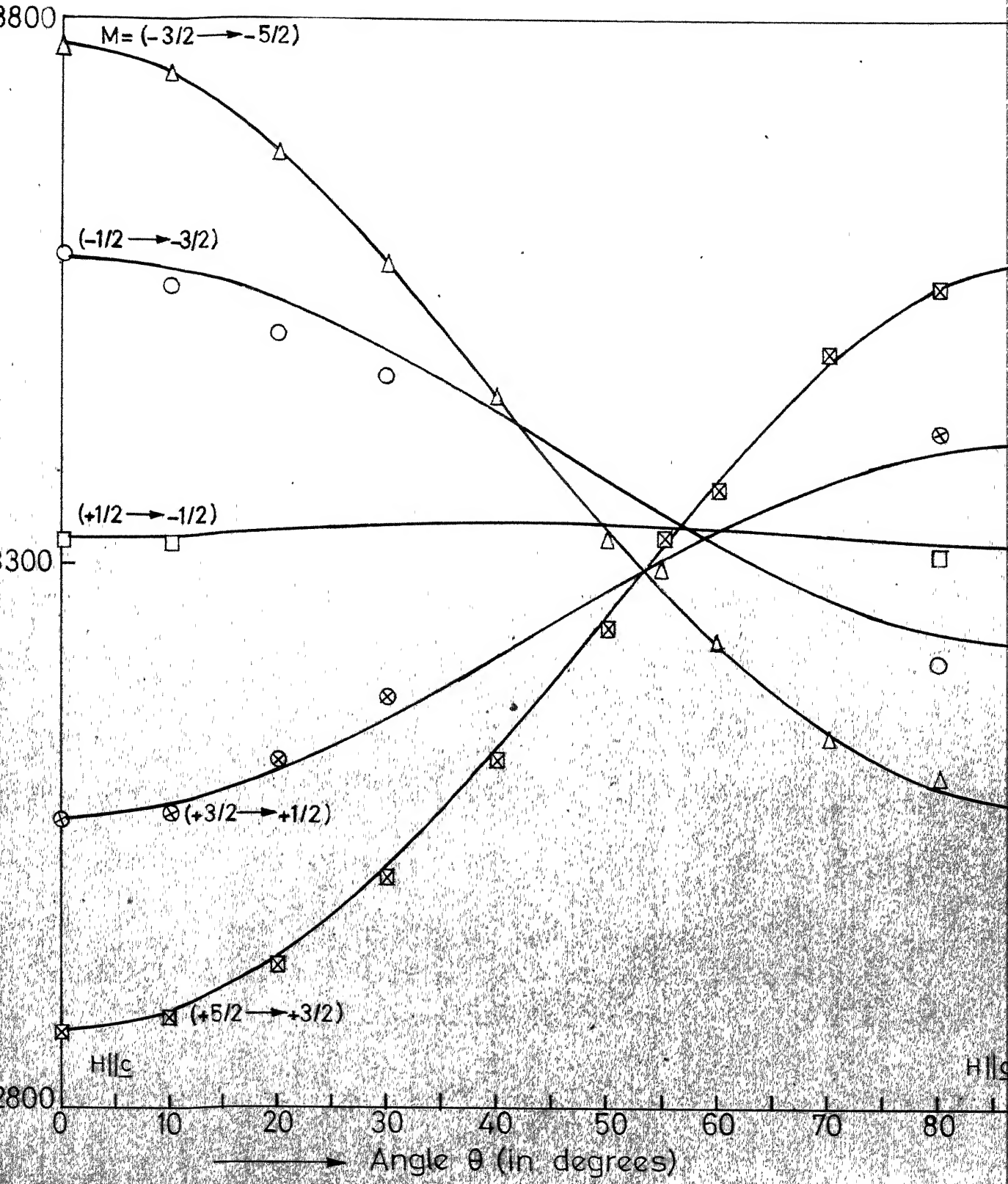

Fig.6.2(b) Angular Variation of fine structure tran.positions in EPR spectrum of Mn^{2+} in $Co(ClO_4)_2 \cdot 6H_2O$ crystal in the a c plane

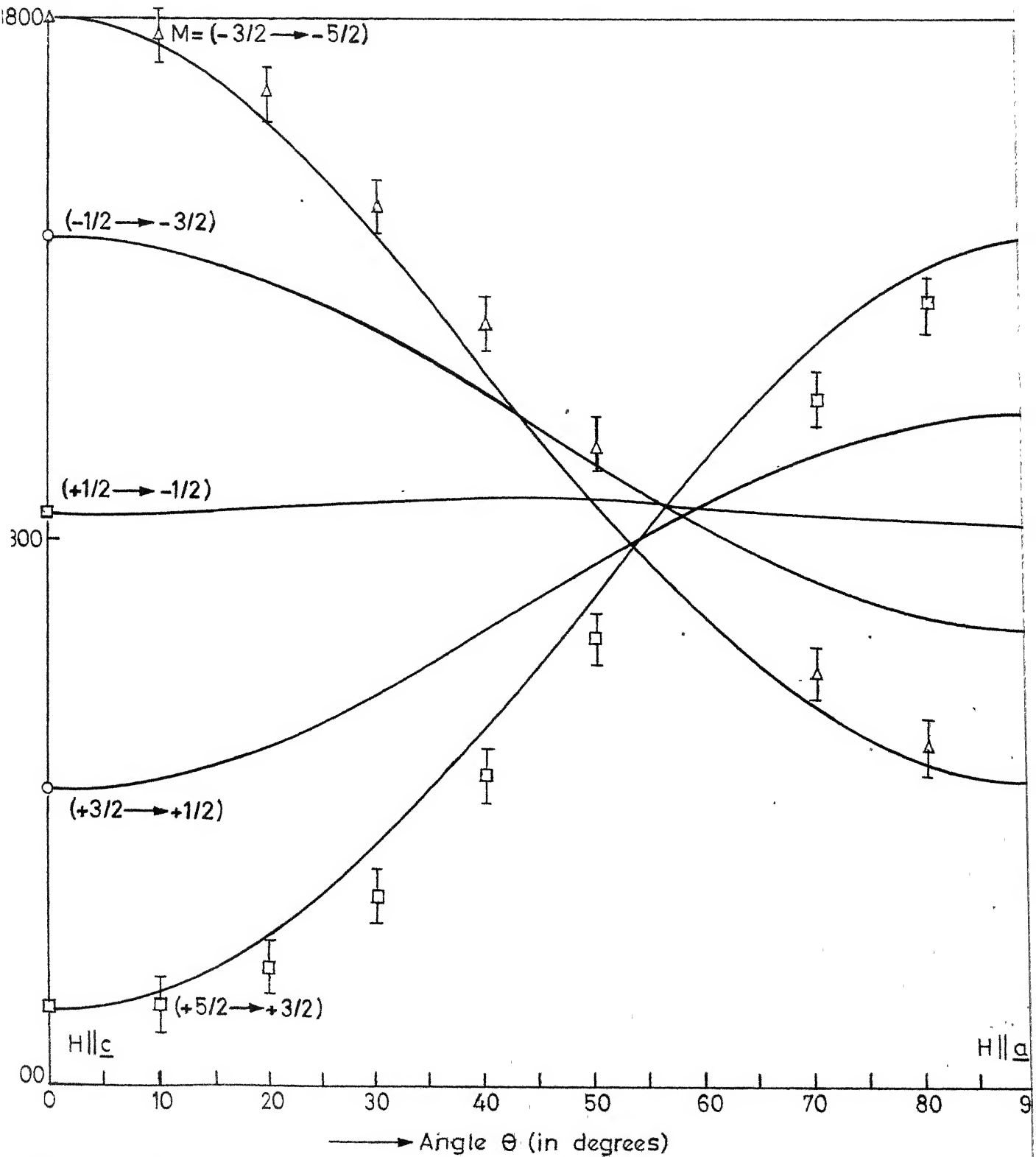

Fig.6.2(c) Angular variation of fine structure tran.positions in a c plane in the EPR spectrum of Mn^{2+} in $Ni(ClO_4)_2 \cdot 6H_2O$.

The angular variation of Mn^{2+} spectra in these crystals can be described by a spin-Hamiltonian for trigonal symmetry given in Chapter III. All the spectra are thus analysed using Eqs. 3.4, 3.5 and 3.8, and the spin-Hamiltonian parameters obtained are listed below in Table 6.2.

Table 6.2 Spin-Hamiltonian Parameters of Mn^{2+} in FePH, CoPH and NiPH

System	$g_{\parallel}$	$g_{\perp}$	D (gauss)	(a-F) (gauss)	A (gauss)	B (gauss
FePH:Mn^{2+}	2.0040 ±.0020	1.9993 ±.0020	121.2 ± 2.0	14.1 ± 2.0	-94.5 ± 3.0	94.6±5
CoPH:Mn^{2+}	2.0026 ±.0020	1.9996 ±.0020	117.6 ± 2.0	13.5 ± 2.0	-93.7 ± 3.0	93.7±5
NiPH:Mn^{2+}	2.0026 ±.0020	1.9987 ±.0020	117.0 ± 2.0	11.0 ± 2.0	-93.0 ± 3.0	93.7±5

A comparision of the parameters in Table 6.2 shows that the coordination of the water octahedron around the divalent ion is same in these compounds and they are stretched in identical manner.

The effect of the paramagnetic host ions Fe^{2+}, Co^{2+} and Ni^{2+} on the EPR spectrum of Mn^{2+} is reflected in the linewidths of the resonance lines which are found much larger compared to the linewidths of the resonance lines of Mn^{2+} in the diamagnetic

hosts MgPH, ZnPH and CdPH. Due to overlap of many lines of Mn^{2+} in paramagnetic hosts, the linewidths of only a few lines of the groups $\pm 5/2 \rightleftharpoons \pm 3/2$ could be measured and compared with those in the diamagnetic hosts. Table 6.3 shows a comparision of the linewidths measured from the spectra of Mn^{2+} for H along the c-axis at room temperature.

Table 6.3 A Comparision of Linewidths in Diamagnetic and Paramagnetic hosts

Mn^{2+} in	$M = +5/2 \rightleftharpoons 3/2$ linewidths in gauss	$-3/2 \rightleftharpoons -5/2$ linewidths in gauss
MgPH	13 , 13	13 , 13
ZnPH	20 , 18	17 , 17
CdPH	18	18
FePH	47 , 36	43 , 53
CoPH	37 , 37	36 , 36
NiPH	46 , 36	45 50

Larger linewidths of Mn^{2+} resonance lines have been observed by Saraswat and Upreti[3] also in cobalt and nickel acetate tetrahydrate single crystals and have been attributed to the magnetic interactions between Mn^{2+} and respective host

paramagnetic ions. The same explanation holds for the observed large linewidths in the present study as well.

From the linewidths of the four lines of $\pm 5/2 \rightleftharpoons \pm 3/2$ groups, it is not possible to predict exactly the behaviour of the lines of the remaining groups ($\pm 3/2 \rightleftharpoons \pm 1/2$) and ($1/2 \rightleftharpoons -1/2$).

TEMPERATURE VARIATION AND STRUCTURAL PHASE TRANSITION STUDIES

No resonance lines of the paramagnetic host ions seem to appear in the range 320 K to 80 K of temperature variation study.

The linewidths of Mn^{2+} resonance lines in paramagnetic hosts are large and are found to increase with the decrease in temperature, therefore, it becomes difficult to make accurate quantitative measurements, as the temperature is decreased. It is possible, however, to obtain some useful information about the hosts. Therefore, a temperature variation study of the Mn^{2+} doped FePH, CoPH and NiPH is made from room temperature to the liquid nitrogen temperature in the manner described in Chapter III.

Spectra for magnetic field H along c :

At room temperature, for H along c, 30-line hyperfine spectra are observed for Mn^{2+} in all the three paramagnetic host lattices. As the temperature is lowered, it is

observed that the fine structure spread of the Mn^{2+} spectra in FePH and CoPH increases very slowly and in CoPH it shows a maximum at 245 ± 5 K. In NiPH, the spread decreases continuously and shows a change in slope at 247 ± 5 K. These temperature are indicated by T_{ab} in Figs. 6.3(b) and 6.3(c). Some structural change in CoPH and NiPH seems to occur at these temperatures but this is not confirmed, because it is not possible to observe the changes in the spectrum other than those in the spread and even the changes in the spread are small. These structural changes can be confirmed by some other studies like specific heat measurement, x-ray etc.

As the temperature goes down further, the spread decreases continuously in CoPH and NiPH but in FePH it remains almost constant and lines become broader. The phase transitions already reported(by Mössbauer study and susceptibility measurements) appear to start at temperatures T_1 (242 K for FePH 161 K for CoPH and 223 K for NiPH) and are nearly complete at temperature T_2 (232 K for FePH, 148 K for CoPH). It is judged from the fact that at T_2, the fine structure disappears and only a merged spectrum is observed, due to the fact that this spectrum is at about 55° from its principal z-axis and contribution of the D term vanishes leaving only hyperfine structure. The temperature T_2 could not be found for NiPH upto the liquid nitrogen temperature and this shows that the

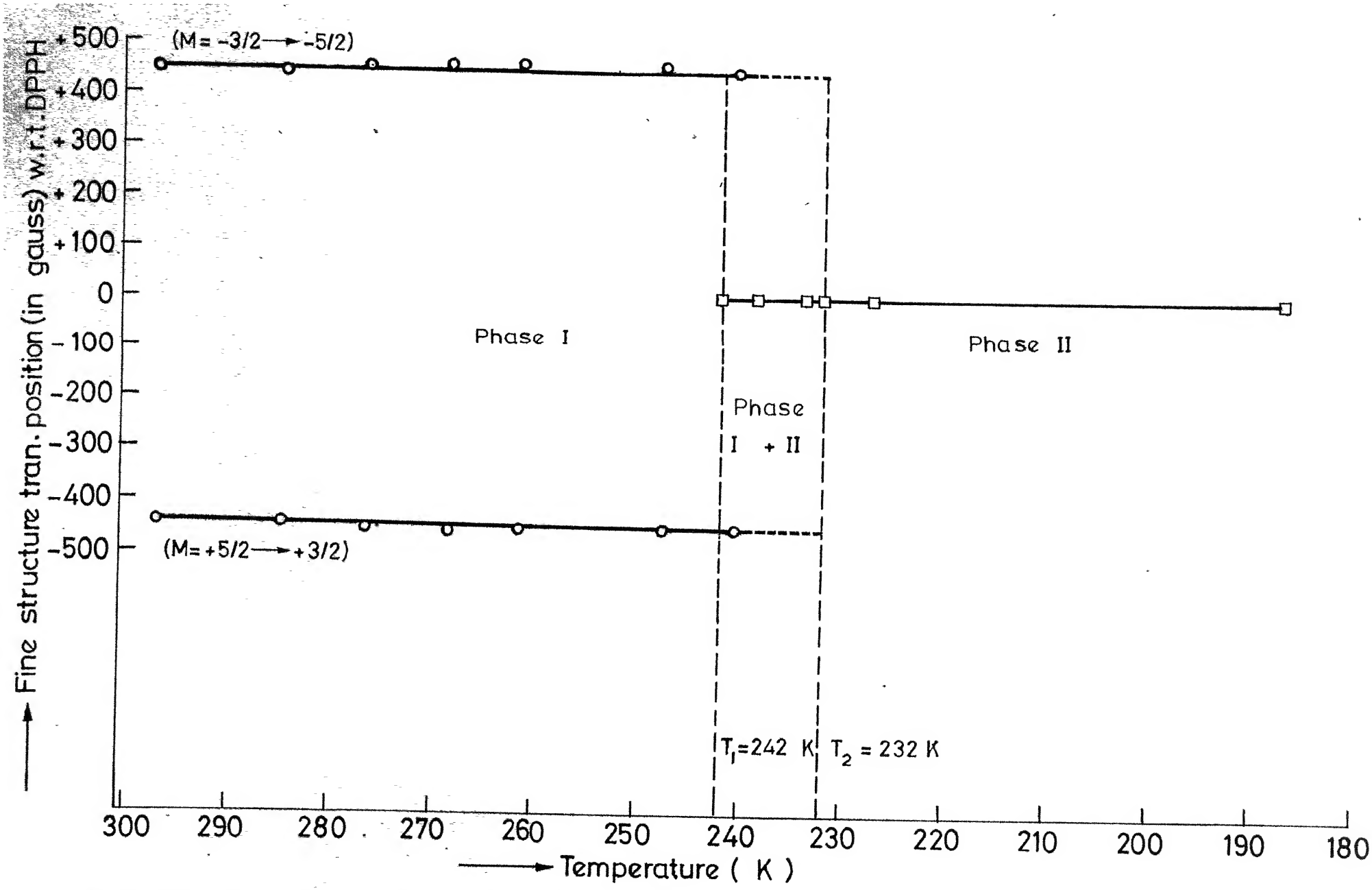

Fig. 6.3(a) Temperature variation of fine structure tran.positions in the EPR spectrum of Mn^{2+} in $Fe(ClO_4)_2 \cdot 6H_2O$ crystal for H||c.

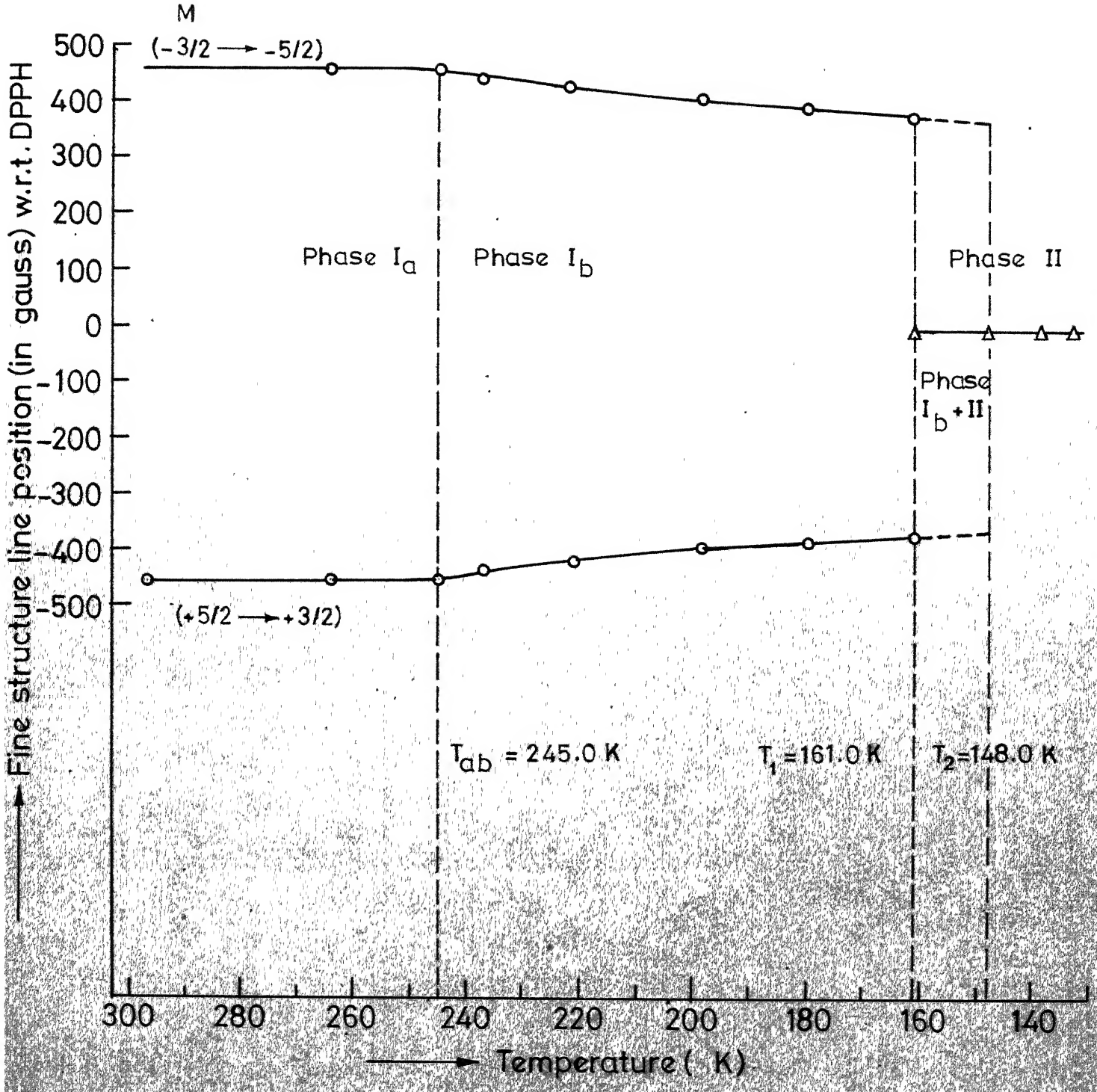

Fig. 6.3(b) Temperature variation of fine structure tran.positions in the EPR spectrum of Mn^{2+} in $Co(ClO_4)_2 \cdot 6H_2O$ crystal for H||c.

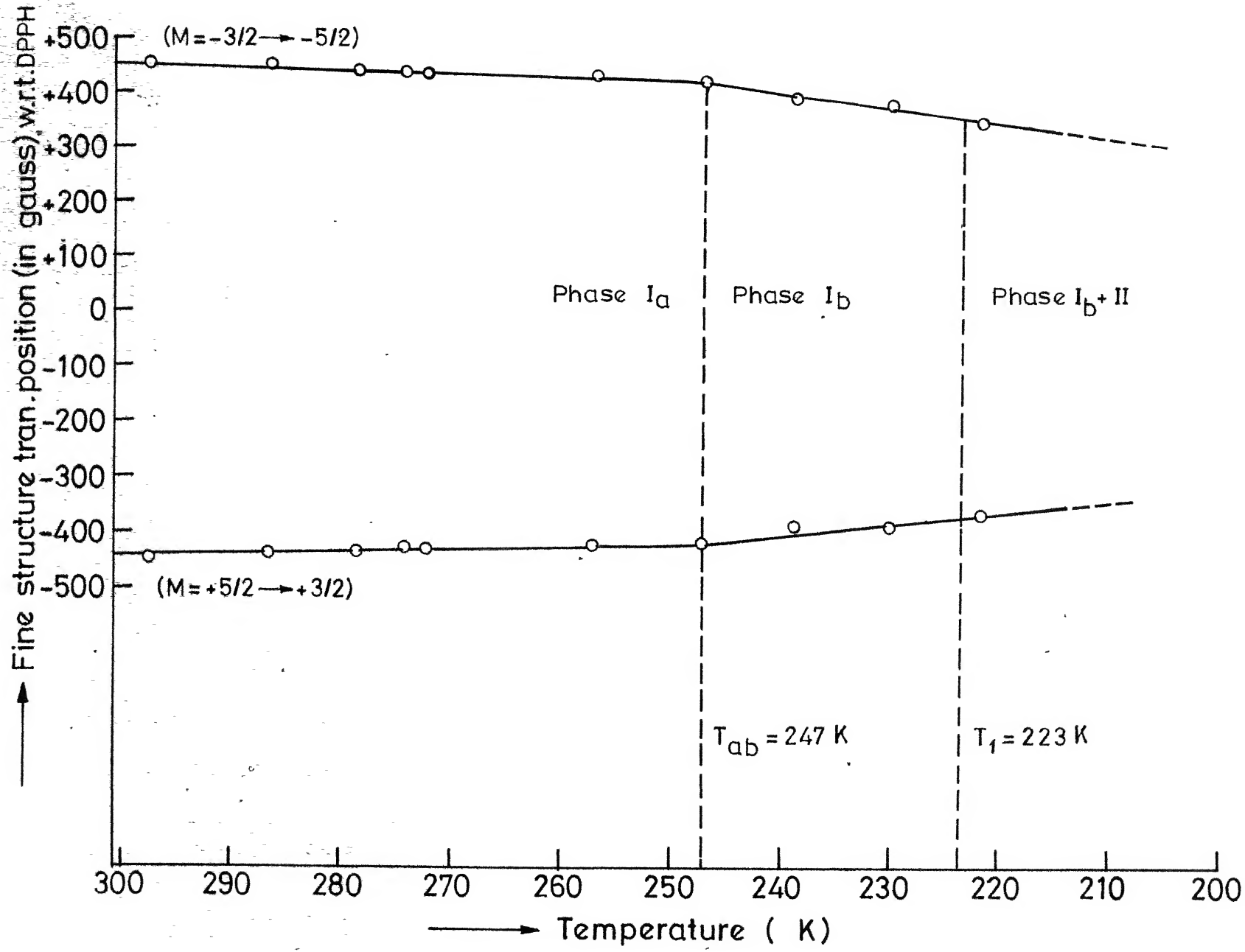

Fig.6.3(c) Temperature variation of fine structure tran. positions in the EPR spectrum of Mn^{2+} in $Ni(ClO_4)_2 \cdot 6H_2O$ crystal for H||c.

nature of the transition in this system is different from those in the other two hosts. Both the phases I and II in FePH, and I_b and II in CoPH coexist in the range T_1 to T_2, while in NiPH probably T_2 is below liquid nitrogen temperature and the phases I_b and II coexist till there. Such a coexistence has been reported by Dézsi I. et al.[4,11]. The transition temperatures for these phase transitions are compared below (Table 6.4) with those obtained by other studies.

Table 6.4 A comparision of Phase Transition Temperatures

System	Present study	Mössbauer study[4]	Susceptibility Measurement[6-9]
FePH:Mn^{2+}	237 ± 5 K	237 ± 15 K	237 ± 1 K
CoPH:Mn^{2+}	154.5 ± 6.5 K	155.5 ± 7.5 K	166 ± 1 K
NiPH:Mn^{2+}	223 ± 5 K	83 K	225 ± 1 K

The transition temperatures in FePH and NiPH obtained in the present study agree with those obtained in the susceptibility measurements while in CoPH it agrees with that found in Mössbauer study. The differences are probably due to presence of impurity ions in EPR and Massbauer studies. The slow conversion from phase I to phase II indicates that the phase transition is of the order higher than one. Transition temperature, 83K, reported by Mossbauer study is probably temperature T_2 for NiPH.

Angular Variation :

The angular variation in the b c plane shows that in all the systems, the nature of the spectra and the principal axes remain same from room temperature to T_1, though the spreads change and lines become broad. Below T_1 the changes observed are discussed separately for each host.

Fig. 6.4 shows the EPR spectra of Mn^{2+} in FePH at different temperatures for the magnetic field H parallel to c. In the phase II, spectra as shown in Fig. 6.4(b), (c), (d) are observed. The angular variation of these spectra in the b c plane shows an extremum (a broad peak with some structure) for H about 36° off the c-axis (Fig. 6.5) on one side and other broader extremum on the otherside of the c-axis for H about 54° off. This indicates clearly that the principal axes have changed their orientation in such a way that c-axis is the axis of minimum spread at about 54° from the new principal z-axis. Identical changes must take place in the other two possible b c planesjust as in the MgPH:Mn^{2+} system and the c-axis is still found to be the common axis of symmetry for all the complexes formed.

Figs. 6.6(a) and 6.6(b) show the spectra of Mn^{2+} in CoPH for H || c at room temperature and in phase II at 145.5 K. The angular variation of the spectrum shown in

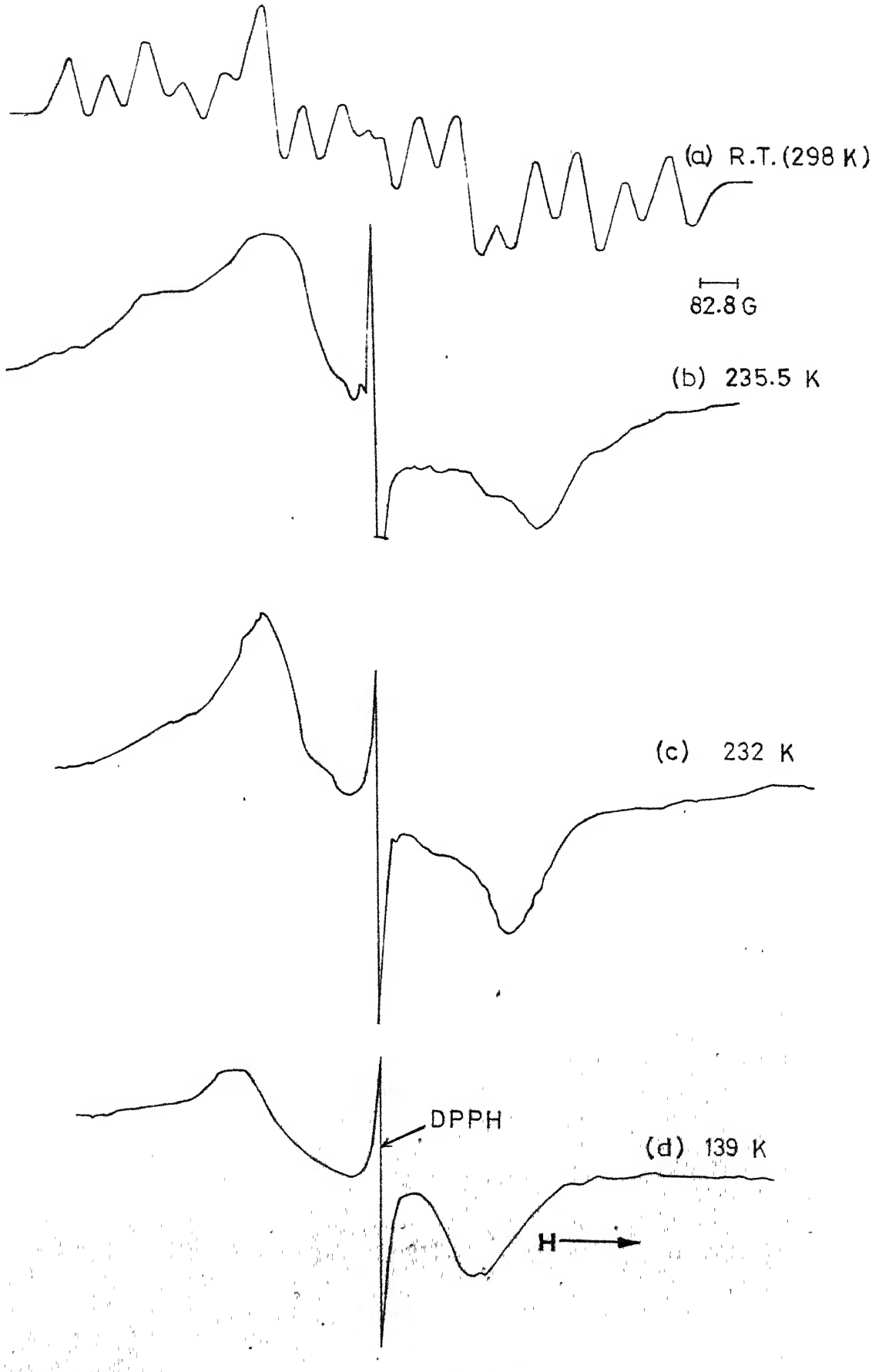

Fig.6.4 The EPR spectra of Mn^{2+} in $Fe(ClO_4)_2 \cdot 6H_2O$ with H||c at different temperatures.

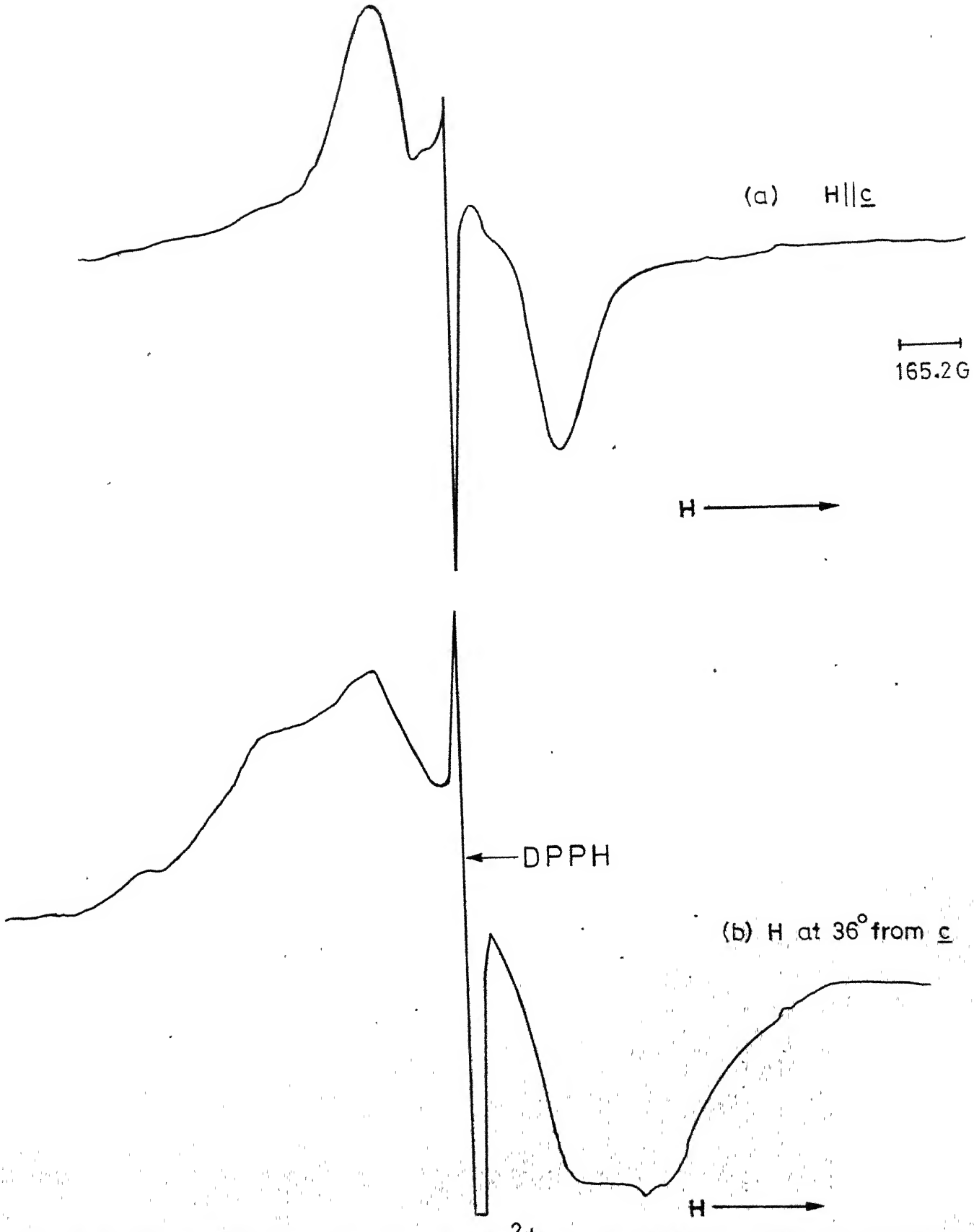

Fig.6.5 The EPR spectrum of Mn^{2+} in $Fe(ClO_4)_2 \cdot 6H_2O$ at 187 K with (a) H||c showing a minimum spread, (b) With H about 36° off c-axis in b c plane: the spectrum shows an extremum.

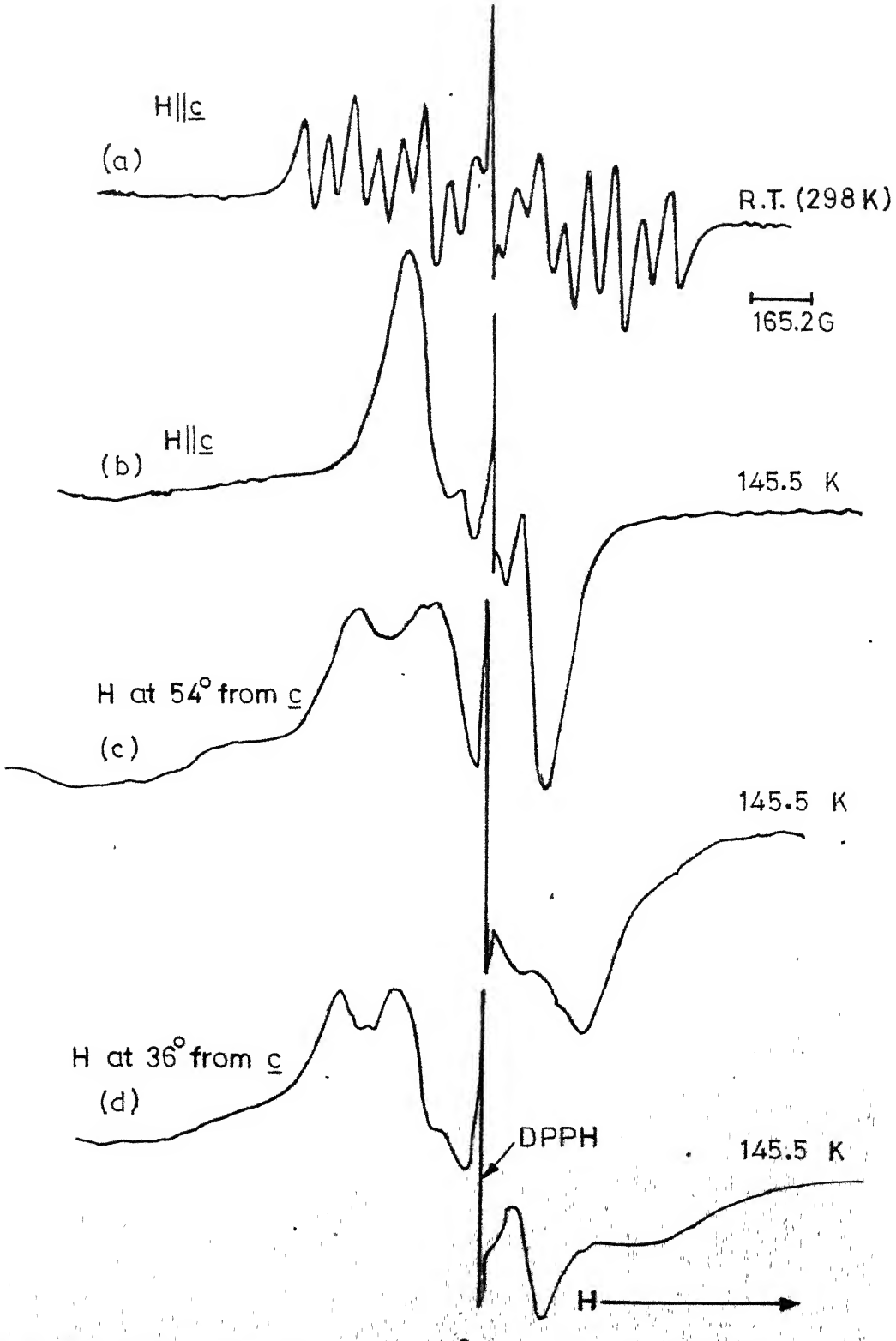

Fig.6.6 The EPR spectra of Mn^{2+} : $Co(ClO_4)_2 \cdot 6H_2O$: for (a) H||c at R.T.,(b) H||c at 145.5 K,(c) H at 54° from c-axis in b c plane,(d) H at 36° from c-axis on the other side in the b c plane.

Fig. 6.6(b) in the b c plane shows an extremum for H at about 54° from the c-axis (Fig. 6.6(c)) and another for H about 36° from the c-axis (Fig.6.6(d)onothersidde of the c-axis. Thus these two extrema are 90° off from each other. Therefore, in this system also the principal axes are turned off from those at room temperature. The same results will be obtained for the other two possible b c planes.

Fig. 6.7(a) shows the EPR spectrum of Mn^{2+} in NiPH for H along c at 109 K. There appears to be some structure though not observable clearly due to broader lines and overlap. The angular variation of this spectrum in the b c plane shows a minimum for H at about 54° off from the c-axis(Fig. 6.7(b))and this behaviour is identical to that at room temperature at which the spectrum for H along c goes to a minimum when magnetic field H is brought to a position about 54° off from the c-axis in the b c plane. This shows that still principal z-axis is parallel to the c-axis.

According to Chaudhuri who observed the phase transition in these system[6-9] from susceptibility measurements, the site symmetry of the divalent cation changes from trigonal (above the transition point) to tetragonal (below the transition point) and the mechanism of the transition[12] is associated to the rotation or rearrangement of the perchlorate tetrahedra. But, from the Mössbauer studies on $Fe(ClO_4)_2 6H_2O$,

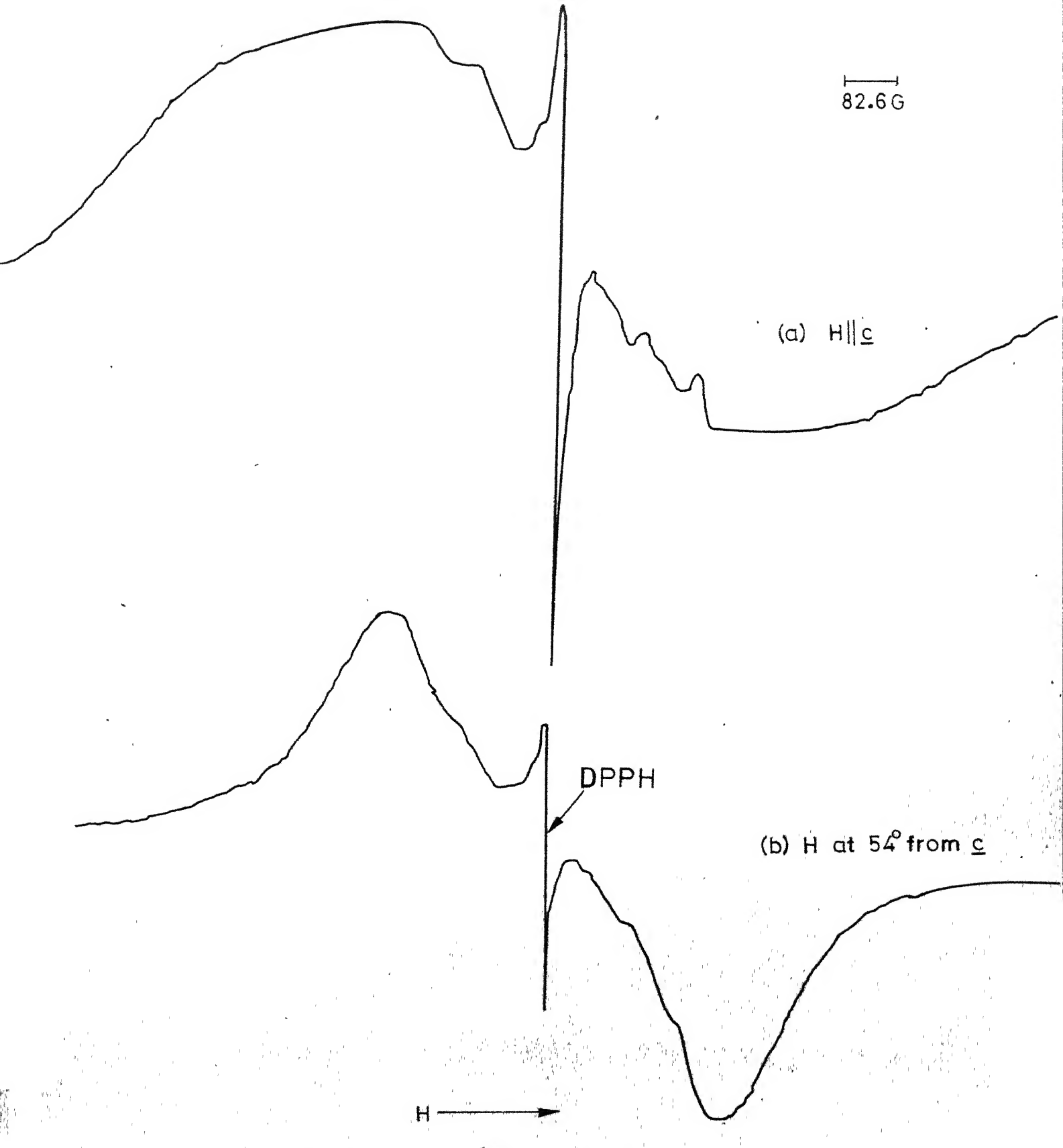

Fig.6.7 The EPR spectra of Mn^{2+} in $Ni(ClO_4)_2 \cdot 6H_2O$ at 109 K: (a) for H||c, (b) for H at 54° from c-axis in b c plane

Reiff et al.[5] suggest that, at this transition, a trigonally elongated octahedron changes into a trigonally compressed octahedron, the three fold axis remaining same and the mechanism of transition being related to disorder of the tetrahedra.

Our observations in FePH and CoPH support the predictions made by Chaudhuri as far as the change in symmetry is concerned. However, exact determination of the symmetry seems difficult due to line broadening and pseudohexagonal structure of the crystals. Further our observations in NiPH support the view of Reiff et al. for the symmetry changes.

REFERENCES

1. Bleaney B., Elliott R.J. and Scovil H.E.D., Proc. Phys. Soc. (Lond.) A-63, 408 (1950).

2. Ono K. and Hayashi I., J. Phys. Soc. Japan 8, 561 (1953).

3. Saraswat R.S. and Upreti G.C., J. Mag. Res. 20,39 (1975). and references therein.

4. Dézsi I. and Keszthelyi L., Solid State Comm. 4, 511(1966).

5. Reiff W.M., Frankel R.B. and Abeledo C.R., Chem. Phys. Lett. 22, 124 (1973).

6. Chaudhuri B.K. and Ghosh D., Phys. Stat. Solidi (a) 23, 649 (1974).

7. Chaudhuri B.K., J. Phys. C: Solid State Phys. 7, 3962 (1974).

8. Chaudhuri B.K., Solid State Comm. 16, 767 (1975).

9. Chaudhuri B.K., Indian J. of Pure and Appld. Phys. 13 363 (1975).

10. West C.D., Z. Kristall. 91A, 480 (1935).

11. Asch L., Dézsi I. Lohner T. and Molnar B., Chem. Phys. Lett. 39, 177 (1976).

12. Chaudhuri B.K., Ind. J. Pure and Appld. Phys. 14, 525 (1976).